

ECOLOGY AND ENERGETICS OF EARLY LIFE STAGES OF
WALLEYE POLLOCK IN THE EASTERN BERING SEA: THE ROLE
OF SPATIAL VARIABILITY ACROSS CLIMATIC CONDITIONS

By

Elizabeth Calvert Siddon

RECOMMENDED:



Dr. Janet T. Duffy-Anderson



Dr. Ron A. Heintz



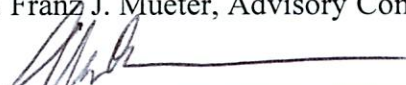
Dr. Nicola Hillgruber



Dr. Brenda L. Norcross




Dr. Franz J. Mueter, Advisory Committee Chair

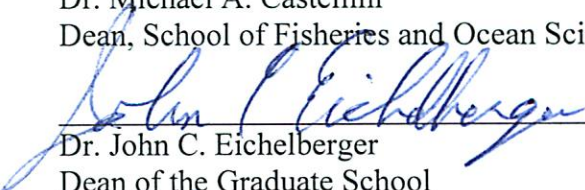


Dr. Milo D. Adkison
Chair, Graduate Program, Fisheries Division

APPROVED:



Dr. Michael A. Castellini
Dean, School of Fisheries and Ocean Sciences



Dr. John C. Eichelberger
Dean of the Graduate School



Date

ECOLOGY AND ENERGETICS OF EARLY LIFE STAGES OF
WALLEYE POLLOCK IN THE EASTERN BERING SEA: THE ROLE
OF SPATIAL VARIABILITY ACROSS CLIMATIC REGIMES

A
THESIS

Presented to the Faculty
of the University of Alaska Fairbanks

in Partial Fulfillment of the Requirements
for the Degree of

DOCTOR OF PHILOSOPHY

By

Elizabeth Calvert Siddon, B.S., M.S.

Fairbanks, Alaska

August 2013

Abstract

Understanding mechanisms behind variability in early life survival of marine fishes can improve predictive capabilities for recruitment success under changing climate conditions. Ecosystem changes in response to climate variability in the eastern Bering Sea affect commercial species including walleye pollock (*Theragra chalcogramma*), which represent an ecologically important component of the ecosystem and support the largest commercial fishery in the United States. The goal of my dissertation was to better understand spatial and temporal dynamics in the ecology of early life stages of walleye pollock in the eastern Bering Sea through: (1) an examination of shifts in larval fish community composition in response to environmental variability across both warm and cold conditions; (2) a quantification of the seasonal progression in energy content of age-0 walleye pollock which provides critical information for predicting overwinter survival and recruitment to age-1 because age-0 walleye pollock rely on sufficient energy reserves to survive their first winter; and (3) a modeling approach to better understand the role of prey quality, prey composition, and water temperature on spatial and temporal patterns of juvenile walleye pollock growth with implications for year-class survival and recruitment success. In the community analysis, I identified a strong cross-shelf gradient delineating slope and shelf assemblages, an influence of water masses from the Gulf of Alaska on species composition, and the importance of nearshore areas for larval fish. Species assemblages differed between warm and cold periods, and larval abundances, including that of walleye pollock, were generally greater in warm years. I identified different energy allocation strategies indicating that distinct ontogenetic stages face different

survival constraints. Larval walleye pollock favored allocation to somatic growth, presumably to escape size-dependent predation, while juveniles allocated energy to lipid storage in late summer. Finally, I provide evidence that a spatial mismatch between juvenile walleye pollock and growth ‘hot spots’ in 2005 contributed to poor recruitment while a higher degree of overlap in 2010 resulted in improved recruitment. I highlight the importance of climate-driven spatial patterns in community structure, prey dynamics, and environmental conditions that influence the growth and survival of an important gadoid population in a sub-arctic marine ecosystem.

Table of Contents

	Page
Signature Page	i
Title Page	iii
Abstract	v
Table of Contents	vii
List of Figures	xii
List of Tables	xviii
Acknowledgements	xxi
Dedication	xxiv
General Introduction	1
Chapter 1: Community-level response of larval fish to environmental variability in the southeastern Bering Sea	7
Abstract	7
1.1 Introduction	9
1.2 Study region	11
1.3 Materials and methods	12
1.3.1 Biological sampling	12
1.3.2 Physical environment sampling	13
1.3.3 Community analyses	15

1.3.4 NMDS by station	16
1.3.5 NMDS by geographic area.....	18
1.4 Results.....	18
1.4.1 Biological sampling.....	18
1.4.2 Physical environment sampling.....	19
1.4.3 Community analyses.....	19
1.4.3.1 NMDS by station	20
1.4.3.2 Generalized Additive Models	20
1.4.3.2.1 Axis 1	20
1.4.3.2.2 Axis 2	21
1.4.3.2.3 Axis 3	22
1.4.3.3 NMDS by geographic area.....	23
1.5 Discussion.....	24
1.6 Acknowledgements.....	30
1.7 References.....	31
Chapter 2: Conceptual model of energy allocation in walleye pollock (<i>Theragra</i>	
<i>chalcogramma</i>) from age-0 to age-1 in the southeastern Bering Sea.....	55
Abstract.....	55
2.1 Introduction.....	57
2.1.1 Study region.....	61
2.2 Materials and methods	62

2.2.1 Biological sampling	62
2.2.2 Chemical analysis	64
2.2.2.1 Energy density	64
2.2.2.2 Proximate composition	65
2.2.3 Statistical analysis	67
2.2.3.1 Cohort-specific patterns from age-0 to age-1	67
2.2.3.2 Seasonal patterns in energy allocation of age-0 fish.....	67
2.3 Results.....	69
2.3.1 Biological sampling	69
2.3.2 Cohort-specific patterns from age-0 to age-1	70
2.3.3 Seasonal patterns in energy allocation of age-0 fish.....	70
2.4 Discussion.....	72
2.5 Conclusions.....	77
2.6 Acknowledgements.....	78
2.7 References.....	79

Chapter 3: Spatial match-mismatch between juvenile fish and prey explains

recruitment variability across contrasting climate conditions in the eastern Bering

Sea	99
Abstract.....	99
3.1 Introduction.....	101
3.2 Materials and methods	103

3.2.1 Ethics statement	103
3.2.2 Modeling approaches	103
3.2.3 Field observations	104
3.2.3.1 Juvenile pollock abundance	105
3.2.3.2 Water temperature.....	105
3.2.3.3 Zooplankton data	106
3.2.3.3.1 Determination of main prey taxa	106
3.2.3.3.2 Zooplankton size.....	107
3.2.3.3.3 Zooplankton abundance.....	107
3.2.3.3.4 Zooplankton biomass.....	108
3.2.3.3.5 Zooplankton energy density.....	108
3.2.3.3.6 Zooplankton vertical profiles.....	109
3.2.4 Bioenergetics model.....	110
3.2.4.1 Bioenergetics sensitivity analyses.....	112
3.2.5 Mechanistic individual-based model	113
3.2.5.1 IBM sensitivity analyses	115
3.2.6 Comparison of observed and predicted prey preferences	116
3.3 Results.....	117
3.3.1 Field observations	117
3.3.1.1 Juvenile pollock abundance	117
3.3.1.2 Water temperature.....	118
3.3.1.3 Zooplankton	118

3.3.1.3.1 Prey taxa.....	118
3.3.1.3.2 Zooplankton abundance.....	119
3.3.1.3.3 Zooplankton biomass.....	119
3.3.1.3.4 Zooplankton energy density.....	120
3.3.1.3.5 Zooplankton vertical profiles.....	120
3.3.2 Bioenergetics model.....	121
3.3.2.1 Bioenergetics sensitivity analyses.....	121
3.3.2.1.1 Effect of water temperature and prey energy density ..	121
3.3.2.1.2 Effect of fish weight and fish energy density ..	122
3.3.3 Mechanistic individual-based model	123
3.3.3.1 IBM sensitivity analyses	124
3.3.4 Spatial comparison of bioenergetics- and IBM-predicted growth.....	125
3.3.5 Comparison of observed and predicted prey preferences	125
3.4 Discussion.....	126
3.5 Conclusions.....	133
3.6 Acknowledgements.....	133
3.7 References.....	134
General Conclusions.....	169
References.....	176

List of Figures

	Page
Chapter 1	
<p>Figure 1.1. (A) Study region showing the location of sampling stations (◆). To investigate changes in larval fish assemblage structure over time, only those stations sampled in at least two years were included in the analyses ('common stations'; Table 1). Depth contours are shown for the 40, 100, 200, and 1000 m isobaths. (B) Predominant currents in the study region include the Aleutian North Slope Current (ANSC), the Bering Slope Current (BSC), and the Alaska Coastal Current (ACC)</p>	42
<p>Figure 1.2. Stations sampled in (A) 2002 and (B) 2008, and corresponding temperature and salinity plots (averaged across the top 20 m) for (C) 2002 and (D) 2008. Samples were collected in 4 geographic areas based on bathymetry: Unimak Pass (*), slope (▲; outside of 200 m isobath), outer domain (+; between 100 m - 200 m isobaths), and shelf (▽; out to 100 m). 2002 was a warm year showing increased mixing of water masses from Unimak Pass to the shelf; 2008 was a cold year with greater distinction of water masses. Note the difference in the x-axis scale in C and D</p>	43
<p>Figure 1.3. Percent contribution to total catch (based on catch per unit effort) of the 5 overall most abundant species by year. The most abundant species were walleye pollock (<i>Theragra chalcogramma</i>), Pacific sand lance (<i>Ammodytes hexapterus</i>), <i>Sebastes</i> spp., northern rock sole (<i>Lepidopsetta polyxystra</i>), and Pacific cod (<i>Gadus macrocephalus</i>) .</p>	44
<p>Figure 1.4. Non-metric multidimensional scaling (NMDS) ordination, based on a Bray-Curtis similarity matrix, depicting the relative similarity in species composition among individual stations sampled across 5 years. Data were 4th root transformed and standardized to species maximum</p>	45
<p>Figure 1.5. (A) Predicted spatial gradient of species composition as indicated by Axis 1 scores from non-metric multidimensional scaling (NMDS) ordination of species-by-station matrix, based on the generalized additive model (GAM) described by Eq. (2). The spatial surface was estimated as a smooth term of latitude and longitude; other covariates were fixed at their mean values. Species composition is predicted to be similar along contours; changes in species composition occur when moving across contours (color gradient). Spearman rank correlations of species positively or negatively correlated with these values were used to determine the main species of the slope versus shelf assemblage, respectively. Depth contours are shown for the 100 and 200 m isobaths</p>	46

Figure 1.5. (B) Predicted measure of species composition (Axis 1 scores from NMDS ordination) as a smooth function of temperature and salinity based on the GAM described by Eq. (2). Stations with salinities less than 29 ($n = 3$) were removed for better visualization of the relative effects of temperature and salinity. Cool colors correspond to the shelf habitat and negative species correlations; warm colors correspond to the slope habitat and positive species correlations (see A). Years are distinguished as follows: 2002 = red, 2003 = brown, 2005 = orange, 2006 = light blue, 2008 = purple..... 47

Figure 1.5. (C) Estimated differences in species composition among years (Axis 1 scores from NMDS ordination) based on the GAM described by Eq. (2). Solid lines reflect the partial response of Axis 1 scores, on a normalized scale, when all other covariates are fixed at their mean values. Dashed lines denote 95% confidence intervals 48

Figure 1.6. (A) Predicted spatial gradient of species composition as indicated by Axis 2 scores from non-metric multidimensional scaling (NMDS) ordination of species-by-station matrix, based on the generalized additive model (GAM) described by Eq. (3). Spearman rank correlations of species positively correlated with these values were used to determine the main species of the Alaska Coastal Current assemblage 49

Figure 1.6. (B) Predicted measure of species composition (Axis 2 scores from NMDS ordination) as a smooth function of temperature and salinity based on the GAM described by Eq. (3). Warm colors correspond to the Alaska Coastal Current waters and positive species correlations (see A). See Fig. 5 for additional description..... 50

Figure 1.7. (A) Predicted spatial gradient of species composition as indicated by Axis 3 scores from non-metric multidimensional scaling (NMDS) ordination of species-by-station matrix, based on the generalized additive model (GAM) described by Eq. (4). Spearman rank correlations of species positively correlated with these values were used to determine the main species of the nearshore assemblage..... 51

Figure 1.7. (B) Predicted measure of species composition (Axis 3 scores from NMDS ordination) as a smooth function of temperature and salinity based on the GAM described by Eq. (4). Warm colors correspond to the nearshore habitat and positive species correlations (see A). See Fig. 5 for additional description 52

Figure 1.8. Non-metric multidimensional scaling (NMDS) ordination, based on a Bray-Curtis similarity matrix, depicting the relative similarity in species composition among geographic areas by year. Outer domain: between 100 and 200 m isobaths; Shelf: within 100 m isobath; Slope: outside of 200 m isobath; Unimak Pass (see Fig. 1.1). Data were 4th root transformed and standardized to species maximum..... 53

Chapter 2

Figure 2.1. (A) Map showing the location of the Bering Sea. (B) Map of the southeastern Bering Sea showing the location of sample collections by age class and year. Sampling for age-0 fish is assumed to encompass the bulk of their distribution based on historical data, while age-1 fish were predominantly sampled from the outer shelf domain (between 100 and 200 m isobaths). Depth contours are shown for the 50 m, 100 m, and 200 m isobaths. 89

Figure 2.2. Plot of energy density (kJ/g dry mass) for the 2008 and 2009 cohorts of walleye pollock (*Theragra chalcogramma*). Errors bars are plotted as ± 1 standard deviation to show the variability in energy density estimates for each sampling interval. Different letters indicate significant differences in energy density within season. Note x-axis is mean sampling date across the age-0 and age-1 seasons. 90

Figure 2.3. Results from generalized additive mixed model (GAMM) regression analyses showing the estimated effects on energy density (kJ/g dry mass) of (a) standard length (SL; mm), (b) spatial location (by year), and (c) year for age-0 walleye pollock (*Theragra chalcogramma*). Dashed lines denote 95% confidence intervals in (a) and (c). Energy densities in (a) are plotted as anomalies because actual values depend on location and year. Spatial contours in (b) correspond to the estimated energy density for a fish of 60 mm SL on September 1. Depth contours are shown for the 50 m, 100 m, and 200 m isobaths. The partial fits by year (c) show the average energy density by year with other covariates fixed at their mean values. 91

Figure 2.4. Results from generalized additive mixed model (GAMM) regression analyses showing the estimated effects on % lipid (on a dry mass basis) of (a) standard length (SL; mm), (b) sampling date, and (c) year for age-0 walleye pollock (*Theragra chalcogramma*). Dashed lines denote 95% confidence intervals. % Lipid values in (a) and (b) are plotted as anomalies because actual values depend on sampling date and year. The range of y-axis values are comparable between (a) and (b), indicating SL and sampling date are similarly important in explaining variability in % lipid. The partial fits by year (c) show the average % lipid by year with other covariates fixed at their mean values... 94

Figure 2.5. Results from generalized additive mixed model (GAMM) regression analyses showing the estimated effects on standard length (SL; mm) of (a) sampling date and (b) year for age-0 walleye pollock (*Theragra chalcogramma*). Dashed lines denote 95% confidence intervals. The partial fits by year (b) show the average SL by year with other covariates fixed at their mean values. 97

Chapter 3

Figure 3.1. (a) Bering Sea with predominant currents in the study region, including the Aleutian North Slope Current (ANSC), the Bering Slope Current (BSC), and the Alaska Coastal Current (ACC). (b) Eastern Bering Sea with locations of sampling stations at which the bioenergetics model and IBM models were run in 2005 (•) and 2010 (□). MC Station (▲) is the representative station used for Monte Carlo simulations. Depth contours are shown for the 50 m, 100 m, and 200 m isobaths. 144

Figure 3.2. Log(CPUE) of juvenile walleye pollock collected in surface trawls in 2005 (a) and 2010 (b). Circle size is proportional to catch at each station; stations with zero catch (×) are on white background. 145

Figure 3.3. Water temperatures in 2005 and 2010 interpolated across all stations (•) sampled by the CTD. Upper row shows the mean temperature in the upper 30 m of the water column. Lower row shows the mean temperature below 40 m. 146

Figure 3.4. Zooplankton prey availability in the eastern Bering Sea in 2005 and 2010. Upper row shows the log of total abundance (a and c) and log of total biomass (g WW; b and d) in each year. Lower row shows the log of total abundance for zooplankton within the optimal size range for 65 mm SL juvenile walleye pollock (5-8% of fish length; e and g) and the biomass-weighted mean energy density (f and h) of available zooplankton prey in each year. The CPUE of juvenile walleye pollock collected in surface trawls is overlaid in e-h. Circle size is proportional to catch at each station (×=zero catch). 147

Figure 3.5. Vertical profiles of abundance for representative main prey taxa from a cold year. (a) *Thysanoessa inermis* has a strong diel migration with distribution shifting from deeper during day to more shallow at night. (b) *Pseudocalanus* sp. displays an opposite behavior, shallow distribution during the day and deeper at night. (c) *Limacina helicina*, the dominant prey item in 2005 and 2010, does not display strong diel migration, with a shallow distribution during day and night. 148

Figure 3.6. Maximum predicted growth of juvenile walleye pollock ($g \cdot g^{-1} \cdot d^{-1}$) from the bioenergetics model. Top row shows growth under the base scenarios for 2005 and 2010 (a and b, respectively). Middle row (c-d) shows changes in predicted growth when temperature is increased by 1 standard deviation (SD). Predicted growth could not be estimated at one station (panel c) in the inner domain under increased temperatures because the water temperature in the upper 30 m was greater than 15 °C ($T_{cm} = 15$ °C in the model). Lower row shows changes in predicted growth when prey energy density is increased by 1 SD in 2005 and 2010 (e and f, respectively). Spatial plots of predicted growth when parameters are lowered by 1 SD are not shown, but can be visualized by subtracting the anomalies (lower two rows) from the base scenario plots (top row). 149

Figure 3.7. Predicted growth ($g \cdot g^{-1} \cdot d^{-1}$) of juvenile walleye pollock over the range of observed temperatures and prey energy density (ω_k) across both 2005 and 2010. The observed fish energy density (v_k) was higher in 2010 ($v_{2010} = 5.292$ kJ $\cdot g^{-1}$ WW; used in plot shown), thus higher metabolic demands, therefore this interpolation demonstrates the range of predicted growth for fish with high energy density. Temperatures included 0-16 °C to show possible range under variable climate conditions; observed range of ω_k across warm and cold years. Black rectangle encompasses the range of temperatures and ω_k observed across 2005 and 2010. Points are shown for average temperature and ω_k conditions in 2005 and 2010. Predicted growth above 15 °C was not possible (black) because the bioenergetics model has a temperature threshold of 15 °C. 151

Figure 3.8. Simulated distribution of growth rates ($g \cdot g^{-1} \cdot d^{-1}$) when fish weight (W) and fish energy (v_i) at a single representative station (see Fig. 1) in 2005 and 2010 is varied over the range of observed values (random draws from a normal distribution with observed mean and SD). Using the base scenario ($W=2.5$ g; $v_{2005} = 3.916$ kJ $\cdot g^{-1}$ WW; $v_{2010} = 5.292$ kJ $\cdot g^{-1}$ WW) ± 1 standard deviation (SD), the model was run 1000 times to estimate the distribution around mean predicted growth. Parameter SDs were calculated across stations after removing the annual means. 152

Figure 3.9. Maximum predicted growth ($g \cdot g^{-1} \cdot d^{-1}$) and average depth of juvenile walleye pollock over 24 hours from the IBM. Top row shows growth (a and c) and average depth (b and d) under the base scenario for a 2.5 g fish in 2005 and 2010. Middle row shows changes in predicted growth (e and g) and average depth (f and h) for 2.0 g fish, highlighting the relative importance of fish size and water temperature (between years). Lower row shows changes in predicted growth (i and k) and average depth (j and l) when uniform vertical distributions of prey are implemented, highlighting the effect of zooplankton diel vertical distribution and migrations on juvenile walleye pollock prey selection. Negative changes in depth indicate a shallower distribution; positive values indicate a deeper distribution. 153

Figure 3.10. Difference in predicted growth of juvenile walleye pollock ($g \cdot g^{-1} \cdot d^{-1}$) between the bioenergetics model and the IBM for 2005 (a) and 2010 (b). Areas of positive differences indicate where maximum growth potential from the bioenergetics model was higher than predicted growth from the IBM. 155

Figure 3.11. Diet comparisons between observed and predicted (IBM) diets of juvenile walleye pollock for main prey taxa (see Table 3.1) in 2005. The left-hand panel shows the mean Chesson indices (unitless) for each prey taxon for observed and predicted diets. Neutral selection varied across stations depending on the number of taxa present. The right-hand panel shows the difference (± 1 standard deviation) in the relative preference of each prey taxa; Chesson values were divided by neutral selection for each station and then predicted values subtracted from observed. Positive values indicate the prey is more prevalent in observed diets (e.g., a value of 2 indicate the taxa is twice as prevalent in observed diets as predicted). Prey taxa abbreviations are as follows: LH = *Limacina helicina*; PS = *Pseudocalanus* sp.; OS = *Oikopleua* sp.; CA = *Centropages abdominalis*; TR = *Thysanoessa raschii*; TS = *Thysanoessa* sp.; AC = *Acartia clausi*; CM = *Calanus marshallae*. 156

Figure 3.12. Diet comparisons between observed and predicted (IBM) diets of juvenile walleye pollock for main prey taxa (see Table 3.1) in 2010. See Figure 11 legend for explanation. Prey taxa abbreviations are as follows: LH = *Limacina helicina*; CM = *Calanus marshallae*; NC = *Neocalanus cristatus*; TR = *Thysanoessa raschii*; EB = *Eucalanus bungii*. 157

Figure 3.13. Conceptual figure of the spatial relationship between juvenile fish abundance (yellow) and zooplankton prey availability (blue). Where these areas overlap (green), juvenile fish are predicted to have higher growth rates and increased survival. Under warm climate conditions, there is reduced spatial overlap between juvenile fish and prey availability, resulting in lower overwinter survival and recruitment success to age-1. In colder conditions, increased spatial overlap between juvenile fish and prey availability results in increased overwinter survival and recruitment to age-1. 158

List of Tables

	Page
Chapter 1	
Table 1.1. Cruise name, year, temperature regime, and dates of cruises. The total number of stations sampled ('bongo tows') and the number of stations used in the analysis ('common stations') by year are shown.....	36
Table 1.2. Percent of total catch (based on number per 10m ²) for species (or species complex) observed in greater than 5% of stations across the study period 2002 to 2008	37
Table 1.3. Spearman rank correlations for the 3 axes (dimensions) interpreted from the non-metric multidimensional scaling (NMDS) ordination by station. Only those species with correlations ≥ 0.4 are shown	39
Table 1.4. Model terms with corresponding significance values for each axis in the generalized additive model (GAM) analyses. Temp: temperature; Sal: salinity; Lat: latitude; Long: longitude; Year: year	40
Table 1.5. Results from the PRIMER routine SIMPER used to identify differences in relative species composition based on geographic area and period using the full station-by-species matrix. The average abundance (catch per unit effort, CPUE, number per 10 m ²) is shown for species that account for a significant amount of observed dissimilarity between periods; species' abundances in bold account for approximately 60% of dissimilarity for the given area. For each geographic area separately, a 1-way analysis of similarity (ANOSIM) was used to test for significant differences in species composition between warm and cold periods using the Bray-Curtis resemblance matrix; the ANOSIM test statistic (R) and significance (p-value) are shown	41
Chapter 2	
Table 2.1. Year, season, sampling dates, and gear used to collect age-0 and age-1 walleye pollock (<i>Theragra chalcogramma</i>). The mean (\pm standard error, <i>n</i>) energy density, % lipid, and standard length (mm) are shown for each cruise by age class.....	85

Table 2.2. Summary of generalized additive mixed model (GAMM) fits for energy density, % lipid, and standard length showing terms, coefficient estimates, standard error (SE) for fixed coefficients, degrees of freedom (d.f.; number of parameters for each term in the model, estimated for smooth terms), and *P*-values. *P*-values for parametric terms (intercept, year coefficients) based on t-test of the null hypothesis that the coefficient is equal to zero; for smooth terms (f_i) based on an approximate F-test (Wood, 2006); for random effects term (σ_a) based on likelihood ratio test. The intercept (α) corresponds to the 2008 means and the subsequent year effects (Y_k) correspond to the difference between that year's mean and the intercept; $f_1, f_2,$ and f_4 are smooth terms (SL = standard length; date = sampling date); f_3 and f_5 are smooth spatial surfaces (lat=latitude; long=longitude) by year k , and ε_{ik} is within-station residual variability. 87

Chapter 3

Table 3.1. Dominant prey taxa included in the models for 2005 and 2010. Prey items cumulatively accounting for at least 90% of the diet by % volume and individually accounting for at least 2% of the diet by % volume were included. Prey taxa common to both years are shown in **bold**. 140

Table 3.2. Parameter definitions and values used in the bioenergetics model to estimate maximum growth potential ($g \cdot g^{-1} \cdot d^{-1}$) of juvenile walleye pollock. Parameters were used as inputs to the bioenergetics model described in [14]. 141

Table 3.3. Summary of sensitivity analyses for the bioenergetics model in 2005 and 2010 showing the minimum, mean, and maximum growth potential over all stations. Base values are predicted maximum growth potential ($g \cdot g^{-1} \cdot d^{-1}$) from the base model scenarios ($W=2.5$ g, Temp=average temperature in upper 30 m, $P=1.0$, ω_k =prey energy density, $\bar{v}_{2005}=3.916$ kJ \cdot g $^{-1}$ WW; $\bar{v}_{2010}=5.292$ kJ \cdot g $^{-1}$ WW). All other values denote the change in growth rate resulting from indicated changes in inputs; therefore (-) effects indicate that varied conditions resulted in lower predicted growth and vice versa. Pooled standard deviations (SDs) for each parameter were calculated across stations after removing the annual means. W and v_t are constant values applied across all station, so changes (± 1 SD) act as a scalar and results in similar spatial patterns across the area. Temperature and ω_k vary across stations. 142

Table 3.4. Summary of sensitivity analyses for the IBM model in 2005 and 2010 showing the minimum, mean, and maximum growth potential and depth over all stations. Base values are predicted growth ($g \cdot g^{-1} \cdot d^{-1}$) and depth of juvenile walleye pollock over 24 hours from the base model scenarios ($W=2.5$ g, zooplankton prey distributed according to

vertical profiles). All other values are predicted changes in growth and depth. Negative changes in depth indicate a shallower distribution; positive values indicate a deeper distribution. Weight is a constant value applied across all station, so varying the parameter acts as a scalar and results in similar spatial patterns across the area. The effect of applying a uniform distribution of zooplankton prey with depth varies across stations.

..... 143

Table 3.A.1. Stage, sampling gear, length range, width, biomass (g, wet weight), and energy density ($\text{kJ}\cdot\text{g}^{-1}$, wet weight) values for the main prey items of juvenile walleye pollock in late summer 2005 and 2010. Biomass estimates were obtained during processing of the zooplankton samples from 2005 (warm) and 2010 (cold) (NA=stage was not collected); energy density values were obtained from zooplankton collected in the EBS during 2004 (warm) and 2010 (cold). Single estimates of energy density (shown in bold) were used when year-specific information was not available for individual taxa.

..... 159

Table 3.A.2. Component equations of the bioenergetics model used to estimate maximum growth potential ($\text{g}\cdot\text{g}^{-1}\cdot\text{d}^{-1}$) of juvenile walleye pollock..... 167

Acknowledgements

I am indebted to my graduate committee for their time, advice, collaboration, and friendship over the last five years. I very much look forward to continuing to work with them over the course of my career. Each of them has found time to meet with me, answer questions, review drafts, or talk about job opportunities among the numerous other things in their busy lives. I have often said over the last few years, and especially as I near the end of my PhD program: “I never want to graduate” because I’ve been so fortunate to work with an amazing group of scientists and people on projects I am really interested in...”if only the pay were better.”

When I was thinking about starting a PhD program, and interested in working on a project dealing with climate effects on fish populations, I found the perfect match with Nicola and the NPRB/BSIERP ichthyoplankton project. Thankfully Nicola believed in my abilities and gave me the opportunity to shape the project to my interests. She introduced me to broad-scale (i.e., weeks at sea) oceanographic survey work in a large collaborative setting, which allowed me to work closely with several NOAA programs, both in Juneau, AK and Seattle, WA.

Having committee members who work for NOAA provided a real-world perspective to everything that I did. I was able to see where my results fit in to the bigger picture. When Nicola moved to Germany in the spring of 2009, Janet became somewhat of my de-facto adviser and has since been the ‘voice of reason’ I’ve looked to for advice along the way. She has provided scientific, career, and life advice, as well as moral support, and is a great example to me of someone balancing work and family life.

Working with Ron and the Nutritional Ecology Lab gave me experience with laboratory techniques and really got me interested in the ecology of commercially important species in support of stock assessment science. But best of all, Ron always made me feel like a colleague more than a student. During our conversations, I felt like he valued my opinion and we were working together on projects.

Brenda has been the matriarch of the committee and a trusted voice throughout my time. I'm not sure whose idea it was for her to serve my committee, hers or mine, which reflects the mutual respect we've had for each other since my days as Associate Editor of *Fishery Bulletin*. Brenda has an uncanny ability to distill conversations down, getting to the pertinent details, a gift I much appreciated during long committee meetings. I look forward to many visits with Aunt Brenda in the future, rain or shine.

Finally, I cannot thank Franz enough for taking over as Committee Chair in 2009. I feel so fortunate to have been able to work with him and learn from him. The focus of my research shifted to a distinctly more quantitative approach that, surprisingly to me at first, proved to be of great interest to me. And who better to learn those skills from than Franz, who is able to teach and discuss complex statistical and modeling topics in a very accessible way. But statistics aside, Franz has been open, extremely approachable, and supportive of everything I do. He has made me feel that the work I've done is important, and encouraged me every step along the way. I have the highest respect for him, both professionally and personally, and look forward to years of collaboration and friendship to come!

I am also very grateful for the funding support I received throughout my graduate career from the North Pacific Research Board. This funding allowed me to conduct the research presented in this dissertation, travel to and present my findings at various scientific conferences, and buy a few groceries along the way. This dissertation is NPRB publication number 431 and BEST-BSIERP Bering Sea Project publication number 105.

The work presented in this dissertation is based on NOAA historical time series and samples collected in the US Exclusive Economic Zone under NOAA permits or granted by the Magnuson - Stevens Fishery Conservation and Management Act; therefore, UAF permits were not required.

Dedication

I would like to dedicate my dissertation to the Shoals Marine Lab, which holds a special place in my heart for two very important reasons: Dr. James A. Coyer and Dr. Christopher E. Siddon.

I have had the immense privilege of learning from, working with, and teaching with Jim Coyer over the last 16 years. I first met Jim as a student in his Underwater Research course at the Shoals Marine Lab the summer after my freshman year at UNH in 1997. I spent the next 10 years of my life conducting subtidal research and pursuing any opportunity that took me underwater. Since 2005, I have returned to the Shoals Marine Lab each summer to co-teach Underwater Research with Jim; I look forward to those 2 weeks for the entire year!

In 2000, Jim invited me to participate in a research mission in Aquarius, ‘the World’s only underwater habitat’. We lived and worked at 60’ below the surface off the coast of Key Largo, FL for 10 days and forever hold the title ‘Aquanaut’. I said to Jim after the mission was completed: “Thanks a lot – I’m 21 and my life is downhill from here.”

It was Jim who encouraged me to apply and pursue my Masters degree with UAF in 2002, following in his footsteps of kelp research, studying canopy-forming kelp communities in southeastern Alaska. As I left for Alaska, he said to me: “Alaska is a wild place, with wild people” and little did I know that 11 years later, I would still be calling this place my home.

After graduating in 2005, I was invited to participate in a research cruise to the Arctic as part of an under-ice dive team (NOAA's Office of Ocean Exploration; Hidden Ocean cruise). Although I have sworn to never go cave diving, and while under-ice diving seemed pretty similar, I knew I couldn't pass up the opportunity. I spent 4 weeks diving under the ice in the Arctic, seeing underwater landscapes few people have ever seen.

Whenever someone asks me how I got to where I am today, the answer is "Jim."

And it was at the Shoals Marine Lab where I met my husband in the summer of 2000. Chris was conducting (diving!) fieldwork for his PhD through Brown University and I was working on the island as staff. While it may very well have been 'love at first sight', it took some time for our relationship to grow. Needless to say, 13 lucky years later I am grateful to have him in my life...everyday. As this chapter of graduate school comes to a close, we very much look forward to our next adventure welcoming Baby Siddon into our lives.

General Introduction

Walleye pollock (*Theragra chalcogramma*) is a gadoid species widely distributed throughout the sub-arctic North Pacific and its marginal seas, including a Japanese Pacific stock centered in coastal areas of southern Hokkaido Island (Ciannelli et al. 2007, Kooka et al. 2007). The centers of distribution for walleye pollock are in the southeastern Bering Sea and Gulf of Alaska. The eastern Bering Sea (EBS) fishery averaged 1.31 million tons annually during 2000-2009 (Ianelli et al. 2009), supporting the largest commercial fishery in the U.S. by weight. Range expansion of walleye pollock through Bering Strait was documented in 1976 (Wolotira et al. 1977) with larval walleye pollock observed in the Chukchi Sea in 1988 (Wyllie Echeverria & McRoy 1992). Whether the observation of walleye pollock north of Bering Strait may represent seasonally migrating portions of the Bering Sea population or resident populations of successfully reproducing walleye pollock in the Chukchi Sea has not been resolved to date.

Fluctuations in the abundance of walleye pollock throughout their range have been linked to large-scale climate forces (i.e., Pacific Decadal Oscillation). One manifestation of shifts in climate conditions was demonstrated by the switch from a benthic- to a pelagic-dominated ecosystem in the EBS following the regime shift of 1976/77 (Hare & Mantua 2000). Groundfish, including walleye pollock, showed strong recruitment following the regime shift, correlated with a general warming of the system due to a positive phase of the Aleutian Low Pressure System (ALPS) (Wyllie Echeverria & Wooster 1998).

The EBS is characterized by a broad continental shelf (> 500 km) with an average depth of only about 70 m and supports a highly productive ecosystem owing to on-shelf flow of nutrient-rich waters. From spring to early fall, persistent oceanographic fronts (Hunt & Stabeno 2002) separate the shelf into three domains: the inner shelf domain (inside of the 50 m depth contour), the middle domain (between 50 and 100 m), and the outer domain (between 100 and 200 m) (Iverson et al. 1979, Coachman 1986). Alternating climate states have resulted in periods of both warm and cold conditions in recent years. The most extensive ice cover and coldest water column temperatures since the early 1970s were observed beginning in 2007 and continued through at least the winter of 2010/11 (Stabeno et al. 2012).

Predominant currents onto the EBS shelf include the Alaska Coastal Current (ACC) that transports lower salinity waters from the Gulf of Alaska through Unimak Pass, and the Aleutian North Slope Current that brings higher salinity oceanic waters to the slope (Schumacher & Stabeno 1998, Stabeno et al. 2006). Current trajectories over the shelf are generally northwestward with the Bering Slope Current flowing along the shelf break and ACC waters following either the 50 m or 100 m isobath (Stabeno et al. 2001).

The Oscillating Control Hypothesis (OCH), initially proposed by Hunt et al. (2002), was revised (Hunt et al. 2011) based in part on new findings regarding the importance of energetic status to fish survival (Heintz et al. in press). The OCH provides a theoretical framework within which to predict ecosystem responses to warm and cold regimes in the EBS. In warm regimes with early ice retreat, stratified waters maintain

production within the pelagic system (Walsh & McRoy 1986, Mueter et al. 2006), which was predicted to result in enhanced survival of species such as walleye pollock (Hunt & Stabeno 2002, Mueter et al. 2006, Moss et al. 2009). However, recent data indicate that changes in prey composition and abundance during a warm regime may be detrimental to walleye pollock survival. Specifically, larger zooplankton taxa, such as lipid-rich *Calanus* spp., were less abundant during recent warm years, which resulted in reduced growth rates and lipid reserves of age-0 walleye pollock and may have increased their predation risk and decreased their overwinter survival (Coyle et al. 2011, Stabeno et al. 2012). In contrast, higher abundances of larger, lipid-rich zooplankton taxa during cold years, combined with lower metabolic demands, allows age-0 walleye pollock to acquire greater lipid reserves by late summer, resulting in increased overwinter survival (Hunt et al. 2011).

The main prey resources for walleye pollock are similar across their distribution range, but prey composition varies based on ontogeny and shifts in available prey due to climate conditions. Early life stages of walleye pollock are gape-limited and feed mainly on copepod nauplii (Hillgruber et al. 1995, Strasburger et al. in press). With increasing size, the diversity of prey increases to include later stages of copepod species (i.e., *Calanus* spp., *Pseudocalanus* spp.), amphipods (*Themisto libellula*), and euphausiids (i.e., *Thysanoessa raschii*) (Farley¹, unpubl. data). Fall condition of walleye pollock is increasingly recognized as a predictor of overwinter success and is hypothesized to be dependent on prey availability early in the growing season to fuel larval development

¹ Farley, EV. NOAA Fisheries, Alaska Fisheries Science Center, Juneau, AK 99801

combined with lipid-rich prey available during fall to allow walleye pollock to store energy reserves for overwintering (Heintz et al. in press).

Under continued warming conditions, walleye pollock populations in sub-arctic ecosystems are hypothesized to face the combined challenges of reduced habitat and prey availability. Northward shifts in species' distributions in response to temperature increases have been observed on the Bering Sea shelf (Mueter et al. 2007, Mueter & Litzow 2008, Spencer 2008). However, available habitat and prey resources may not be able to support extensive northward shifts. Some prey populations may be able to evolve and/or shift their distributions concurrent with walleye pollock populations, but shortened day lengths (and subsequent growing seasons) combined with more persistent ice cover may restrict the northward distribution of walleye pollock, ultimately limiting their abundance under a warming scenario. The reproductive contribution of northern segments of the walleye pollock population will affect the ability of walleye pollock to respond to climate warming.

Forecasted summer sea surface temperatures in the Bering Sea are predicted to rise by 2°C by 2050 (Hollowed et al. 2009) while declines in recruitment to age-1 of walleye pollock of 32-58% are also predicted by 2050 (Mueter et al. 2011). Warm temperature conditions result in reduced prey quality and low energy density of juvenile walleye pollock in late summer (Hunt et al. 2011), lowering year class survival and recruitment success. Climate-driven changes in prey dynamics may have ecosystem-level consequences via bottom-up control of fish populations in sub-arctic marine ecosystems. Understanding mechanisms behind recruitment variability, and underlying spatial

patterns in the relationships, may inform the discussion of climate effects on predator-prey interactions and recruitment success of marine fishes.

This dissertation examines spatial and temporal dynamics in the ecology of early life stages of walleye pollock in the EBS to better evaluate potential consequences of climate change on walleye pollock and the broader ecosystem. The goal of my first chapter was to quantify how spring larval fish assemblages respond to environmental variability, in particular temperature variability, and to examine what delineates community composition in the EBS. Characterizing patterns in larval fish community composition for the waters north of the Alaska Peninsula is of particular interest because this region includes known spawning and nursery areas for a variety of ecologically and economically important groundfish species, including walleye pollock (Lanksbury et al. 2007, Bacheler et al. 2010). In addition, the influx of larvae advected through Unimak Pass from the Gulf of Alaska (e.g., northern rock sole, *Lepidopsetta polyxystra*; Lanksbury et al. 2007) may have important ecological consequences due to their potential impacts on local populations.

Despite the important role of walleye pollock in the EBS pelagic ecosystem, and the relationship between age-0 energy density in late summer and overwinter survival (Heintz et al. in press), the energy allocation patterns during age-0 remain poorly understood. The second chapter describes larval and juvenile strategies for growth and energy storage in age-0 walleye pollock. By maximizing growth and transitioning through the larval period rapidly, larvae minimize exposure to size-dependent predation during this stage. However, overwinter survival is higher in fish that are both larger and

have increased lipid reserves, indicating that energy allocation during the juvenile stage will not only favor lipid storage but also support increasing fish size (i.e., critical size and period hypothesis; Beamish & Mahnken 2001, Heintz & Vollenweider 2010). I hypothesized that the age-0 walleye pollock energy allocation strategy (i.e., favoring growth vs. storage) will differ seasonally among life stages and I tested this by contrasting body compositions of larval and juvenile fish. Specifically, the goals of this study were to (1) describe cohort-specific patterns in energy density for walleye pollock from age-0 to age-1, and (2) describe seasonal patterns in energy allocation during larval and juvenile (age-0) development leading to estimates of energy levels prior to their first winter.

Finally, the objectives of the third chapter were to (1) estimate spatial differences in maximum growth potential of juvenile walleye pollock on the EBS shelf using a bioenergetics modeling approach, (2) quantify the impact of temperature and prey quality on spatial variability in growth potential, (3) compare maximum growth potential to predicted growth from an individual-based model (IBM), and (4) compare observed and predicted (from IBM) prey preferences in order to better understand mechanistic prey selection leading to differences in modeled growth. I hypothesized that differences in prey species composition and quality lead to bottom-up control of juvenile walleye pollock growth and survival in representative warm and cold years in the EBS.

Chapter 1: Community-level response of larval fish to environmental variability in the southeastern Bering Sea²

Abstract

Oceanographic conditions in the southeastern Bering Sea are affected by large-scale climatic drivers (e.g., Pacific Decadal Oscillation, Aleutian Low Pressure System). Ecosystem changes in response to climate variability should be monitored, as the Bering Sea supports the largest commercial fishery in the USA (walleye pollock *Theragra chalcogramma*). This analysis examined shifts in larval fish community composition in the southeastern Bering Sea in response to environmental variability across both warm and cold periods. Larvae were sampled in spring (May) during 5 cruises between 2002 and 2008 using oblique 60 cm bongo tows. Non-metric multidimensional scaling (NMDS) was used to quantify variability and reduce multi-species abundance data to major modes of species composition. Generalized additive models (GAMs) characterized spatial and temporal differences in assemblage structure as a function of environmental covariates. We identified a strong cross-shelf gradient delineating slope and shelf assemblages, an influence of water masses from the Gulf of Alaska on species composition, and the importance of nearshore areas for larval fish. Species assemblages differed between warm and cold periods, and larval abundances were generally greater in warm years. High abundances of walleye pollock in warm years contributed most to differences in Unimak Pass, outer domain, and shelf areas (geographic areas in the study

² Siddon, E.C., Duffy-Anderson, J.T., Mueter, F.J. 2011. Community-level response of larval fish to environmental variability in the southeastern Bering Sea. Marine Ecology Progress Series 426: 225-239.

region defined based on bathymetry). *Sebastes* spp. contributed to differences over the slope with increased abundances in cold years. We propose that community-level patterns in larval fish composition may reflect species-specific responses to climate change and that early life stages may be primary indicators of environmental change.

1.1 Introduction

Climate variability affects marine ecosystems through direct effects on ocean temperatures; an underlying warming trend (IPCC 2007) is therefore likely to affect commercial, recreational, and subsistence fisheries. Community-level consequences of environmental variability arise because species have different temperature tolerances (physiological optima and limits) and mobility to stay within their preferred thermal range (Pörtner et al. 2001). Populations or species with higher temperature optima will have a competitive advantage in warm conditions, resulting in species turnover and changes in community composition (e.g., Chavez & Messie 2009). In addition to direct responses of fish and other organisms, temperature changes are modulated by simultaneous changes in food availability and predation pressure, which are more difficult to predict because they interact in non-linear ways (Ciannelli et al. 2004).

Most previous studies have focused on temperature effects to adult demersal fish and shellfish communities (Brander et al. 2003, Perry et al. 2005, Mueter et al. 2007, Mueter & Litzow 2008, Spencer 2008). Less work has been done to investigate changes in the pelagic community structure or early life stages of fishes (Duffy-Anderson et al. 2006, Brodeur et al. 2008, Doyle et al. 2009). The pelagic distribution of ichthyoplankton is related to the spawning locations of adult fish (Doyle et al. 2002). After spawning, larval drift is subject to advection of water masses (Lanksbury et al. 2005), which is strongly influenced by wind stress and varies interannually as a result of basin-scale climate variability. Transport pathways can lead to differential survival of larvae based on life history characteristics (Doyle et al. 2009), predator abundances (Hunt et al. 2002),

or availability of suitable juvenile habitat (Wilderbuer et al. 2002). Understanding variability in ichthyoplankton assemblage structure may indicate ecosystem-level and/or species-specific responses to climate change.

The southeastern Bering Sea has experienced both warm and cold conditions (as defined in Hunt et al. 2002, 2011) in recent years, offering an opportunity to examine changes in larval fish community compositions. Underlying this variability is a long-term warming trend of approximately 0.1°C per decade, with the most pronounced increases occurring during summer months (F. Mueter unpubl. data). Historically, sea surface temperatures (SSTs) in the Bering Sea were cool in the early 20th century followed by a relatively warm period from 1925 to the mid- to late 1940s. Temperatures in the 1950s to early 1970s were also cool, but increased after the 1976–77 regime shift (Hare & Mantua 2000). The Bering Sea has been generally warmer following this regime shift, and the highest summer temperatures since the beginning of the last century were observed between 2002 and 2005. However, the most extensive ice cover and coldest water column temperatures since the early 1970s were observed from 2006 to at least the end of 2010. While water-column temperatures have been much lower recently, average SSTs over the shelf during late summer have stayed relatively high (Mueter et al. 2009).

The goal of this work is to quantify how spring larval fish assemblages respond to environmental variability, in particular temperature variability, and to examine what delineates community composition in the southeastern Bering Sea. Characterizing patterns in larval fish community composition for the waters north of the Alaska Peninsula is of particular interest because this region includes known spawning and

nursery areas for a variety of ecologically and economically important groundfish species (Lanksbury et al. 2007, Bacheler et al. 2010). In addition, the influx of larvae advected through Unimak Pass from the Gulf of Alaska (e.g., northern rock sole *Lepidopsetta polyxystra*) (Lanksbury et al. 2007) may have important ecological consequences as these species interact with local populations.

1.2 Study Region

The southeastern Bering Sea is characterized by a broad continental shelf (>500 km wide) with an average depth of only about 70 m and supports a highly productive ecosystem owing to on-shelf flow of nutrient-rich waters. From spring to early fall, persistent oceanographic fronts (Hunt & Stabeno 2002) separate the shelf into 3 domains: the inner shelf domain (inside of the 50 m isobath), the middle domain (between 50 and 100 m isobaths), and the outer domain (between 100 and 200 m isobaths) (Iverson et al. 1979, Coachman 1986).

Predominant currents onto the southeastern Bering Sea shelf include the Alaska Coastal Current (ACC) that transports lower salinity waters from the Gulf of Alaska through Unimak Pass, and the Aleutian North Slope Current that brings higher salinity oceanic waters to the slope (Schumacher & Stabeno 1998, Stabeno et al. 2006). Current trajectories over the shelf are generally northwestward with the Bering Slope Current flowing along the shelf break and ACC waters following either the 50 or 100 m isobath (Stabeno et al. 2001).

The ACC flows counterclockwise around the Gulf of Alaska and southwestward along the Alaskan Peninsula; it branches through Unimak Pass, which represents the

major conduit of flow between the Gulf of Alaska and the Bering Sea shelf (Ladd et al. 2005). The volume of ACC water advected through Unimak Pass varies seasonally and interannually (Stabeno et al. 2002). Freshwater discharge into the Gulf of Alaska can be used as a proxy for the strength of the ACC and, presumably, flow through Unimak Pass (Weingartner et al. 2005). Average discharge in March for 2002 to 2005 was $9764 \text{ m}^3 \text{ s}^{-1}$ versus $1872 \text{ m}^3 \text{ s}^{-1}$ for 2006 to 2008 (T. Royer unpubl. data based on formulae in Royer 1982) suggesting greater flow through Unimak Pass in warm years. The direction of ACC waters entering the Bering Sea varies based on differences in forcing mechanisms (e.g. wind speed and direction) that affect water column structure and front formation. The onset and location of fronts affect water current trajectories (Kachel et al. 2002) and, therefore, transport pathways of larvae (Duffy-Anderson et al. 2006).

1.3 Materials and methods

1.3.1 Biological sampling

Data on spring larval fish assemblage structure were collected during 5 research cruises in the southeastern Bering Sea (Fig. 1.1) between 2002 and 2008 using 60 cm bongo nets fitted with either 335 μm (2008) or 505 μm (2002, 2003, 2005, 2006) mesh; previous research determined that abundances of collected larvae are comparable between the 2 mesh sizes (Shima & Bailey 1994, Boeing & Duffy-Anderson 2008, Duffy-Anderson et al. 2010). Cruises occurred in May of each year (Table 1.1). During all cruises, quantitative oblique tows were made to a maximum depth of 300 m (or to within 10 m of the substratum), allowing for vertically integrated estimates of larval fish abundance. The

ship speed was monitored and adjusted (1.5 to 2.5 knots) throughout each tow to maintain a wire angle of 45° from the ship to the bongo net. The nets were equipped with a calibrated 40 m flow meter; therefore, catch rates were standardized to catch per unit effort (CPUE; number · 10 m⁻²). Sampling occurred 24-hours a day and it was assumed that vertically integrated abundance estimates were not affected by diel vertical migrations. The geographic coverage of the sampling grid varied each year; to investigate changes in larval fish assemblage structure over time, only those stations sampled in at least two years were included in the analyses ('common stations'; Table 1.1; Fig. 1.1).

After retrieval of the bongo nets, all fish larvae were removed from the codends and a volume displacement measurement of remaining zooplankton (including small gelatinous zooplankton; large jellyfish were removed so as not to bias the displacement volume) was taken as a coarse measure of zooplankton wet weight biomass and an index of overall production at each station (Napp et al. 2002, Coyle et al. 2008, 2011). All samples were preserved at sea in 5% buffered formalin seawater solution. Fish larvae were sorted, identified to the lowest possible taxonomic level, measured (mm standard length [SL]), and enumerated at the Plankton Sorting and Identification Center in Szczecin, Poland. Identifications were verified at the Alaska Fisheries Science Center, NOAA (National Oceanic and Atmospheric Administration) in Seattle, Washington, USA.

1.3.2 Physical environment sampling

A Sea-Bird SBE 19 CTD was attached in-line between the bongo nets and the wire terminus to provide real-time estimates of temperature, conductivity, and pressure over

the towed path. An estimate of the water temperature within the study area each year was calculated by averaging the sampled water column temperature across all stations in a given year. Temperature and salinity measurements were averaged throughout the sampled water column at each station for comparison with the vertically integrated larval fish abundances to determine the characteristics of the water column when larvae were present. Larvae likely resulted from different water masses (e.g., above and below the pycnocline), but any effect of averaging was consistent across the study region (Duffy-Anderson et al. 2006). Temperature and salinity were also averaged within the top 20 m (surface layer) to visualize and identify water mass characteristics by geographic areas (see below). Water column profiles varied from well-mixed nearshore stations to more stratified offshore stations. Surface water characteristics best captured broad differences by area and provided a reasonable metric to track the less-saline (i.e., less dense) ACC water through Unimak Pass and subsequent mixing on the shelf.

Four distinct geographic areas were examined for the analyses, and stations were grouped as follows: Unimak Pass, slope (outside of 200 m isobath), outer domain (between 100 and 200 m isobaths), and shelf (within 100 m isobath). Very few stations were sampled within the inner domain (inside of 50 m) therefore these were combined with the middle domain (between 50 and 100 m) stations and comprised the shelf area. Surface (top 20 m) measurements of temperature and salinity distinguished unique water masses within each geographic area. Unimak Pass and the outer domain water masses had intermediate salinities, with Unimak Pass stations having relatively colder temperatures. Slope waters had the highest salinities and warmest temperatures while

shelf waters had lower salinities and colder water temperatures (Fig. 1.2).

1.3.3 Community analyses

To quantify variability in species composition over time and space, we used non-metric multidimensional scaling (NMDS) to reduce multi-species abundance data to their major modes of variability (PRIMER 6, v6.1.11) (Clarke & Gorley 2006). NMDS allowed us to detect patterns in the biological data first and then interpret those patterns in relation to the environmental data (Field et al. 1982) using generalized additive models (GAMs). NMDS is also more robust to violations of assumptions than other methods (e.g. detrended correspondence analysis or principle components analysis) (Minchin 1987). Stations at which no larval fish were caught ($n = 8$) and rare species, defined as those present at less than 5% of the stations across all years, were removed from the analyses. Rare species likely do not contribute to broad-scale temporal and spatial patterns (Duffy-Anderson et al. 2006), therefore our approach allowed for detection of substantial shifts in species composition between years.

Larval fish abundance data were highly right-skewed, therefore a 4th root transformation ($CPUE^{0.25}$) was used to reduce the influence of samples with very high abundances. Transformed data were standardized to species maxima (i.e. each value was divided by the maximum $CPUE^{0.25}$ value for the corresponding species) to give equal weight to all species, regardless of their average numerical abundance (Field et al. 1982). Bray-Curtis similarity matrices were then computed to examine differences in assemblage structure among (1) individual stations and (2) by geographic area based on larval fish composition, followed by ordinations using NMDS to visualize similarities in

species composition among stations or areas. The NMDS algorithm attempts to arrange samples (either stations or areas) such that pairwise distances in the ordination plot match Bray-Curtis similarities as closely as possible; thus, samples closer together in the ordination plot have a more similar species composition than samples farther apart. The final configuration of stations (areas) was determined by minimizing Kruskal's stress statistic (Kruskal 1964), and the number of dimensions for the final ordinations was chosen as the smallest number of dimensions that achieved a stress of no more than 0.2. A stress of 0.1 or lower is considered a good fit (Kruskal 1964) and we defined a stress of less than 0.2 as acceptable.

1.3.4 NMDS by station

The final station-by-species matrix included 318 stations (Table 1.1) and 31 prevalent species (or species complexes) (see Table 1.2). The ordination axes in the NMDS plot, consisting of dimensionless values or scores for each station, were used as the response variable for modeling differences in assemblage structure in space and as a function of environmental covariates using GAMs. Spearman rank correlations were used to identify those species whose abundances were most strongly correlated (positively or negatively) with the axis scores and which therefore contributed most to the observed patterns of species composition. Only species for which the absolute correlation with a given ordination axis was equal to or larger than 0.4 were further examined.

A GAM approach was used for modeling species composition to avoid pre-specifying a functional relationship between the response and predictor variables. GAMs quantify the relationship between a set of predictors and the response through non-

parametric smooth functions of the predictor variables (e.g. a smooth spatial surface can be fit as a function of latitude and longitude). The optimum amount of smoothing was chosen through a cross-validation approach as implemented in the R package ‘mgcv’ (Wood 2006). Appropriate (biologically meaningful) covariates (year, temperature, salinity, zooplankton displacement volume, latitude, and longitude) were selected to explain variability in larval fish assemblage structure. Station depth (bathymetry) is strongly confounded with the spatial term (latitude and longitude), and the estimated spatial surface captures any effects of location whether related to bathymetry, distance from shore, or other variables. Therefore, we did not include station depth as a covariate in the model.

The full model included a categorical year term to allow for differences in the average response between years (subscript t denotes different years), a smooth function (f) of temperature and salinity to allow for possible interactions, a smooth function of zooplankton displacement volume, and a smooth spatial surface (interaction term for latitude and longitude):

$$\text{Axis 1} = \text{Year}_t + f_1(\text{temperature, salinity}) + f_2(\text{zooplankton displacement volume}) + f_3(\text{latitude, longitude}) + \varepsilon \quad (\text{Eq. 1})$$

Alternative models were considered that included separate smooth terms for temperature and salinity or eliminated one or more variables from the model (e.g., no zooplankton displacement volume term). Based on Akaike’s Information Criterion (AIC) (Akaike 1973, Burnham & Anderson 2002) and the amount of variability explained by

each model (adjusted R^2 values), a best fit model was selected for characterizing the estimated effects of environmental variability on species composition for each axis.

1.3.5 NMDS by geographic area

We compared species composition by geographic area by averaging the CPUE for each species across all stations within a given area, which resulted in an area-by-species matrix that included 20 year-area combinations ($n = 5$ years; $n = 4$ areas) and 31 species. The PRIMER routine MVDISP, which measured the relative dispersion of yearly values within each area, was used to compare the variability in species composition by area across the study period. To examine differences in species composition between the warm period (years 2002, 2003, and 2005) and cold period (years 2006 and 2008), a 1-way analysis of similarity (ANOSIM) tested for pairwise differences between each area-period combination. Separate ANOSIM tests were performed for each area to further test whether species compositions were significantly different between warm and cold periods. A SIMPER (similarity percentages) analysis was then performed using the full station-by-species matrix to determine the contribution of individual species responsible for the dissimilarity between areas and periods.

1.4 Results

1.4.1 Biological sampling

A total of 31 species or species complexes (e.g. *Sebastes* spp.) representing 14 different families were collected during 5 cruises over the 7 yr sampling period and were included in the community analyses. Walleye pollock *Theragra chalcogramma* was numerically the most abundant species in the assemblage (66% of total catch), followed by Pacific

sand lance *Ammodytes hexapterus*, rockfishes *Sebastes* spp., northern rock sole, and Pacific cod *Gadus macrocephalus* (Table 1.2). Individual species abundances varied interannually; for example, walleye pollock comprised a maximum of 85% of the total catch in 2002 to a minimum of 29% in 2006 (Fig. 1.3). Fish larvae were generally more abundant in the warm years than in the cold years, especially flathead sole *Hippoglossoides elassodon*, northern rock sole, and Pacific sand lance. Rare species, though not included in the analyses, were sampled in either warm years (e.g. high cockscomb *Anoplarchus purpurescens* and Greenland halibut *Reinhardtius hippoglossoides*) or cold years (e.g. Arctic cod *Boreogadus saida*).

1.4.2 Physical environment sampling

The average water column temperature varied considerably between the warmer years of 2002, 2003, and 2005 (3.86, 4.75, and 4.16°C, respectively) and the colder years of 2006 and 2008 (3.39 and 2.0°C, respectively). This provided an environmental continuum against which to investigate changes in larval fish species composition. Water mass characteristics were unique at slope, outer domain, and shelf stations in cold years (Fig. 1.2D), but the outer domain and shelf waters were not as clearly separated in warm years (Fig. 1.2C). Unimak Pass stations generally displayed similar characteristics to outer domain waters; however, in 2002 and 2005, stations on the east side of Unimak Pass displayed characteristics of shelf waters, whereas stations on the west side of Unimak Pass were more similar to slope waters based on differences in salinity, indicating flow in both directions through Unimak Pass.

1.4.3 Community analyses

1.4.3.1 NMDS by station

The ordination of individual stations (Fig. 1.4) condensed information on the abundance of each species and afforded both community-level and species-specific gradients to be described across the study area. GAMs illustrated 3 patterns in species composition that captured important habitat attributes for larval fish distributions as described below.

Spearman rank correlations with the NMDS axis scores showed which individual species contributed most to the observed gradients. The first axis captured the greatest amount of variability in species composition, which was corroborated by strong species' correlations, both positive and negative. Several species were strongly positively correlated with the second and third axes; however, no species were strongly negatively correlated with these axes (Table 1.3).

1.4.3.2 Generalized Additive Models

1.4.3.2.1 Axis 1

The first axis described a gradient between a slope assemblage (species positively correlated with Axis 1) and a shelf assemblage (negatively correlated with Axis 1) that was resilient to interannual differences in species abundances (Fig. 1.5A). The slope assemblage was characterized by *Sebastes* spp. and *Atheresthes* spp., as well as deeper-water species such as Pacific blacksmelt (*Bathylagus pacificus*). In contrast, the shelf assemblage was characterized by Alaska plaice (*Pleuronectes quadrituberculatus*), Pacific sand lance, walleye pollock, and northern rock sole (Table 1.3).

The best model for Axis 1 scores was described as:

$$\text{Axis 1} \sim \text{Year}_t + f(\text{Temperature, Salinity}) + f(\text{Latitude, Longitude}) \quad (\text{Eq. 2})$$

and included a significant categorical year term denoting a difference in the average value of the response among years, a significant smooth term of temperature and salinity, and a smooth spatial term (latitude and longitude) (Table 1.4). Although temperature and salinity were confounded with the spatial term, the latter largely captured residual variability not explained by either temperature or salinity. Zooplankton displacement volume was not significant in the full model described by Eq. (1) and was dropped from the best model. The model explained a significant proportion of the variability in species composition along the first axis (adjusted $R^2 = 0.865$; $n = 318$).

Both temperature and salinity had a strong influence on species composition (Fig. 1.5B). The slope assemblage (positive correlations) was more common at higher temperatures and at higher salinities, while the shelf assemblage (negative correlations) was found at lower temperatures and salinities, corroborating the cross-shelf spatial pattern described above. In addition, we found significant variability in species composition among years (Fig. 1.5C) that was not explained by local water mass characteristics or spatial patterns. Species abundances were generally higher in warm years, driven by shelf species such as Pacific sand lance, flathead sole, and northern rock sole

1.4.3.2.2 Axis 2

The second axis identified a plume of similar species composition originating in Unimak Pass and extending onto the shelf. Fig. 1.6A shows the average spatial pattern across all years, though the spatial extent of the plume varied between years. Species strongly correlated with this plume of water included flathead sole, Pacific cod, and northern rock sole (Table 1.3).

The best model for Axis 2 was described as:

$$\text{Axis 2} \sim f(\text{Temperature, Salinity}) + f(\text{Latitude, Longitude}) \quad (\text{Eq. 3})$$

and included a significant smooth term of temperature and salinity and a smooth spatial term (Table 1.4), however the year and zooplankton displacement volume terms were not significant. The model explained additional variability in species composition along the second axis of the NMDS ordination (adjusted $R^2 = 0.423$; $n = 318$).

The water mass associated with the plume of species originating from the Unimak Pass region had warmer temperatures and lower salinities than surrounding waters (Fig. 1.6B). The ACC carries lower salinity waters from the Gulf of Alaska through Unimak Pass (Stabeno et al. 2002) and may have influenced the spatial distribution (i.e. plume) of species assemblages. After accounting for the effects of temperature and salinity, as well as the spatial pattern, there was no significant effect of year in Axis 2 scores, suggesting that interannual variability in species compositions was fully accounted for by interannual differences in water mass characteristics.

1.4.3.2.3 Axis 3

The third axis delineated species that were associated with nearshore habitats in waters north of the Alaska Peninsula (Fig. 1.7A). Species strongly positively correlated with Axis 3 included Pacific cod, Pacific sand lance, and sturgeon poacher *Podothecus acipenserinus* (Table 1.3).

The best model for Axis 3 was described as:

$$\text{Axis 3} \sim f(\text{Temperature, Salinity}) + f(\text{Latitude, Longitude}) \quad (\text{Eq. 4})$$

and included a significant smooth term of temperature and salinity and a smooth spatial term (latitude and longitude) (Table 1.4), whereas the year and zooplankton displacement volume terms were not significant. The model explained additional variability in species composition along the third axis (adjusted $R^2 = 0.458$; $n = 318$).

Temperature and salinity helped to distinguish the spatial pattern. Nearshore waters had warmer temperatures and lower salinities, whereas offshore waters had cooler temperatures and higher salinities (Fig. 1.7B). The nearshore species assemblage may reflect spawning habitat preferences of the adult stages.

1.4.3.3 NMDS by geographic area

The ordination by area (Fig. 1.8) allowed detection of changes in species composition across broader geographic areas by year. The ordination showed a clear gradient in species assemblages from the slope to the shelf. Unimak Pass assemblages were more similar to outer domain assemblages in warm years, but less so in cold years. Species compositions were more variable between warm and cold periods for Unimak Pass, the outer domain, and shelf areas. In contrast, the slope assemblage was less variable across the study period based on average rank dissimilarity (MVDISP; Unimak Pass = 1.44; slope = 0.63; outer domain = 0.8; shelf = 1.13). Pairwise comparisons showed the highest dissimilarity among years for Unimak Pass and the lowest dissimilarity slope stations (Index of Multivariate Dispersion [IMD] = -0.76, where -1 would indicate maximum difference).

All unique area-by-period combinations showed significant differences in species assemblages (ANOSIM; $p < 0.05$), except slope assemblages between warm and cold

periods ($p = 0.08$) and between Unimak Pass and outer domain assemblages in warm ($p = 0.19$) and cold ($p = 0.1$) periods. Within each area, species compositions were significantly different between warm and cold periods ($p < 0.05$ for all), though the difference on the slope was only weakly significant ($p = 0.041$). SIMPER then identified which individual species contributed most to assemblage differences between the warm and cold periods for each area. The average abundance of *Sebastes* spp. contributed most to differences in the slope assemblage, with more *Sebastes* spp. in cold years. The abundance of walleye pollock contributed most to assemblage differences in Unimak Pass, outer domain, and shelf areas with greater abundances of walleye pollock during the warm period (Table 1.5).

1.5 Discussion

Larval fish community composition in the southeastern Bering Sea was delineated by strong spatial patterns related to differences in water column temperature and/or salinity. Interannual differences in assemblage composition were attributed to species-specific responses to warm or cold conditions. Larval abundances were generally higher in warm years with high abundances of walleye pollock contributing most to differences in Unimak Pass, outer domain, and shelf areas between warm and cold periods. Assemblages over the slope were less variable between years and may be somewhat insulated from interannual variability. The slope assemblage was consistently dominated by *Sebastes* spp. with increased abundances in cold years. Therefore, community-level patterns in larval fish composition may reflect species-specific responses to envi-

ronmental variability.

Cross-shelf assemblage structure was primarily associated with a geographic and/or salinity gradient that distinguished slope and shelf communities. Salinities are higher over the slope due to the oceanic influence of the Aleutian North Slope Current and lower on the shelf due to increased freshwater from the mainland and from the ACC flowing through Unimak Pass. The advection of slope waters onto the shelf can be seen in the spatial pattern of predicted species composition according to Axis 1 (Fig. 1.5A). A finger of slope-derived species extended onto the shelf indicating larval transport through Bering Canyon. The cross-shelf gradient, largely driven by differences in spawning habitat for slope and shelf species, appears resilient to environmental variability between warm and cold years.

The observation of unique slope and shelf assemblages corroborates previous patterns (Doyle et al. 2002) and provides information on spawning habitats of adult fish. Although larval *Sebastes* spp. (slope assemblage) cannot easily be identified to species, many adult distributions follow the shelf break and slope habitats in the southeastern Bering Sea (e.g. Pacific ocean perch *Sebastes alutus*; Brodeur 2001). Juvenile *Atheresthes* spp., comprising arrowtooth flounder *A. stomias* and Kamchatka flounder *A. evermanni*, are widely distributed on the continental shelf and begin recruiting to the slope habitat after about age-4 (Wilderbuer et al. 2009). In recent years, their abundance has increased, leading to a greater trophic impact; adult arrowtooth flounder are known to be voracious predators on juvenile walleye pollock (Livingston & Jurado-Molina 2000, Knoth & Foy 2008, Ianelli et al. 2009). Larval pollock, however, were predominant in the

shelf assemblage in our study, indicating spatial separation from adult arrowtooth flounder and from larval aggregations of *Atheresthes* spp. over the slope. Alaska plaice spawn along the north side of the Alaska Peninsula in April and May, and eggs and larvae drift north and northeast over the shelf (Duffy-Anderson et al. 2010). While the drift trajectories vary interannually, the general current flow retains Alaska plaice within the shelf habitat.

The advection of ACC waters through Unimak Pass (Ladd et al. 2005) may affect the distribution of larval fish on the southeastern Bering Sea shelf. Water in Unimak Pass is similar to the outer domain water mass, especially in cold years, indicating directional flow of ACC water onto the outer Bering Sea shelf. Warm years with greater inflow of ACC water (T. Royer unpubl. data) may result in increased mixing and subsequent blending of water mass characteristics over the shelf (Fig. 1.2C). In cold years, inflow of ACC water is reduced, resulting in a clearer distinction of water masses (Fig. 1.2D).

Species entrained in, or advected by, ACC waters within Unimak Pass and the Bering Sea shelf included Pacific cod and northern rock sole, with higher overall abundances of these species in warm years. The trawling grounds around Unimak Pass are some of the most productive fishing areas for Pacific cod in the Bering Sea (Connors & Munro 2008), and just northeast of Unimak Pass is a major spawning area (Shimada & Kimura 1994). Pacific cod larvae caught in and near Unimak Pass in this study may reflect these well-known spawning areas and/or reflect the contribution of Pacific cod spawned in the Gulf of Alaska to Bering Sea populations. Previous research on northern rock sole has identified spawning areas west of Unimak Pass along the Aleutian Islands

and in the Gulf of Alaska with advection through Unimak Pass. Transport pathways follow the middle and outer shelf or flow eastward along the Alaska Peninsula (Lanksbury et al. 2007). Differential survival of northern rock sole depends on transport to adequate nursery grounds in the coastal domain (Wilderbuer et al. 2002, Lanksbury et al. 2007). Unfortunately, our sampling design cannot resolve whether these larvae originated in the Gulf of Alaska or were entrained in ACC waters within Unimak Pass and nearby spawning grounds. The impact of Gulf of Alaska larvae on Bering Sea populations, and the degree to which the populations are connected, are important ecological (i.e. competition, predation) and fisheries management (number of sub-populations) questions. To address the connectedness of these populations, future work tracking larvae from different spawning grounds using genetic markers, otolith microchemistry, or differential growth rates could improve the resolution of Gulf of Alaska larval contributions to Bering Sea populations.

The importance of nearshore habitats to Pacific cod, *Bathymaster* spp., and Pacific sand lance could reflect preferred spawning grounds of adult fish (e.g. Pacific cod; Shimada & Kimura 1994). The onshore-offshore gradient in species composition was more difficult to interpret because correlations with individual species' CPUEs were weaker than for the other axes. In addition, the third NMDS axis captured residual variability not already accounted for in the first or second axes. However, the importance of nearshore habitat and an onshore-offshore gradient in species composition are biologically reasonable; therefore, we believe our interpretation of this axis is realistic.

The 3 spatial patterns of larval fish assemblages identified from the NMDS ordination axes are not exclusive; individual species can be correlated with more than one gradient, thereby capturing different influences on larval distribution. For example, Pacific sand lance was strongly correlated with the first and third axes. The first axis described Pacific sand lance as a shelf species, while the third axis further associated larval sand lance with the nearshore environment of the shelf habitat. Pacific cod was correlated with the second and third axes. The second axis highlighted the importance of ACC waters in the distribution of larval Pacific cod while the third axis identified the nearshore environment as important, likely due to the spawning preferences of adult fish.

The analytical approach of multivariate ordination followed by GAMs as an exploratory regression technique successfully highlighted the main delineations of species compositions and modeled the response of the assemblage to environmental covariates. However, caution should be used when interpreting such results, as spurious (i.e. non-biologically relevant) outcomes are possible due to the flexible nature of GAMs. We are confident in our interpretations of the model results based on current knowledge of the Bering Sea ecosystem and believe our approach captured underlying mechanisms that determine larval fish species compositions in the southeastern Bering Sea.

While the timing of surveys used for this study was consistent across years, differential temperature effects on early life history events (e.g. spawning) could affect our interpretations. If colder temperatures result in delayed adult spawning activities or reduced rates of ichthyoplankton development, the fixed timing of our surveys could have been mismatched to the variable timing of larval production. Further, the timing of

front formation in the region can also affect the distribution of larvae. For example, the Bering Sea Inner Front is a seasonally established hydrographic front that sets up in the vicinity of the 40 m isobath in spring and persists through late autumn (Schumacher & Stabeno 1998, Kachel et al. 2002). We hypothesize that if cold conditions persist over the shelf into late spring, the timing of the set up of the Inner Front would be delayed, resulting in continued retention of larvae in northward moving currents along the 100 and 200 m isobaths and potentially out of our east-west survey area (Lanksbury et al. 2007).

The Oscillating Control Hypothesis (Hunt et al. 2002; revised in Hunt et al. 2011) provides a theoretical framework within which to predict ecosystem responses to warm and cold regimes in the southeastern Bering Sea. In warm regimes with early ice retreat, stratified waters maintain production within the pelagic system (Mueter et al. 2006), resulting in enhanced survival of species such as walleye pollock (Hunt & Stabeno 2002, Mueter et al. 2006, Moss et al. 2009). This is supported by the observation in the current study of high larval walleye pollock abundances in the warm years of 2002, 2003, and 2005. However, recent data show that in warm regimes, larger zooplankton taxa (e.g. large calanoid copepods and euphausiids) are less abundant, thus reducing growth rates and lipid reserves of young-of-year walleye pollock and thereby increasing predation risk and decreasing overwinter survival (Hunt et al. 2011). Therefore, a discontinuity exists between early spring conditions (i.e. water column temperature and prey availability), larval abundance, and the abundance of age-1 walleye pollock observed following the first winter. Although higher abundances of larval walleye pollock may not be indicative of eventual year-class strength, community-level analyses may provide information on

ecological interactions affecting specific populations.

Our study was the first to look at changes in larval fish community composition within the southeastern Bering Sea over a time period that included both warm and cold periods. Significant differences in assemblage structure were detected, supporting the hypothesis that early life stages may be primary indicators of environmental change. The biological shifts between warm and cold regimes are difficult to predict due to direct and indirect species responses; a better understanding of non-linear environmental effects will increase predictive and management capabilities. The eastern Bering Sea walleye pollock fishery averaged 1.31 million tons annually between 2000 and 2009 (Ianelli et al. 2009), representing the largest commercial fishery in the USA by weight. Therefore, it is important to understand the mechanisms underlying interannual variability in this stock.

1.6 Acknowledgements

We thank the officers and crew of NOAA's RVs 'Miller Freeman' and 'Oscar Dyson'. Funding was provided through NOAA's NPCREP and EcoFOCI programs, as well as the North Pacific Research Board (NPRB) Bering Sea Integrated Ecosystem Research Program (BSIERP). We thank 3 anonymous reviewers for providing helpful comments that improved the manuscript. This research is contribution EcoFOCI-0759 to NOAA's Fisheries-Oceanography Coordinated Investigations, NPRB 285, and BEST-BSIERP 17.

1.7 References

- Akaike H (1973) Information theory as an extension of the maximum likelihood principle. In BN Petrov and F Csaki (eds) Second International Symposium on Information Theory. Akademiai Kiado, Budapest, p. 267-281
- Bacheler NM, Ciannelli L, Bailey KM, Duffy-Anderson JT (2010) Spatial and temporal patterns of walleye pollock (*Theragra chalcogramma*) spawning in the eastern Bering Sea inferred from egg and larval distributions. *Fish Oceanogr* 19(2): 107-120
- Boeing WJ, Duffy-Anderson JT (2008) Ichthyoplankton dynamics and biodiversity in the Gulf of Alaska: Responses to environmental change. *Ecol Indicators* 8: 292-302
- Brander KM, Blom G, Borges MF, Erzini K, Henderson G, MacKenzie BR, Mendes H, Santos AMP, Toresen P (2003) Changes in fish distribution in the eastern North Atlantic: are we seeing a coherent response to changing temperature? *ICES Mar Sci Symp* 219: 260-273
- Brodeur RD (2001) Habitat-specific distribution of Pacific ocean perch (*Sebastes alutus*) in Pribilof Canyon, Bering Sea. *Cont Shelf Res* 21: 227-224
- Brodeur RD, Peterson WT, Auth TD, Soulen HL, Parnel MM, Emerson AA (2008) Abundance and diversity of coastal fish larvae as indicators of recent changes in ocean and climate conditions in the Oregon upwelling zone. *Mar Ecol Prog Ser* 366: 187-202
- Burnham KP, Anderson DR (2002) Model selection and multi-model inference: a practical information-theoretic approach, Springer-Verlag, New York, NY.
- Chavez FP, Messié M (2009) A comparison of Eastern Boundary Upwelling Ecosystems. *Prog Oceanogr* 83(1-4): 80-96
- Ciannelli L, Chan K-S, Bailey KM, Stenseth NC (2004) Nonadditive effects of the environment on the survival of a large marine fish population. *Ecology* 85(12): 3418-3427
- Clarke KR, Gorley RN (2006) PRIMER v6: User manual/tutorial. PRIMER-E: Plymouth
- Coachman LK (1986) Circulation, water masses, and fluxes on the southeastern Bering Sea shelf. *Cont Shelf Res* 5(1-2): 23-108
- Connors ME, Munro P (2008) Effects of commercial fishing on local abundance of Pacific cod (*Gadus macrocephalus*) in the Bering Sea. *Fish Bull* 106: 281-292

- Coyle KO, Pinchuk AI, Eisner LB, Napp JM (2008) Zooplankton species composition, abundance and biomass on the eastern Bering Sea shelf during summer: The potential role of water-column stability and nutrients in structuring the zooplankton community. *Deep-Sea Res II* 55: 1775-1791
- Coyle KO, Eisner LB, Mueter FJ, Pinchuk AI, Janout MA, Cieciel KD, Farley EV, Andrews AG (2011) Climate change in the southeastern Bering Sea: impacts on pollock stocks and implications for the Oscillating Control Hypothesis. *Fish Oceanogr* 20: 139-156
- Doyle MJ, Mier KL, Busby MS, Brodeur RD (2002) Regional variation in springtime ichthyoplankton assemblages in the northeast Pacific Ocean. *Prog Oceanogr* 53: 247-281
- Doyle MJ, Picquelle SJ, Mier KL, Spillane MC, Bond NA (2009) Larval fish abundance and physical forcing in the Gulf of Alaska, 1981-2003. *Prog Oceanogr* 80: 163-187
- Duffy-Anderson JT, Busby MS, Mier KL, Deliyaniades CM, Stabeno PJ (2006) Spatial and temporal patterns in summer ichthyoplankton assemblages on the eastern Bering Sea shelf 1996-2000. *Fish Oceanogr* 15: 80-94
- Duffy-Anderson JT, Doyle MJ, Mier KL, Stabeno PJ, Wilderbuer TK (2010) Early life ecology of Alaska plaice (*Pleuronectes quadrituberculatus*) in the eastern Bering Sea: seasonality, distribution, and dispersal. *J Sea Res* 64: 3-14
- Field JG, Clarke KR, Warwick RM (1982) A practical strategy for analyzing multispecies distribution patterns. *Mar Ecol Prog Ser* 8: 37-52
- Hare SR, Mantua NJ (2000) Empirical evidence for North Pacific regime shifts in 1977 and 1989. *Prog Oceanogr* 47: 103-145
- Hunt GL Jr, Stabeno PJ (2002) Climate change and the control of energy flow in the southeastern Bering Sea. *Prog Oceanogr* 55: 5-22
- Hunt GL Jr, Stabeno PJ, Walters G, Sinclair E, Brodeur RD, Napp JM, Bond NA (2002) Climate change and control of the southeastern Bering Sea pelagic ecosystem. *Deep-Sea Res Part II* 49: 5821-5853
- Hunt Jr., G.L., Coyle, K.O., Eisner, L., Farley, E.V., Heintz, R., Mueter, F.J., Napp, J.M., Overland, J.E., Ressler, P.H., Salo, S., Stabeno, P.J., 2011. Climate impacts on eastern Bering Sea foodwebs: A synthesis of new data and an assessment of the Oscillating Control Hypothesis. *ICES J Mar Sci* 68(6): 1230-1243.
- Ianelli JN, Barbeaux S, Honkalehto T, Kotwicki S, Aydin K, Williamson N (2009) Assessment of the Walleye Pollock stock in the Eastern Bering Sea. In: *Stock assessment*

and fishery evaluation report for the groundfish resources of the Bering Sea/Aleutian Islands regions. North Pacific Fishery Management Council, 605 W. 4th Ave., Suite 306, Anchorage, AK, p 49-148

IPCC (Intergovernmental Panel on Climate Change) (2007) Climate Change 2007: the physical science basis. Solomon S, Qin D, Manning M, Chen Z and others (eds) Contribution of Working Group I to the Fourth Assessment Report of the Intergovernmental Panel on Climate Change. Cambridge University Press, Cambridge

Iverson RL, Coachman LK, Cooney RT, English TS, Goering JJ, Hunt GL Jr, Macauley MC, McRoy CP, Reeburgh WS, Whitledge TE (1979) Ecological significance of fronts in the southeastern Bering Sea. In RJ Livingston (ed) Ecological Processes in Coastal and Marine Systems. Plenum Press, New York, NY. p. 437-466

Kachel NB, Hunt GL Jr, Salo SA, Schumacher JD, Stabeno PJ, Whitledge TE (2002) Characteristics and variability of the inner front of the southeastern Bering Sea. Deep-Sea Res Part II 49: 5889-5909

Knoth BA, Foy RJ (2008) Temporal variability in the food habits of arrowtooth flounder (*Atheresthes stomias*) in the western Gulf of Alaska. NOAA Tech Memo NMFS-AFSC 184

Kruskal JB (1964) Multidimensional scaling by optimizing goodness of fit to a nonmetric hypothesis. Psychometrika 29: 1-27

Ladd C, Hunt GL Jr, Mordy CW, Salo SA, Stabeno PJ (2005) Marine environment of the eastern and central Aleutian Islands. Fish Oceanogr 14(Suppl. 1): 22-38

Lanksbury JA, Duffy-Anderson JT, Mier KL, Wilson MT (2005) Ichthyoplankton abundance, distribution, and assemblage structure in the Gulf of Alaska during September 2000 and 2001. Est Coast Shelf Sci 64: 775-785

Lanksbury JA, Duffy-Anderson JT, Mier KL, Busby MS, Stabeno PJ (2007) Distribution and transport patterns of northern rock sole, *Lepidopsetta polyxystra*, larvae in the southeastern Bering Sea. Prog Oceanogr 72: 39-62

Livingston PA, Jurado-Molina J (2000) A multispecies virtual populations analysis of the eastern Bering Sea. J Mar Sci 57: 294-299

Minchin PR (1987) An evaluation of the relative robustness of techniques for ecological ordination. Vegetatio 69: 89-101

- Moss JH, Farley EV, Feldman AM, Ianelli JN (2009) Spatial distribution, energetic status, and food habits of eastern Bering Sea age-0 walleye pollock. *Trans Am Fish Soc* 138: 497-505
- Mueter FJ, Litzow MA (2008) Sea ice retreat alters the biogeography of the Bering Sea continental shelf. *Ecol Appl* 18(2): 309-320
- Mueter FJ, Ladd C, Palmer MC, Norcross BL (2006) Bottom-up and top-down controls of walleye pollock (*Theragra chalcogramma*) on the Eastern Bering Sea shelf. *Prog Oceanogr* 68:152–183
- Mueter FJ, Hunt GL Jr, Litzow MA (2007) The Eastern Bering Sea shelf: a highly productive seasonally ice-covered sea. ICES CM2007/D:04, available at www.ices.dk/products/CMdocs/CM-2007/D/D0407.pdf
- Mueter FJ, Broms C, Drinkwater KF, Friedland KD, Hare JA, Hunt GL Jr, Melle W (2009) Ecosystem responses to recent oceanographic variability in high-latitude Northern Hemisphere ecosystems. *Prog Oceanogr* 81: 93-110
- Napp JM, Baier CT, Brodeur RD, Coyle KO, Shiga N, Mier K (2002) Interannual and decadal variability in zooplankton communities of the southeast Bering Sea shelf. *Deep-Sea Res II* 49: 5991-6008
- Perry AL, Low PJ, Ellis JR, Reynolds JD (2005) Climate change and distribution shifts in marine fishes. *Science* 308: 1912-1915
- Pörtner HO, Berdal B, Blust R, Brix O, Colosimo A, Wachter BD, Giuliani A, Johansen T, Fischer T, Knust R, Lannig G, Naevdal G, Nedenes A, Nyhammer G, Sartoris FJ, Serendero I, Sirabella P, Thorkildsen S, Zakhartsev M (2001) Climate induced temperature effects on growth performance, fecundity and recruitment in marine fish: developing a hypothesis for cause and effect relationships in Atlantic cod (*Gadus morhua*) and common eelpout (*Zoarces viviparus*). *Cont Shelf Res* 21: 1975-1997
- Royer TC (1982) Coastal freshwater discharge in the Northeast Pacific. *J Geophys Res* 87(C3): 2017–2021
- Schumacher JD, Stabeno PJ (1998) The continental shelf of the Bering Sea. In AR Robinson and KH Brink (eds) *The Sea: The global coastal ocean: regional studies and synthesis*. John Wiley and Sons, New York, NY. p. 789-822
- Shima M, Bailey KM (1994) Comparative analysis of ichthyoplankton sampling gear for early life stages of walleye pollock (*Theragra chalcogramma*). *Fish Oceanogr* 3(1): 50-59

- Shimada AM, Kimura DK (1994) Seasonal movements of Pacific cod, *Gadus macrocephalus*, in the eastern Bering Sea and adjacent waters based on tag-recapture data. *Fish Bull* 92: 800-816
- Spencer PD (2008) Density-independent and density-dependent factors affecting temporal changes in spatial distributions of eastern Bering Sea flatfish. *Fish Oceanogr* 17: 396-410
- Stabeno PJ, Bond NA, Kachel NB, Salo SA, Schumacher JD (2001) On the temporal variability of the physical environment over the south-eastern Bering Sea. *Fish Oceanogr* 10(1): 81-98
- Stabeno PJ, Reed RK, Napp JM (2002) Transport through Unimak Pass, Alaska. *Deep-Sea Res Part II* 49: 5919-5930
- Stabeno PJ, Hunt GL Jr, Napp JM, Schumacher JD (2006) Physical forcing of ecosystem dynamics on the Bering Sea shelf. In AR Robinson and KH Brink (eds) *The Sea: The global coastal ocean: Interdisciplinary regional studies and syntheses, Part B*. Harvard University Press, Cambridge, MA. p. 1177–1212
- Weingartner TJ, Danielson SL, Royer TC (2005) Freshwater variability and predictability in the Alaska Coastal Current. *Deep-Sea Res Part II* 52: 169-191
- Wilderbuer TK, Hollowed AB, Ingraham WJ Jr, Spencer PD, Connors ME, Bond NA, Walters GE (2002) Flatfish recruitment response to decadal climatic variability and ocean conditions in the eastern Bering Sea. *Prog Oceanogr* 55: 235-247
- Wilderbuer TK, Nichol DG, Aydin K (2009) Arrowtooth Flounder. In: Stock assessment and fishery evaluation report for the groundfish resources of the Bering Sea/Aleutian Islands regions. North Pacific Fishery Management Council, Anchorage, AK, p 677-740
- Wood SN (2006) *Generalized Additive Models: An introduction with R*. Chapman & Hall/CRC, Boca Raton, FL

Table 1.1. Cruise name, year, temperature regime, and dates of cruises. The total number of stations sampled ('bongo tows') and the number of stations used in the analysis ('common stations') by year are shown

Cruise	Year	Temperature regime	Dates	Bongo tows	Common stations
3MF02	2002	Warm	May 13- May 21	81	65
4MF03	2003	Warm	May 18- May 24	60	58
5MF05	2005	Warm	May 10- May 20	91	68
3MF06	2006	Cold	May 9- May 18	90	75
3DY08	2008	Cold	May 13- May 21	65	52
			TOTALS	387	318

Table 1.2. Percent of total catch (based on number per 10m²) for species (or species complex) observed in greater than 5% of stations across the study period 2002 to 2008

Family	Taxon	Common name	% Total catch
Gadidae	<i>Theragra chalcogramma</i>	Walleye pollock	66.44
Ammodytidae	<i>Ammodytes hexapterus</i>	Pacific sand lance	10.72
Scorpaenidae	<i>Sebastes</i> spp.	Rockfishes	8.86
Pleuronectidae	<i>Lepidopsetta polyxystra</i>	Northern rock sole	4.55
Gadidae	<i>Gadus macrocephalus</i>	Pacific cod	1.86
Pleuronectidae	<i>Hippoglossoides elassodon</i>	Flathead sole	1.53
Pleuronectidae	<i>Platichthys stellatus</i>	Starry flounder	1.32
Bathymasteridae	<i>Bathymaster</i> spp.		0.95
Gadidae	Unidentified Gadidae		0.86
Pleuronectidae	<i>Pleuronectes quadrituberculatus</i>	Alaska plaice	0.72
Pleuronectidae	<i>Atheresthes</i> spp.		0.29
Stichaeidae	<i>Poroclinus rothrocki</i>	Whitebarred prickleback	0.26
Bathylagidae	<i>Bathylagus pacificus</i>	Pacific blacksmelt	0.17
Cottidae	<i>Icelus</i> spp.		0.17
Liparidae	<i>Liparis</i> spp.		0.13
Cottidae	<i>Myoxocephalus</i> spp.		0.13
Stichaeidae	<i>Anoplarchus insignis</i>	Slender cockscomb	0.11
Cryptacanthodidae	<i>Cryptacanthodes aleutensis</i>	Dwarf wrymouth	0.10
Pleuronectidae	<i>Hippoglossus stenolepis</i>	Pacific halibut	0.10
Bathylagidae	<i>Leuroglossus schmidti</i>	Northern smoothtongue	0.10
Stichaeidae	<i>Anoplarchus</i> spp.		0.09
Pleuronectidae	<i>Lepidopsetta bilineata</i>	Southern rock sole	0.09

Table 1.2. Continued

Myctophidae	<i>Stenobranchius leucopsarus</i>	Northern lampfish	0.08
Cottidae	<i>Icelinus</i> spp.		0.07
Cottidae	<i>Hemilepidotus hemilepidotus</i>	Red Irish lord	0.05
Hexagrammidae	<i>Hexagrammos decagrammus</i>	Kelp greenling	0.05
Agonidae	<i>Bathyagonus alascanus</i>	Gray starsnout	0.04
Agonidae	<i>Bathyagonus infraspinatus</i>	Spinycheek starsnout	0.04
Agonidae	<i>Podothecus acipenserinus</i>	Sturgeon poacher	0.04
Cottidae	<i>Artedius harringtoni</i>	Scalyhead sculpin	0.03
Psychrolutidae	<i>Psychrolutes paradoxus</i>	Tadpole sculpin	0.03

Table 1.3. Spearman rank correlations for the 3 axes (dimensions) interpreted from the non-metric multidimensional scaling (NMDS) ordination by station. Only those species with correlations ≥ 0.4 are shown

Axis 1		Axis 2		Axis 3	
Species	Correlation	Species	Correlation	Species	Correlation
<i>Sebastes</i> spp.	0.82	<i>Hippoglossoides elassodon</i>	0.70	<i>Gadus macrocephalus</i>	0.48
<i>Atheresthes</i> spp.	0.66	<i>Gadus macrocephalus</i>	0.51	<i>Bathymaster</i> spp.	0.46
<i>Bathymaster</i> spp.	0.57	<i>Lepidopsetta polyxystra</i>	0.41	<i>Ammodytes hexapterus</i>	0.41
<i>Bathylagus pacificus</i>	0.55			<i>Podothecus acipenserinus</i>	0.40
<i>Leuroglossus schmidti</i>	0.53				
<i>Pleuronectes quadrituberculatus</i>	-0.58				
<i>Ammodytes hexapterus</i>	-0.57				
<i>Theragra chalcogramma</i>	-0.48				
<i>Lepidopsetta polyxystra</i>	-0.40				

Table 1.4. Model terms with corresponding significance values for each axis in the generalized additive model (GAM) analyses. Temp: temperature; Sal: salinity; Lat: latitude; Long: longitude; Year_t: year

Axis	Term	df	F-value	p-value	Adjusted R ²
1					0.865
	Year _t	4	6.952	<0.001	
	Temp x Sal	16.16	8.851	<0.001	
	Lat x Long	6.59	5.778	<0.001	
2					0.423
	Temp x Sal	11.79	8.280	<0.001	
	Lat x Long	13.92	4.531	<0.001	
3					0.458
	Temp x Sal	10.94	2.815	0.002	
	Lat x Long	17.27	8.281	<0.001	

Table 1.5. Results from the PRIMER routine SIMPER used to identify differences in relative species composition based on geographic area and period using the full station-by-species matrix. The average abundance (catch per unit effort, CPUE, number per 10 m²) is shown for species that account for a significant amount of observed dissimilarity between periods; species' abundances in **bold** account for approximately 60% of dissimilarity for the given area. For each geographic area separately, a 1-way analysis of similarity (ANOSIM) was used to test for significant differences in species composition between warm and cold periods using the Bray-Curtis resemblance matrix; the ANOSIM test statistic (R) and significance (p-value) are shown

Geographic Area	Period	<i>Theragra chalcogramma</i>	<i>Sebastes</i> spp.	<i>Ammodytes hexapterus</i>	<i>Bathymaster</i> spp.	<i>Gadus macrocephalus</i>	ANOSIM (R)	ANOSIM (p-value)
Unimak Pass	Warm	270.8	46.9	66.5	49.1	218.8	0.45	0.001
	Cold	8.1	73.1	19.6	2.1	24.5		
Slope	Warm	67.4	495.3	33.9	37.7	16.2	0.04	0.041
	Cold	48.5	717.5	1.3	41.8	4.2		
Outer domain	Warm	259.6	32.6	28.8	26.6	51.8	0.13	0.003
	Cold	87.1	62.2	9.1	0.8	14.9		
Shelf	Warm	3079.6	0.3	308.9	1.4	19.7	0.22	0.001
	Cold	463.2	0	343.7	0	5.6		

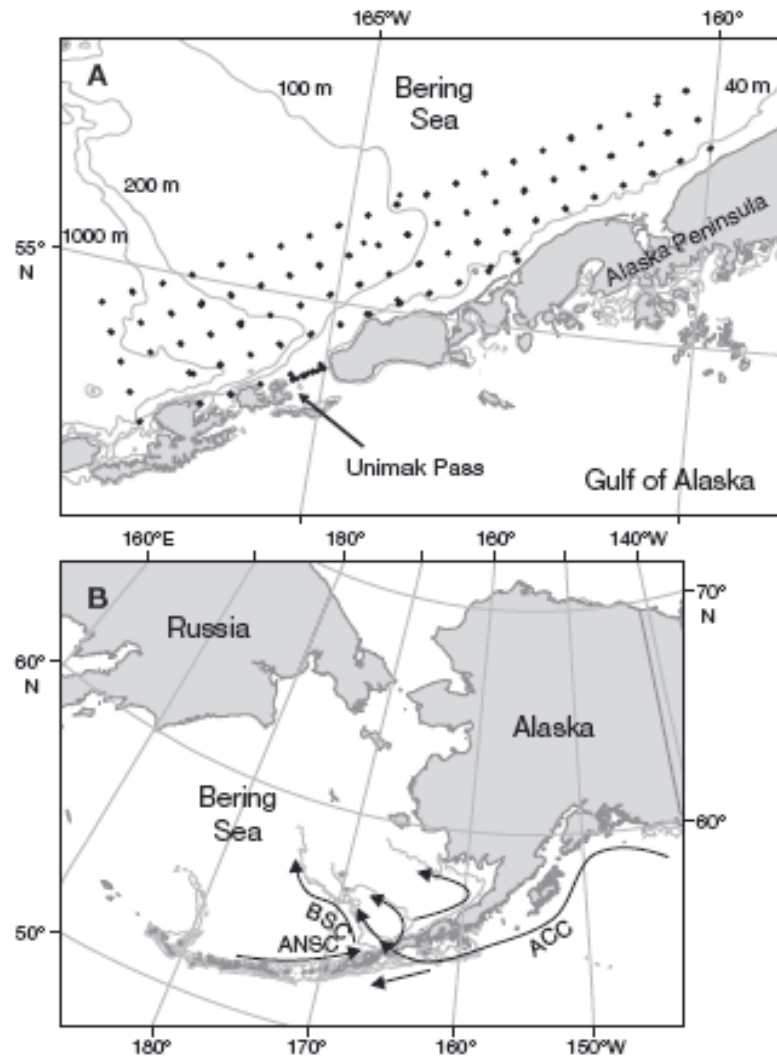


Figure 1.1. (A) Study region showing the location of sampling stations (\blacklozenge). To investigate changes in larval fish assemblage structure over time, only those stations sampled in at least two years were included in the analyses ('common stations'; Table 1.1). Depth contours are shown for the 40, 100, 200, and 1000 m isobaths. (B) Predominant currents in the study region include the Aleutian North Slope Current (ANSC), the Bering Slope Current (BSC), and the Alaska Coastal Current (ACC)

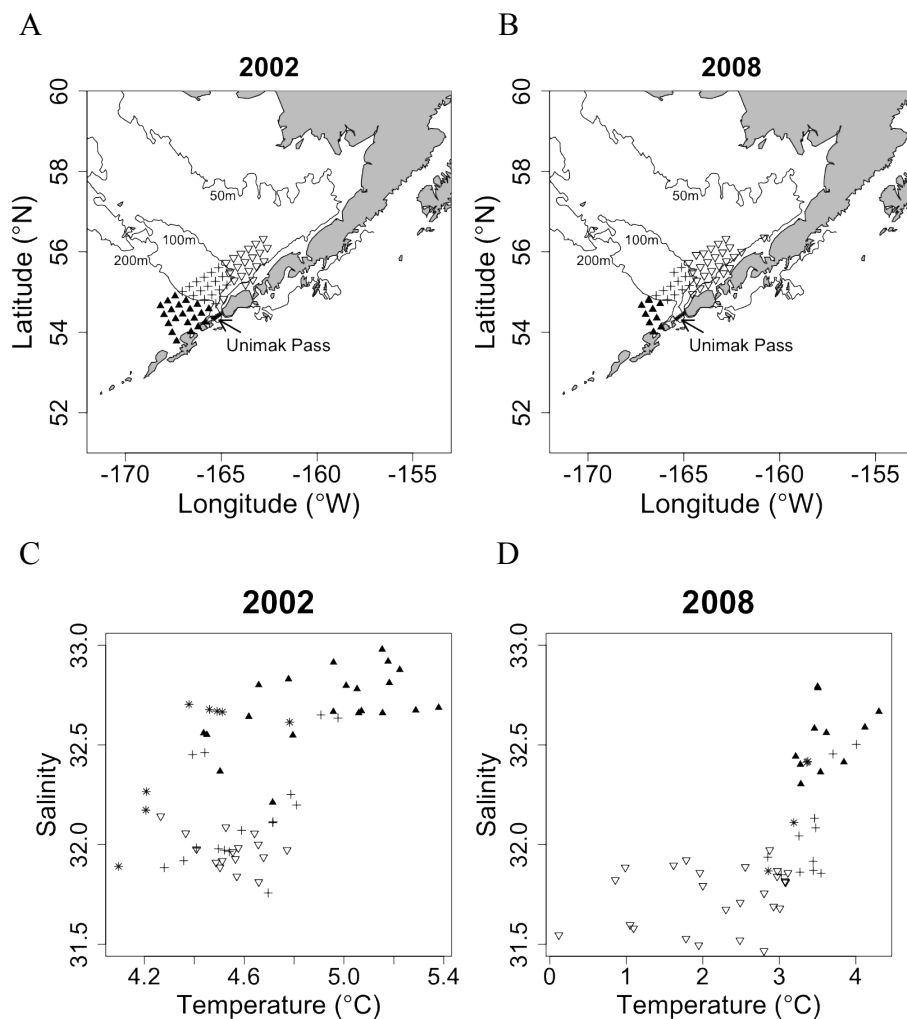


Figure 1.2. Stations sampled in (A) 2002 and (B) 2008, and corresponding temperature and salinity plots (averaged across the top 20 m) for (C) 2002 and (D) 2008. Samples were collected in 4 geographic areas based on bathymetry: Unimak Pass (*), slope (▲; outside of 200 m isobath), outer domain (+; between 100 m - 200 m isobaths), and shelf (▽; out to 100 m). 2002 was a warm year showing increased mixing of water masses from Unimak Pass to the shelf; 2008 was a cold year with greater distinction of water masses. Note the difference in the x-axis scale in C and D

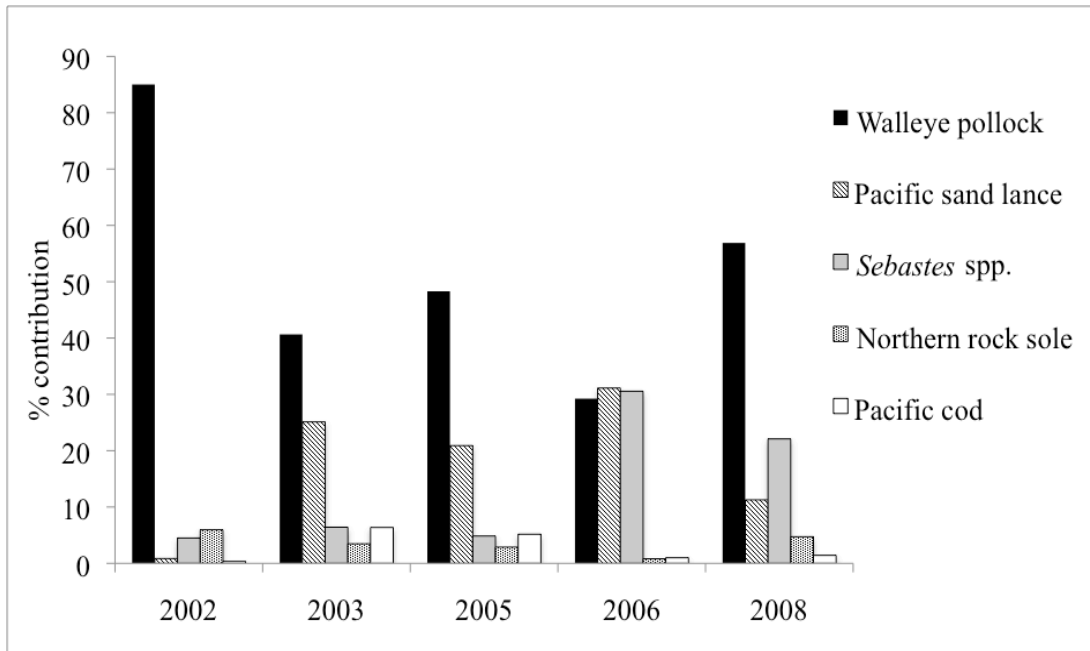


Figure 1.3. Percent contribution to total catch (based on catch per unit effort) of the 5 overall most abundant species by year. The most abundant species were walleye pollock (*Theragra chalcogramma*), Pacific sand lance (*Ammodytes hexapterus*), *Sebastes* spp., northern rock sole (*Lepidopsetta polyxystra*), and Pacific cod (*Gadus macrocephalus*)

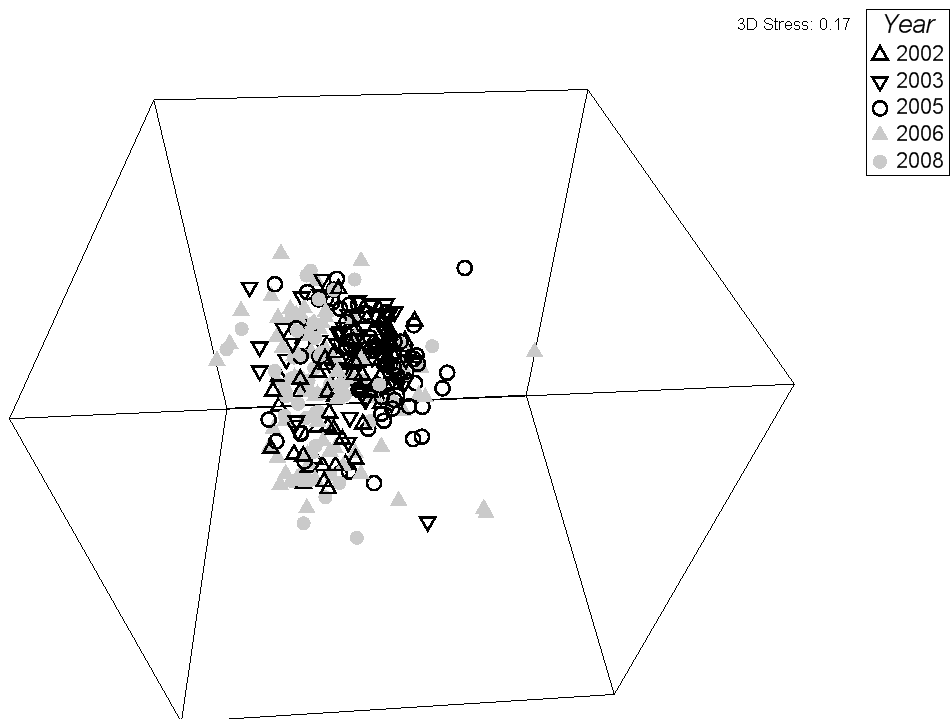


Figure 1.4. Non-metric multidimensional scaling (NMDS) ordination, based on a Bray-Curtis similarity matrix, depicting the relative similarity in species composition among individual stations sampled across 5 years. Data were 4th root transformed and standardized to species maximum

(A)

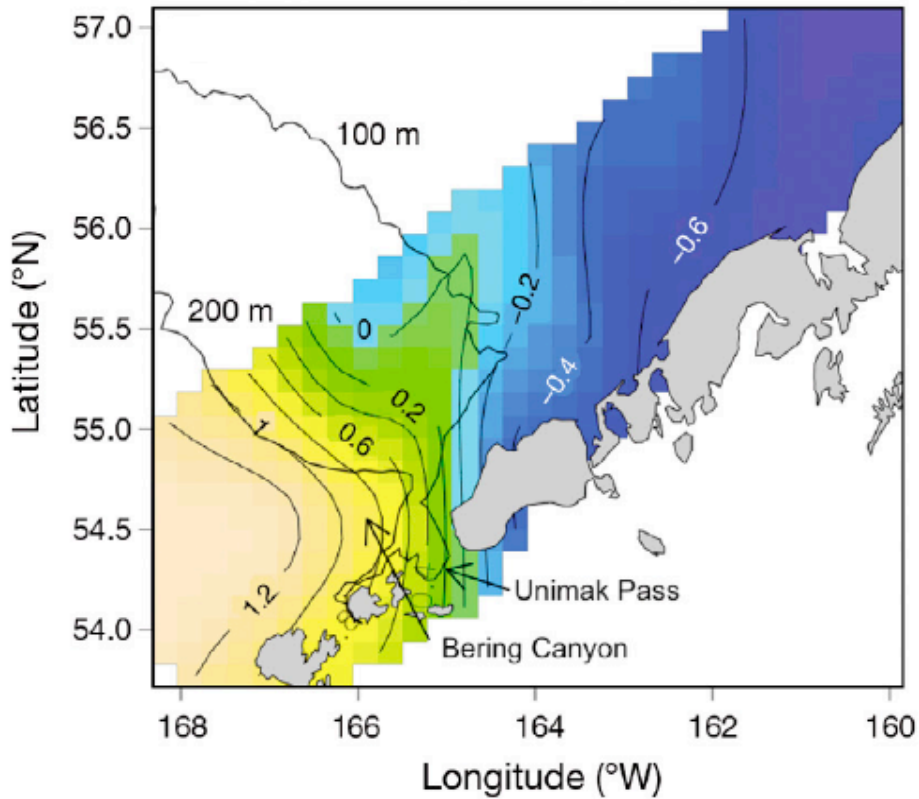


Figure 1.5. (A) Predicted spatial gradient of species composition as indicated by Axis 1 scores from non-metric multidimensional scaling (NMDS) ordination of species-by-station matrix, based on the generalized additive model (GAM) described by Eq. (2). The spatial surface was estimated as a smooth term of latitude and longitude; other covariates were fixed at their mean values. Species composition is predicted to be similar along contours; changes in species composition occur when moving across contours (color gradient). Spearman rank correlations of species positively or negatively correlated with these values were used to determine the main species of the slope versus shelf assemblage, respectively. Depth contours are shown for the 100 and 200 m isobaths

(B)

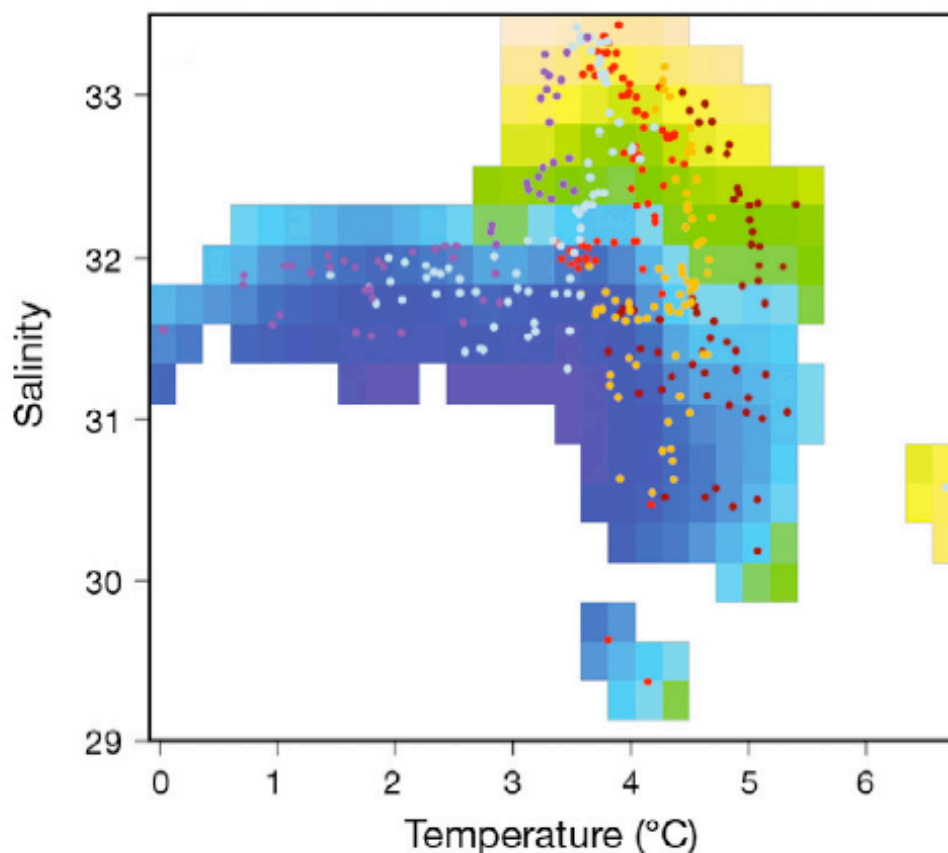


Figure 1.5. (B) Predicted measure of species composition (Axis 1 scores from NMDS ordination) as a smooth function of temperature and salinity based on the GAM described by Eq. (2). Stations with salinities less than 29 ($n = 3$) were removed for better visualization of the relative effects of temperature and salinity. Cool colors correspond to the shelf habitat and negative species correlations; warm colors correspond to the slope habitat and positive species correlations (see A). Years are distinguished as follows: 2002 = red, 2003 = brown, 2005 = orange, 2006 = light blue, 2008 = purple

(C)

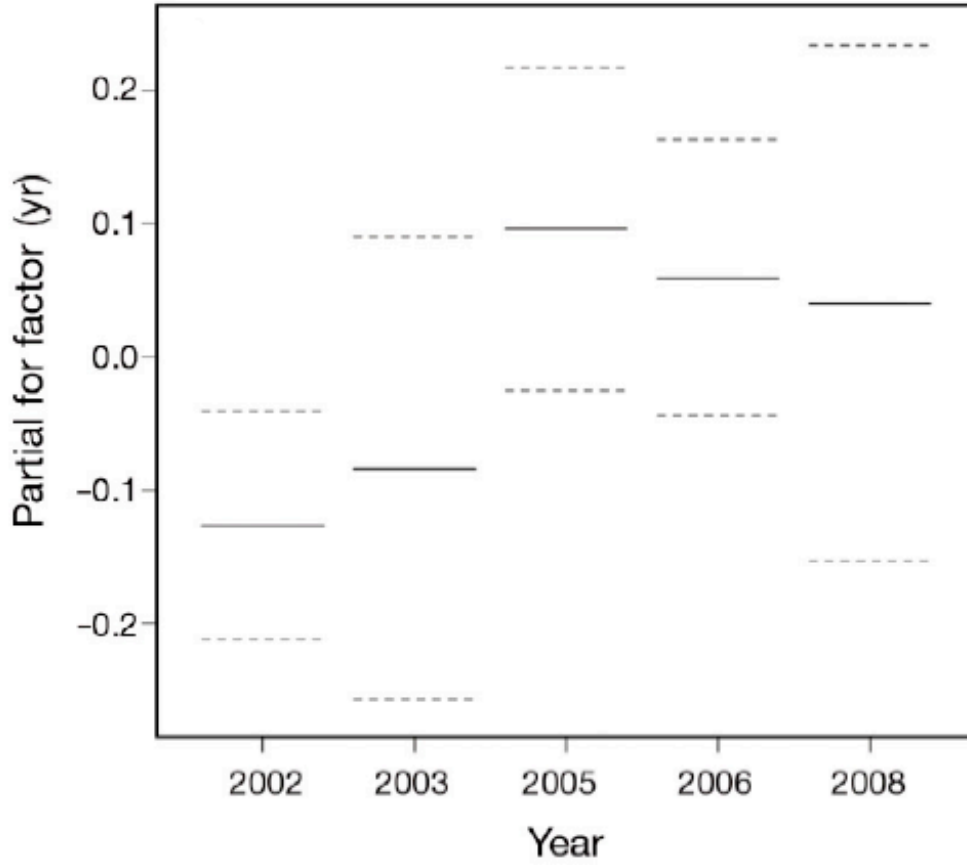


Figure 1.5. (C) Estimated differences in species composition among years (Axis 1 scores from NMDS ordination) based on the GAM described by Eq. (2). Solid lines reflect the partial response of Axis 1 scores, on a normalized scale, when all other covariates are fixed at their mean values. Dashed lines denote 95% confidence intervals

(A)

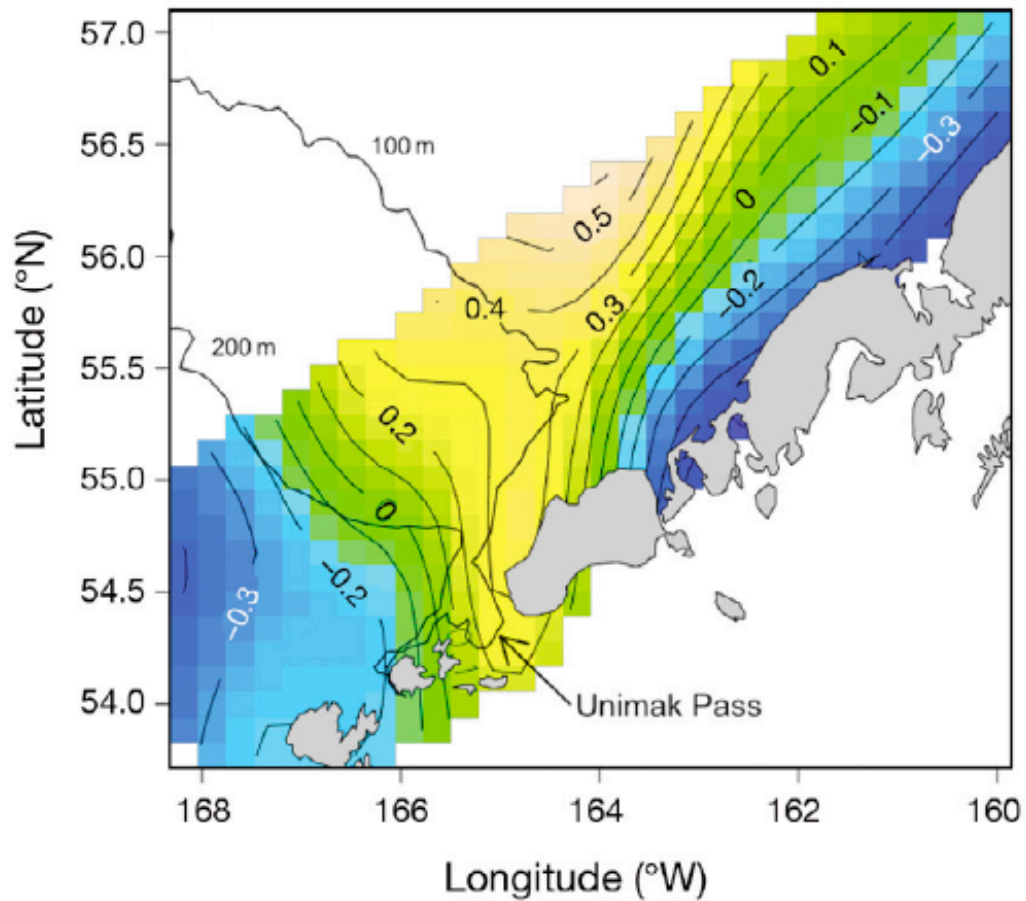


Figure 1.6. (A) Predicted spatial gradient of species composition as indicated by Axis 2 scores from non-metric multidimensional scaling (NMDS) ordination of species-by-station matrix, based on the generalized additive model (GAM) described by Eq. (3). Spearman rank correlations of species positively correlated with these values were used to determine the main species of the Alaska Coastal Current assemblage

(B)

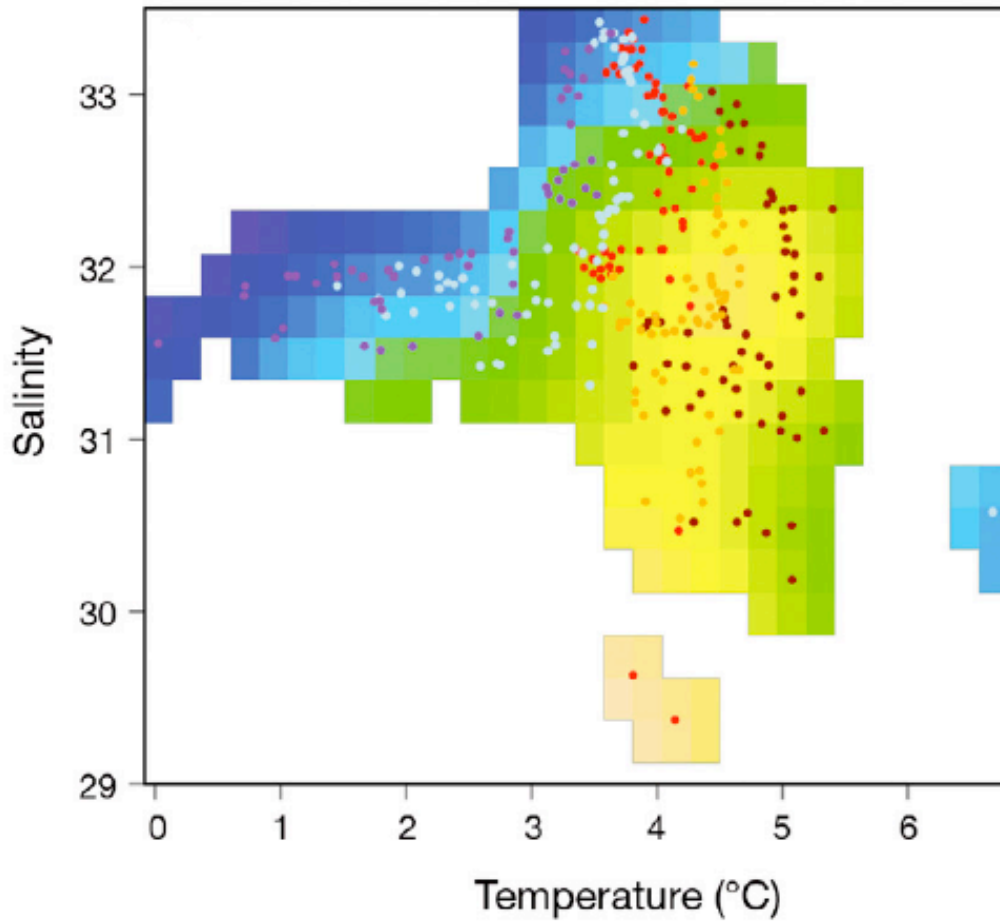


Figure 1.6. (B) Predicted measure of species composition (Axis 2 scores from NMDS ordination) as a smooth function of temperature and salinity based on the GAM described by Eq. (3). Warm colors correspond to the Alaska Coastal Current waters and positive species correlations (see A). See Fig. 1.5 for additional description

(A)

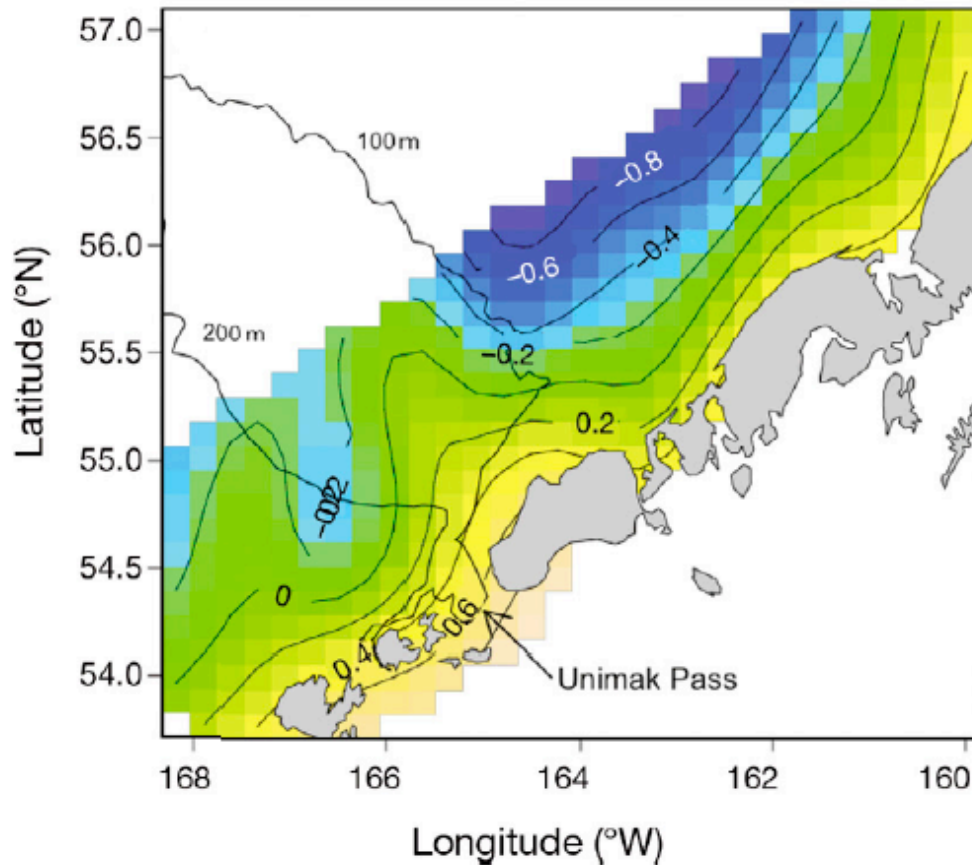


Figure 1.7. (A) Predicted spatial gradient of species composition as indicated by Axis 3 scores from non-metric multidimensional scaling (NMDS) ordination of species-by-station matrix, based on the generalized additive model (GAM) described by Eq. (4). Spearman rank correlations of species positively correlated with these values were used to determine the main species of the nearshore assemblage

(B)

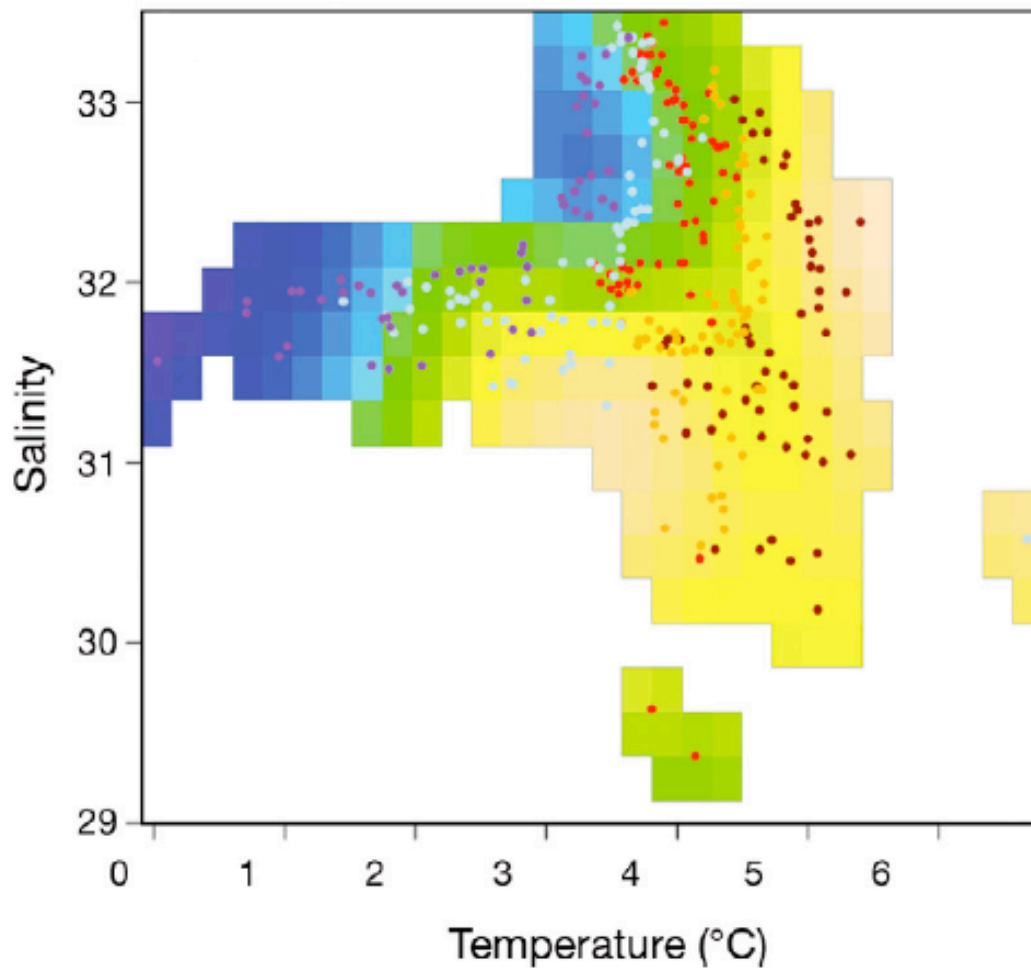


Figure 1.7. (B) Predicted measure of species composition (Axis 3 scores from NMDS ordination) as a smooth function of temperature and salinity based on the GAM described by Eq. (4). Warm colors correspond to the nearshore habitat and positive species correlations (see A). See Fig. 1.5 for additional description

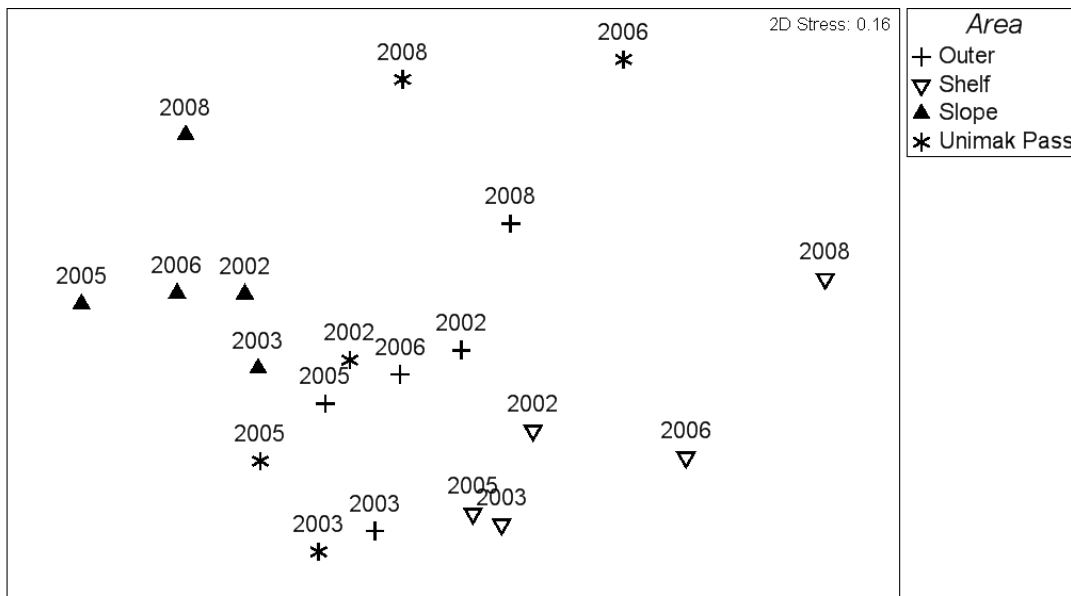


Figure 1.8. Non-metric multidimensional scaling (NMDS) ordination, based on a Bray-Curtis similarity matrix, depicting the relative similarity in species composition among geographic areas by year. Outer domain: between 100 and 200 m isobaths; Shelf: within 100 m isobath; Slope: outside of 200 m isobath; Unimak Pass (see Fig. 1.1). Data were 4th root transformed and standardized to species maximum

Chapter 2: Conceptual model of energy allocation in walleye pollock

(Theragra chalcogramma) from age-0 to age-1 in the southeastern Bering Sea³

Abstract

Walleye pollock (*Theragra chalcogramma*) support the largest commercial fishery in the United States and are an ecologically important component of the southeastern Bering Sea (SEBS) pelagic ecosystem. Alternating climate states influence the survival of walleye pollock through bottom-up control of zooplankton communities and possible top-down control of predator abundance. Quantifying the seasonal progression and spatial trends in energy content of walleye pollock provides critical information for predicting overwinter survival and recruitment to age-1 because age-0 walleye pollock rely on energy reserves to survive their first winter. Age-0 and age-1 walleye pollock were collected in the SEBS from May to September 2008-2010. Energetic status was determined through quantification of energy density (kJ/g) and proximate composition (i.e., % lipid, % moisture) with variation in energy density primarily driven by variability in % lipid. Energy densities remained relatively low during the larval phase in spring, consistent with energy allocation to somatic growth and development. Lipid acquisition rates increased rapidly after transformation to the juvenile form (25-40 mm standard length), with energy allocation to lipid storage leading to higher energy densities in late summer. This transition in energy allocation strategies is a physiological manifestation of

³ Siddon, E.C., Heintz, R.A., and Mueter, F.J. 2013. Conceptual model of energy allocation in walleye pollock (*Theragra chalcogramma*) from age-0 to age-1 in the southeastern Bering Sea. Deep-Sea Res. II. <http://dx.doi.org/10.1016/j.dsr2.2012.12.007>.

survival constraints associated with distinct ontogenetic stages; a strategy favoring growth to escape size-dependent predation appears limited to larval development while juvenile fish allocate proportionally more mass to lipid storage in late summer. We propose that the time after the end of larval development and before the onset of winter represents a short critical period for energy storage in age-0 walleye pollock, and that overwinter survival depends on accumulating sufficient stores the previous growing season and consequently may be an important determinant of recruitment success.

2.1 Introduction

Multiple factors during the early life stages of fishes result in variable recruitment success, including prey availability and environmental conditions (Cushing 1982). Variability in the spatial and temporal overlap of predator and prey (match/mismatch hypothesis; Cushing, 1969, 1990), as well as differences in prey quality (Sogard and Olla, 2000; Litzow et al., 2006), affect fish growth and energy storage, which may directly affect differences in year-class success of many marine fish species, such as walleye pollock, *Theragra chalcogramma* (Hunt et al., 2011). In addition, cold water temperatures generally delay ontogenetic development of walleye pollock (Blood 2002; Smart et al., in press) while also lowering routine metabolic demands (Ciannelli et al., 1998). Such constraints affect larval fishes' ability to achieve sufficient size and energy reserves prior to their first winter (Sogard and Olla, 2000; Heintz and Vollenweider, 2010).

In high latitude systems, winter is a period of low light, cold temperatures, and reduced prey availability, and is therefore a significant source of mortality and determinant of recruitment success of marine fishes (Hurst, 2007). Overwintering survival is likely size-dependent because most sources of mortality tend to select against the smallest individuals (Houde 1987; Bailey and Houde, 1989; Paul and Paul, 1999; Sogard and Olla, 2000). The 'critical size and period hypothesis' (Beamish and Mahnken, 2001) emphasizes the importance of increased body size in late summer and fall as indicative of winter survival (e.g., Moss et al., 2005). Lab studies have experimentally corroborated the effects of size on rates of energy depletion (Schultz et al., 1998), which

are proportionally greater in smaller individuals (e.g., Atlantic silverside, *Menidia menidia*; Schultz and Conover, 1999 and walleye pollock; Kooka et al., 2007) due to higher weight-specific metabolism. Given the shorter growing season in high latitudes, marine fishes in these systems may have adapted to grow particularly fast in response to size-selective winter mortality (Conover 1990).

Energy allocation strategies in larval and juvenile fish reflect competing physiological demands of somatic growth versus lipid storage (Post and Parkinson, 2001) and are a response to differing survival constraints. Somatic growth is important during the larval phase, as small fish are more susceptible to size-dependent predation. In contrast, lipid storage is important when fish face periods of food scarcity. By comparing the energy density and proximate composition (i.e., % lipid) of fish during early life stages, differing allocation strategies as well as the relative importance of these survival constraints can be identified. Fish with low energy density and % lipid values are allocating energy to growth and development; those with relatively high energy density and % lipid values are allocating proportionally more energy to storage.

Understanding variability of survival during the early life stages of commercially important species is pivotal to fisheries management in predicting year-class success (Megrey et al., 1996) and subsequent recruitment to the fishery. Numerous studies have established empirical links between recruitment and environmental variability (see Beamish and McFarland, 1989), but incorporating the impacts of climate variability on survival into stock assessments requires knowledge of the mechanistic responses to alternate climate states (Hollowed et al., 2009). The energetic status of age-0 walleye

pollock in late summer is increasingly recognized as a predictor of age-1 abundance during the following summer in the southeastern Bering Sea (SEBS; Heintz et al., in press).

The Oscillating Control Hypothesis (OCH), initially proposed by Hunt et al. (2002), was revised (Hunt et al., 2011) based in part on new findings regarding the importance of energetic status to fish survival (Heintz et al., in press). The OCH provides a theoretical framework within which to predict ecosystem responses to warm and cold regimes in the SEBS. In warm regimes with early ice retreat, stratified waters maintain production within the pelagic system (Walsh and McRoy, 1986), which was predicted to result in enhanced survival of species such as walleye pollock (Hunt and Stabeno, 2002; Mueter et al., 2006; Moss et al., 2009). However, recent data indicate that changes in prey composition and abundance during a warm regime may be detrimental to walleye pollock survival. Specifically, larger zooplankton taxa, such as lipid-rich *Calanus* spp., were less abundant during recent warm years, which resulted in reduced growth rates and lipid reserves of age-0 walleye pollock and may have increased their predation risk and decreased their overwinter survival (Coyle et al., 2011; Stabeno et al., 2012). In contrast, higher abundances of larger, lipid-rich zooplankton taxa during cold years, combined with lower metabolic demands, allowed age-0 walleye pollock to acquire greater lipid reserves by late summer, resulting in increased overwinter survival (Hunt et al., 2011).

Walleye pollock are major consumers of zooplankton at all life history stages (Aydin et al., 2007) with pronounced changes in prey preference throughout their early life (Kendall and Nakatani, 1992; Hillgruber et al., 1995; Ciannelli et al., 2004). Larvae

begin diel vertical migration at approximately 10 mm standard length (SL; Kendall et al., 1994; Smart et al., in press) with more pronounced vertical behavior and nocturnal feeding occurring at approximately 50 mm SL (Brodeur et al., 2000), coinciding with increased gape size and shifts to larger prey (i.e., euphausiids; Ciannelli et al., 1998). Ontogenetic changes in habitat preference (Brodeur et al., 2000) as well as visual acuity (Copp and Kovac, 1996) affect the vertical behavior of larval and juvenile fish. Walleye pollock are also an important forage species for other predators, including arrowtooth flounder, *Atheresthes stomias*, Pacific cod, *Gadus macrocephalus*, skates, flathead sole, *Hippoglossoides elassodon*, Pacific halibut, *Hippoglossus stenolepis*, seabirds, and marine mammals (Aydin and Mueter, 2007). In addition, older age classes exhibit strong cannibalism on age-0 walleye pollock (Wespestad and Quinn, 1996), especially in warmer climate regimes (Hunt et al., 2011).

Despite the important role of walleye pollock in the SEBS pelagic ecosystem, and the relationship between age-0 energy density in late-summer and overwinter survival (Heintz et al., in press), the energy allocation patterns during age-0 remain poorly understood. This paper describes larval and juvenile strategies for growth and energy storage in age-0 walleye pollock. By maximizing growth and transitioning through the larval period rapidly, larvae minimize exposure to size-dependent predation during this stage. However, overwinter survival is higher in fish that are both larger and have increased lipid reserves, indicating that energy allocation during the juvenile stage will favor lipid storage while also increasing fish size (i.e., critical size and period hypothesis; Beamish and Mahnken, 2001; Heintz and Vollenweider, 2010). We hypothesize that

energy allocation strategies (i.e., favoring growth vs. storage) will differ seasonally among life stages and we tested this by contrasting body compositions of larval and juvenile fish. The goals of this study were to: (1) describe cohort-specific patterns in energy density for walleye pollock from age-0 to age-1, and (2) describe seasonal patterns in energy allocation during larval and juvenile (age-0) development leading to estimates of energy levels prior to their first winter.

2.1.1 Study region

The SEBS is characterized by a broad (>500 km) and shallow continental shelf that supports a highly productive ecosystem owing to on-shelf flow of nutrient-rich waters (Stabeno et al., 1999; 2001). Alternating climate states have resulted in periods of both warm and cold conditions in recent years. The most extensive ice cover and coldest water column temperatures since the early 1970s were observed beginning in 2007 and continued through at least the winter of 2010/2011 (Stabeno et al., 2012).

Current trajectories over the shelf are generally northwestward with the Bering Slope Current flowing along the shelf break and Alaska Coastal Current waters following either the 50 m or 100 m isobaths (Stabeno et al., 2001). The onset and location of fronts affect current trajectories (Kachel et al., 2002) and, therefore, transport pathways of larvae (Duffy-Anderson et al., 2006). The main spawning areas for walleye pollock over the SEBS shelf include north of Unimak Island and along the Alaska Peninsula and around the Pribilof Islands (Hinckley 1987; Bacheler et al., 2010). Larvae are generally advected northward over the shelf with slope-spawned larvae advected onto the shelf via

the Bering Slope Current, as inferred from their spawning locations and summer distributions (Bacheler et al., 2010).

2.2 Materials and methods

2.2.1 Biological sampling

Age-0 and age-1 walleye pollock were collected from 13 research surveys conducted in the SEBS between May and September 2008-2010 (Table 2.1; Fig. 2.1). The geographic coverage varied across cruises. Sampling for age-0 fish is assumed to encompass the bulk of their distribution based on historical data (Bacheler et al., 2010), while age-1 fish were predominantly sampled from the outer shelf domain (between 100 and 200 m isobaths; Fig. 2.1). Gear type, mesh size, and sampling depth also varied across cruises to target the life stages occurring at the time of sampling (Table 2.1; Shima and Bailey, 1994).

Vertically integrated oblique bongo tows were made during spring cruises to a maximum depth of 300 m (or to within 10 m of the seafloor) to sample larval walleye pollock. During mid-summer, larval walleye pollock were sampled from the drogue net of the MOCNESS (Multiple Opening/Closing Net and Environmental Sensing System), which was open during deployment, thereby providing vertically integrated samples to a maximum depth of 100 m (or to within 10 m of the seafloor). Bongo and MOCNESS sampling occurred 24 hours a day, therefore it was assumed that vertically integrated sampling was not affected by diel vertical migrations of walleye pollock. The ship speed was monitored and adjusted (1.5-2.5 knots) throughout all bongo and MOCNESS tows to maintain a wire angle of 45°. Surface and midwater rope trawls were used to sample age-

0 and age-1 walleye pollock during late summer. Sampling was conducted during daytime only with the surface and midwater rope trawl sampling above and below the pycnocline, respectively, as determined by water column profiles of temperature and salinity obtained using a Sea-Bird SBE-911 CTD. Fish were predominantly observed and collected from surface waters in 2008 and from the surface and midwater in 2009; in 2010, only walleye pollock collected from surface rope trawls were used in the analyses in order to facilitate interannual comparisons across 2008-2010. In addition to the surface and midwater trawls, the beam trawl sampled near-bottom fishes during late summer as walleye pollock begin to descend in the water column. Methot trawls were used to target midwater walleye pollock from observed acoustics layers (Table 2.1). Beam and Methot trawl sampling occurred 24 hours a day. For this study, we combined walleye pollock from different vertical layers, assuming that vertical differences in energy content are negligible.

After retrieval of the gear, walleye pollock were selected from the catch to represent the size range observed in each haul. Fish were flash frozen (-80 °C) for later chemical analysis at the Alaska Fisheries Science Center, NOAA (National Oceanic and Atmospheric Administration) in Juneau, Alaska, USA. Larvae were measured to the nearest 0.01 mm length (standard, fork, or total) while juvenile and age-1 fish were measured to the nearest mm fork length (FL). All lengths were converted to SL using established conversions for walleye pollock preserved by freezing (Buchheister and Wilson, 2005). Fish were classified as age-0 (larvae <30 mm SL; juvenile >30 mm and

<100 mm SL; Matarese et al., 1989) or age-1 (>100 mm SL and <200 mm SL) based on length-frequency distributions.

2.2.2 Chemical analysis

Stomach contents of fish >8 mm SL were removed prior to chemical analysis so as not to affect estimates of energy density or % lipid.

2.2.2.1 Energy density

Energy density (ED; kJ/g dry mass) was estimated directly using bomb calorimetry or indirectly from estimates of % lipid (see 2.2.2 Proximate composition). Larvae were dried in a drying oven (60 °C) to a constant weight and all data are presented on a dry mass basis. Homogenized tissue was pressed into a pellet form and a Parr Instrument 6725 Semimicro Calorimeter with 6772 Precision Thermometer and 1109A Oxygen Bomb was used to measure the energy released from combustion of the sample pellets. The minimum pellet weight was set at 0.025 g of dry material based on the limits of instrument detection; samples were composited within stations as needed to attain sufficient dry masses for larvae collected in spring and mid-summer. Juvenile and age-1 fish were dried to a constant weight at 135 °C using a LECO Thermogravimetric Analyzer (TGA) 601 or 701 which provided % moisture values used to convert wet mass to dry mass equivalents. The dried tissue was homogenized and processed using the bomb calorimeter as described above. Moisture analysis for juvenile and age-1 fish was replicated when sufficient sample mass was available to ensure the coefficient of variation (CV) for % moisture was less than 1 standard deviation (SD). When sufficient sample mass was not available, we relied on the CV for a reference material (dried adult

walleye pollock homogenate) to obtain duplicate estimates of energy density or % moisture processed with each batch of fish ($n = 17$ for energy density; $n = 15$ for % moisture).

Quality assurance (QA) procedures for the bomb calorimeter included (1) duplicate tissue estimates (sample or walleye pollock reference material) to evaluate precision and (2) duplicate reference material (benzoic acid standard) to evaluate precision and accuracy. Predetermined limits for variation observed in QA samples were set, where precision estimates from duplicate tissue and reference samples must not vary by more than 1.5 SD or 15% CV and reference samples must not vary by more than 15% CV for accuracy. QA samples did not exceed these limits for any batch of samples used in this study.

2.2.2.2 Proximate composition

For larvae, a sulfo-phospho-vanillin (SPV) colorimetric analysis (Van Handel 1985) was performed to determine % lipid composition, which is presented on a dry mass basis. Dried material was sonicated in 2:1 (by volume) chloroform:methanol solvent in glass centrifuge tubes for 60 minutes. Washes of 0.88% KCl and 1:1 (by volume) methanol:water were performed on the extracts as in the modified Folch extraction method (Vollenweider et al., 2011). Resulting chloroform extracts were evaporated in a LabConco RapidVap for 30 minutes at 40 °C and 250 mbar until reduced to approximately 1 ml in volume. Extracts were evaporated to dryness in 12 mm test tubes on a heating block at 75 °C and then allowed to cool. Concentrated sulfuric acid was added to the tubes prior to incubation at 100 °C for 10 minutes with subsequent cooling.

The SPV reagent (1.2 mg/ml vanillin in 80% phosphoric acid) was added to each tube and allowed to develop for 10 minutes. Absorption was measured on an Agilent 8453 Spectrophotometer at 490 nm and extrapolated from species-specific calibration curves determined prior to analysis. For juvenile and age-1 fish, proximate composition analysis was performed as previously described (Vollenweider et al., 2011), with lipid extractions utilizing a Dionex ASE (accelerated solvent extractor) 200 and a modified Folch extraction procedure using a 2:1 (by volume) chloroform:methanol solvent mixture. Measurements of % lipid for juvenile and age-1 fish were converted to dry mass equivalents using estimates of % moisture obtained from the TGA (see above).

QA procedures for the SPV data included two blank runs to estimate background absorption, two method blank samples containing all analysis reagents but no lipid extract to evaluate contamination and reagent absorption, and two reference samples (adult walleye pollock homogenate) to examine precision and accuracy for each batch of 15 samples. Mean background absorbance was subtracted from sample absorbance values. Method blank samples had to be < 10 mg of lipid and walleye pollock reference samples had to vary by < 1 SD and be accurate within 15% of the established lipid value. ASE samples used similar QA criteria except that the method blank samples were allowed to be as high as 0.1 mg of lipid (due to much higher analyzed lipid masses).

To compare energy densities of walleye pollock from age-0 to age-1 for the cohort analysis, a linear regression was used to predict energy density estimates from % lipid values for age-1 fish collected during two cruises (summer 2009 Methot trawl and late-summer 2009 rope trawl surveys; Table 2.1). All age-1 fish processed for both

energy density and % lipid ($n = 83$) were used to develop a regression relationship, $ED = 20.1 + 0.76 * \% \text{ lipid}$ ($R^2 = 0.79$), that was used to predict energy density. The size of the fish used in the regression ranged from 109 to 194 mm SL. Direct estimates of energy density from the bomb calorimeter were used when available.

2.2.3 Statistical analysis

2.2.3.1 Cohort-specific patterns from age-0 to age-1

Cohort-specific patterns in energy density from age-0 to age-1 were examined to determine the extent of interannual variation in the seasonal patterns using two complete cohorts. The 2008 cohort was sampled as age-0 fish in mid- and late-summer 2008, and as age-1 fish in summer and late-summer 2009. The 2009 cohort was sampled as age-0 fish in mid- and late-summer 2009, and as age-1 fish in summer 2010. Energy densities were compared between age-0 fish in mid-summer, age-0 fish in late-summer, and age-1 fish using separate one-way ANOVAs (analysis of variance).

2.2.3.2 Seasonal patterns in energy allocation of age-0 fish

Seasonal patterns in energy allocation during age-0 larval and juvenile development were analyzed using generalized additive mixed models (GAMMs) to identify the seasonal timing and size (i.e., length) at which walleye pollock shift energy allocation strategies from growth to lipid storage. These models do not specify a fixed functional form, but rather quantify the relationship between a set of predictors and the response variable through non-parametric smooth functions of the predictor variables. The optimum amount of smoothing was chosen by generalized cross-validation as implemented in the R package 'mgcv' (Wood 2006).

Variability in energy density and % lipid during the larval and juvenile stages were modeled as a function of SL to estimate changes in energy allocation with fish size. Fish for which SL measurements were not available were removed from models ($n = 5$ and 6 for energy density and % lipid, respectively). Models for energy density, % lipid, and SL included sampling date (date) to estimate seasonal trends, a year term to account for differences in the mean response among years, and a spatial smooth term (thin-plate regression spline fit to latitude and longitude) to describe and account for differences in the mean energy density, % lipid, or SL across stations and to reduce spatial autocorrelation. Based on residual diagnostics, estimates of energy density and % lipid identified as influential outliers ($n = 5$ and 8 , respectively) were removed from further analyses; removing these outliers did not affect our conclusions. The sampling area differed among cruises as did the number of fish processed per station, therefore modeling approaches that accounted for spatial patterns and/or included a random station effect were compared using Akaike Information Criterion (AIC) (Akaike 1973; Burnham and Anderson, 2002). The full models included station as a random effect to account for variability among stations (a_i), in addition to within-station residual variability (ε_{ik}):

$$y = \alpha + f_1(\text{SL}) + f_2(\text{date}) + f_3(\text{latitude, longitude})_k + Y_k + a_i + \varepsilon_{ik}$$

$$\text{SL} = \alpha + f_4(\text{date}) + f_5(\text{latitude, longitude})_k + Y_k + a_i + \varepsilon_{ik}$$

$$a_i \sim N(0, \sigma_a^2)$$

$$\varepsilon_{ik} \sim N(0, \sigma_e^2)$$

where y is energy density or % lipid, f_1 , f_2 , and f_4 are smooth functions of the predictor variables, f_3 and f_5 are smooth spatial surfaces for a given year k (with degrees of freedom

limited to five to restrict flexibility in the fitted surface), and Y_k is the year-specific intercept for year k . The random effects a_i and residuals ε_{ik} are assumed to be independent and normally distributed with mean 0 and variances σ_a^2 and σ_e^2 , respectively.

Random effects and residuals from the models were examined for normality, homoscedasticity, and independence by plotting them against all relevant covariates and by examining spatial patterns in the random station effects by year. Each term in the full model was evaluated for significance and dropped from the model if it was not significant. Differences in spatial variability across years were evaluated by comparing the full model to a model that fit a single smooth spatial surface across years using AIC. Residual diagnostics for all resulting best models showed no unusual trends and no evidence of remaining spatial autocorrelation; diagnostic plots are not presented.

2.3 Results

2.3.1 Biological sampling

A total of 1501 age-0 and age-1 walleye pollock collected from 13 cruises over the 3-year sampling period were measured for standard length with 341 estimates of energy density (kJ/g) from bomb calorimetry ($n = 257$ age-0 including 13 composite samples, $n = 84$ age-1) and 423 estimates of % lipid ($n = 285$ age-0 including 41 composite samples, $n = 135$ age-1) (Table 2.1). The overall mean energy density (\pm SE) of age-0 and age-1 walleye pollock was 22.43 ± 0.11 and 23.67 ± 0.12 (kJ/g dry mass), respectively, and overall mean % lipid (\pm SE) for age-0 and age-1 fish was 10.58 ± 0.40 and 20.53 ± 0.49 (on dry mass basis), respectively.

2.3.2 Cohort-specific patterns from age-0 to age-1

The 2008 and 2009 cohorts had similar seasonal patterns of energy density overall. Age-0 fish from both cohorts had low mean energy densities in mid-summer with no significant difference between cohorts (1-way ANOVA: $F_{(1,9)} = 1.07$, $P = 0.33$). There was a short period from mid-July to mid-September during which energy density rapidly increased by approximately 25% in late-summer 2008 and 2009 (Table 2.1, Fig. 2.2). Energy density of age-0 fish during late-summer 2008 was significantly higher during the rope trawl survey (mean sampling date = September 27) than the beam trawl survey (mean sampling date = September 9), with late-summer 2009 having an intermediate energy density (1-way ANOVA: $F_{(2,120)} = 7.04$, $P < 0.01$). Age-1 fish of both the 2008 and 2009 cohorts had energy densities similar to those of age-0 fish the previous year in late summer. However, the 2009 cohort had significantly greater energy density at age-1 than the 2008 cohort (1-way ANOVA: $F_{(2, 85)} = 13.68$, $P < 0.001$; Fig. 2.2).

2.3.3 Seasonal patterns in energy allocation of age-0 fish

Patterns in energy density, % lipid, and SL were described using unique combinations of explanatory variables. Variability in energy density was best explained by SL, a spatial smooth term, a random station effect, and year (adjusted $R^2 = 0.688$; $n = 247$). Patterns in % lipid were best explained by SL, sampling date, a random station effect, and year (adjusted $R^2 = 0.847$; $n = 271$) while patterns in SL were best explained by sampling date, a spatial smooth term, a random station effect, and year (adjusted $R^2 = 0.955$; $n = 1365$) (Table 2.2). The effect of fish length is difficult to separate from the seasonal pattern because SL is strongly correlated with sampling date in larvae that were measured

for energy density ($r = 0.56$) and for % lipid ($r = 0.91$), although largely uncorrelated for juveniles (energy density $r = 0.086$; % lipid $r = -0.35$). Therefore, for juveniles, we can statistically separate the apparent effects of size from the seasonal pattern of fish condition.

Patterns in energy density for larval walleye pollock had large uncertainty because samples had to be composited to acquire sufficient dry mass for analytical processing. Sampling date was not significant in the full model indicating that changes in energy density are primarily driven by changes in fish length rather than seasonal changes. For a given location and year, energy density was below average at small sizes, increased to above-average energy densities at around 55 mm, and reached an asymptote at approximately 75 mm SL (Fig. 2.3a). The spatial patterns in energy density varied significantly among years, although the relative effect of sampling location was small compared to the importance of SL in explaining patterns of variability (e.g., small range of predicted values in Fig. 2.3b). Average energy density was highest in 2008, lowest in 2009, and intermediate in 2010 (Fig. 2.3c).

Percent lipid in larvae seems to decrease with increasing length up to 20 mm SL; patterns are uncertain for fish 20-40 mm SL due to lack of samples. In fish >40 mm SL, % lipid increases linearly with increasing size (Fig. 2.4a). Lipid content increased linearly over time, although variability in these estimates was high (Fig. 2.4b). The magnitude of the effect of SL on lipid content was comparable to that of the seasonal effect, as indicated by the range in % lipid anomalies between Figures 4a and 4b. The average % lipid of age-0 walleye pollock differed significantly from 2008 to 2010 (Fig. 2.4c), but

we did not see a consistent trend in average energy density over the same time period (Fig. 2.3c). However, we do not have estimates of % lipid for all sampling periods in all years of the study, therefore we cannot fully address interannual differences in % lipid.

Walleye pollock lengths increased slowly during spring, but rapidly after approximately July 15. Fish lengths reached an asymptote in late summer, between approximately August 20 and September 15, before showing an increasing trend again over the remaining sampling period. Fish lengths were more variable in late summer than in spring and mid-summer (Fig. 2.5a). The spatial patterns in SL were inconsistent across years (plots not shown), but the seasonal changes in fish length were robust across years. The average SL of fish was lowest in 2008, highest in 2009, and intermediate in 2010 (Fig. 2.5b).

Patterns in average energy density and % lipid differed among years. Although changes in energy density are primarily driven by changes in % lipid, fish size (i.e., length) also contributes to total energy content. For example, fish in 2008 had high energy density and % lipid, but were smaller relative to fish in 2009 that had intermediate % lipid leading to lower overall energy density (Figs. 2.3c, 2.4c, and 2.5b).

2.4 Discussion

This study provides estimates of energy density and % lipid for age-0 and age-1 walleye pollock and proposes a conceptual model of how energy allocation strategies shift in age-0 walleye pollock during the larval and juvenile phases. This shift represents adaptations to survival constraints associated with distinct ontogenetic stages; a strategy favoring

allocation to growth in order to escape size-dependent predation appears limited to larval development while juvenile fish (> 30mm) adopt a strategy to increase lipid storage in late summer (Fig. 2.4a). This allocation strategy has potentially important consequences for overwinter survival (Post and Parkinson, 2001). For example, age-0 Pacific herring, *Clupea pallasii*, in Prince William Sound, Alaska, rely on energy stores for overwinter survival (Norcross et al., 2001), impacting year-class success (Paul and Paul, 1998). In the SEBS, the energy density of walleye pollock in late summer is directly correlated with observed differences in year-class strength between alternating climate states (Hunt et al., 2011; Heintz et al., in press). We propose that late summer (July-September) represents a critical period for energy storage in age-0 walleye pollock, and that overwinter survival is dependent on sufficient storage in the previous growing season and may be an important determinant of recruitment success.

Differences in energy storage result from differences in the quantity and quality of prey during the age-0 period (Heintz et al., in press). Higher abundances of larger, lipid-rich zooplankton taxa during cold years, combined with lower metabolic demands, allow age-0 walleye pollock to acquire greater lipid reserves by late summer, resulting in increased overwinter survival (Hunt et al., 2011). In the cold years of 2006-2010, the zooplankton community over the Bering Sea shelf was dominated by large copepods (e.g., *Calanus marshallae*) and euphausiids (e.g., *Thysanoessa raschii*). Under warmer conditions (2002-2005), smaller zooplankton taxa were dominant (e.g., *Pseudocalanus* spp., *Acartia* spp., Coyle et al., 2011; Stabeno et al., 2012) and the lack of larger prey appeared to have limited growth and energy storage, leading to poor energy levels and

reduced year-class recruitment. The limited availability of large zooplankton coincided with increased rates of cannibalism by older age classes of walleye pollock, as well as high predation rates by juvenile salmon, further reducing age-0 survival in warm years (Coyle et al., 2011). Hence, prey quality may be as important as the thermal regime for determining overwinter survival (Hurst 2007), although prey availability and prey quality were closely linked to temperature conditions in recent years (Coyle et al., 2011).

The 2008 and 2009 cohorts showed similar seasonal patterns of energy density overall, with observed differences in late-summer age-0 fish likely reflecting the difference in mean sampling date between cruises; this highlights late summer as a period of rapidly increasing energy density in walleye pollock. Differences between the late-summer 2008 age-0 fish sampled during the rope trawl and beam trawl surveys could also be due to surface fishes (sampled by the rope trawl survey) having higher energy density than bottom-associated fishes (beam trawl survey). Energy densities are presumed to decrease during late winter when water column temperatures, prey availability, and feeding rates decrease, although patterns in energy density after late-summer sampling are unknown. Energy density of walleye pollock collected in southeastern Alaska continued to increase between September and December sampling intervals, but declined between December and March (Heintz and Vollenweider, 2010). Age-1 fish in the current study appear to achieve energy densities the following summer that are comparable to the preceding late-summer period. The 2009 cohort had significantly higher energy densities by age-1, which could be due to differential overwinter survival, reduced winter energy loss for the 2009 cohort leading to less of an energy deficit in

spring 2010, and/or differences in prey availability for age-1 fish during their second summer. The 2009 cohort also likely experienced less intra-species competition as the size of the 2009 year-class estimate remains well below the 2008 estimate (Ianelli et al., 2011).

During spring through mid-summer, low energy density and % lipid values indicate fish preferentially allocate energy to development with little increase in overall fish growth during the larval stage. The decrease in lipid content with length as larvae increase from ~5 – 15 mm (Fig. 2.4a) likely reflects decreasing energy stores as larvae adapt to capturing prey and allocate energy to completion of larval development. During summer, walleye pollock appear to be growing in length while also increasing lipid stores, although patterns are poorly defined due to lack of samples during this period. That said, late July – August may be a period when energetic demands are highest based on metabolic demands in warmer water temperatures (Ciannelli et al., 1998). The length at transformation from larval to juvenile form occurs at 25-40 mm SL (Matarese et al., 1989; Brown et al., 2001) and marks a threshold after which % lipid acquisition rates increased linearly with size, leading to higher energy density in late summer as energy is allocated to storage for overwinter survival. Our samples fall on either side of this size range, supporting the inference that fish below this length range (i.e., larvae) are allocating energy to development and fish above this length range (i.e., juveniles) favor energy storage relative to accumulation during the larval phase.

This study was conducted during three cold years in the SEBS (Stabeno et al., 2012), therefore delayed development times likely resulted in smaller fish sizes relative

to warmer years (Smart et al., in press). Age-0 juvenile walleye pollock reached an asymptotic length at approximately 60 mm SL in late summer, which may correspond to a shift in prey preferences with increasing gape size (i.e., switch to euphausiids; Brodeur 1998; Sturdevant et al., 2001) and associated foraging capability (e.g., Ciannelli et al., 2002). However, there is potential confounding between sampling date, year, and gear type that could account for the observed patterns in fish length due to differences in sampling dates among years and the use of different gears with potentially different size selectivity. An asymptotic energy density occurred when fish reached approximately 75 mm SL, similar to that observed for walleye pollock near the Pribilof Islands (asymptotic energy density at 80 mm SL) during 1994-1996 and 1999, with 1995 and 1999 also being cold years (Ciannelli et al., 2002).

While our study focused on seasonal patterns in energy allocation, spatial patterns in the distribution and energetic condition of fish relative to prey may be equally important in determining recruitment success. Significant spatial patterns were observed among years in the best models for energy density and fish length; due to confounding between sampling location and date, we cannot statistically differentiate the relative effect of sampling location. However, the relative importance of the spatial smooth terms was minimal compared to the effect of other covariates in the best models. Therefore, we believe that the patterns observed in energy density as a function of standard length, and in length as a function of sampling date, are robust.

Age-0 walleye pollock in the Gulf of Alaska during late-summer experience spatially variable habitat conditions for growth due to differences in water temperature

and prey (Mazur et al., 2007). Once larvae are capable of diel vertical migration, their position in the water column (i.e., above or below the pycnocline) also affects temperature-dependent metabolic rates, as well as trade-offs in foraging times versus predation risk (Sogard and Olla, 1996). As such, both the horizontal and vertical distributions of larvae affect their growth and energetic condition. Juvenile walleye pollock are capable of selecting habitat based on temperature, prey availability, and predator abundance (Kooka et al., 2007). Consequently, we plan to incorporate both local-scale environmental conditions and estimates of prey availability into a bioenergetics model to quantify fine-scale spatial variability in growth potential and to support the development of predictive models for recruitment success of walleye pollock in the SEBS.

2.5 Conclusions

Larval and juvenile walleye pollock face competing demands for available energy resources. We identified differing energy allocation strategies indicating that distinct ontogenetic stages face different survival constraints. Larval fish favored allocation to somatic growth, presumably in order to escape size-dependent predation, while juvenile fish allocated energy to lipid storage in late summer. We propose that late summer (July-September) represents a critical period for energy storage in age-0 walleye pollock and that subsequent energy levels provide an early metric for the prediction of overwinter survival and recruitment success to age-1.

2.6 Acknowledgments

We thank the officers and crew of the NOAA ships *Miller Freeman* and *Oscar Dyson*, the USCG vessel *Healy*, and the R/Vs *Knorr* (WHOI) and *Thompson* (UW). Funding was provided through the North Pacific Research Board (NPRB) Bering Sea Integrated Ecosystem Research Program (BSIERP) and NOAA's North Pacific Climate Regimes and Ecosystem Productivity Program (NPCREP). NOAA's EcoFOCI, MACE, and BASIS programs kindly conducted additional sampling for this project. We thank Drs. Thomas Hurst, Matthew Wilson, and one anonymous reviewer for providing helpful comments that greatly improved the manuscript. This research is NPRB publication #360 and BEST-BSIERP Bering Sea Project #67. Figure 2.1 courtesy of Ross Parnell-Turner, University of Cambridge. Reference to trade names does not imply endorsement by the National Marine Fisheries Service (NMFS), NOAA. The findings and conclusions in the paper are those of the authors and do not necessarily represent the views of the NMFS, NOAA.

2.7 References

- Akaike, H., 1973. Information theory as an extension of the maximum likelihood principle. In: Petrov, B.N., Csaki, F. (Eds.), Second International Symposium on Information Theory. Akademiai Kiado, Budapest, pp. 267 – 281.
- Aydin, K., Mueter, F.J., 2007. The Bering Sea - A dynamic food web perspective. *Deep-Sea Res. II* 54, 2501-2525.
- Aydin, K., Gaichas, S., Ortiz, I., Kinzey, D., Friday, N., 2007. A Comparison of the Bering Sea, Gulf of Alaska, and Aleutian Islands Large Marine Ecosystems Through Food Web Modeling. NOAA Tech. Memo. NMFS-AFSC-178. 298 p.
- Bacheler, N.M., Ciannelli, L., Bailey, K.M., Duffy-Anderson, J.T., 2010. Spatial and temporal patterns of walleye pollock (*Theragra chalcogramma*) spawning in the eastern Bering Sea inferred from egg and larval distributions. *Fish. Oceanogr.* 19 (2), 107-120.
- Bailey, K.M., Houde, E.D., 1989. Predation on early developmental stages of marine fishes and the recruitment problem. *Adv. Mar. Biol.* 25, 1–83.
- Beamish, R.J., Mahnken, C., 2001. A critical size and period hypothesis to explain natural regulation of salmon abundance and the linkage to climate and climate change. *Prog. Oceanogr.* 49, 423-437.
- Beamish, R.J., McFarlane, G.A. (Eds.), 1989. Effects of ocean variability on recruitment and an evaluation of parameters used in stock assessment models. *Can. Spec. Publ. Fish. Aquat. Sci.* 108, 379 pp.
- Blood, D.M., 2002. Low-temperature incubation of walleye pollock (*Theragra chalcogramma*) eggs from the southeast Bering Sea shelf and Shelikof Strait, Gulf of Alaska. *Deep-Sea Res. II* 49, 6095–6108.
- Brodeur, R.D., 1998. Prey selection by age-0 walleye pollock, *Theragra chalcogramma*, in nearshore waters of the Gulf of Alaska. *Environ. Biol. Fish.* 51, 175-186.
- Brodeur, R.D., Wilson, M.T., Ciannelli, L., 2000. Spatial and temporal variability in feeding and condition of age-0 walleye pollock (*Theragra chalcogramma*) in frontal regions of the Bering Sea. *ICES J. Mar. Sci.* 57, 256–264.
- Brown, A.L., Busby, M.S., Mier, K.L., 2001. Walleye pollock *Theragra chalcogramma* during transformation from the larval to juvenile stage: otolith and osteological development. *Mar. Biol.* 139, 845-851.

- Buchheister, A., Wilson, M.T., 2005. Shrinkage correction and length conversion equations for *Theragra chalcogramma*, *Mallotus villosus* and *Thaleichthys pacificus*. J. Fish Biol. 67, 541-548.
- Burnham, K.P., Anderson, D.R., 2002. Model Selection and Multi-Model Inference: A Practical Information-Theoretic Approach, Springer-Verlag, New York, NY. 488 pp.
- Ciannelli, L., Brodeur, R.D., Buckley, T.W., 1998. Development and application of a bioenergetics model for juvenile walleye pollock. J. Fish Biol. 52, 879-898.
- Ciannelli, L., Paul, A.J., Brodeur, R.D., 2002. Regional, interannual and size-related variation of age 0 year walleye pollock whole body energy content around the Pribilof Islands, Bering Sea. J. Fish Biol. 60, 1267-1279.
- Ciannelli, L., Brodeur, R.D., Napp, J.M., 2004. Foraging impact on zooplankton by age-0 walleye pollock (*Theragra chalcogramma*) around a front in the southeast Bering Sea. Mar. Biol. 144, 515-526.
- Conover, D.O., 1990. The relation between capacity for growth and length of growing season: evidence for and implications of countergradient variation. Trans. Am. Fish. Soc. 119 (3), 416-430.
- Copp, G.H., Kovac, V., 1996. When do fish with indirect development become juveniles? Can. J. Fish. Aquat. Sci. 53, 746-752.
- Coyle, K.O., Eisner, L.B., Mueter, F.J., Pinchuk, A.I., Janout, M.A., Cieciel, K.D., Farley, E.V., Andrews, A.G., 2011. Climate change in the southeastern Bering Sea: impacts on pollock stocks and implications for the Oscillating Control Hypothesis. Fish. Oceanogr. 20 (2), 139-156.
- Cushing, D.H., 1969. The regularity of the spawning season of some fishes. J. Cons. Int. Explor. Mer 33, 81-97.
- Cushing, D.H., 1982. Climate and Fisheries. Academic Press: London. ISBN 0-12-199720-0. 373 pp.
- Cushing, D.H., 1990. Plankton production and year-class strength in fish populations: an update of the match/mismatch hypothesis. Adv. Mar. Biol. 26, 250-293.
- Duffy-Anderson, J.T., Busby, M.S., Mier, K.L., Deliyaniades, C.M., Stabeno, P.J., 2006. Spatial and temporal patterns in summer ichthyoplankton assemblages on the eastern Bering Sea shelf 1996-2000. Fish. Oceanogr. 15, 80-94.

- Heintz, R.A., Vollenweider, J.J., 2010. Influence of size on the sources of energy consumed by overwintering walleye pollock (*Theragra chalcogramma*). J. Exp. Mar. Biol. Ecol. 393 (1-2), 43-50.
- Heintz, R.A., Siddon, E.C., Farley, E.V., in press. Climate-related changes in the nutritional condition of young-of-year (YOY) walleye pollock (*Theragra chalcogramma*) from the southeastern Bering Sea. Deep-Sea Res. II.
- Hillgruber, N., Haldorson, L.J., Paul, A.J., 1995. Feeding selectivity of larval walleye pollock *Theragra chalcogramma* in the oceanic domain of the Bering Sea. Mar. Ecol. Prog. Ser. 120, 1-10.
- Hinckley, S., 1987. The reproductive biology of walleye pollock, *Theragra chalcogramma*, in the Bering Sea, with reference to spawning stock structure. Fish. Bull. 85(3), 481-498.
- Hollowed, A.B., Bond, N.A., Wilderbuer, T.K., Stockhausen, W.T., A'mar, Z.T., Beamish, R.J., Overland, J.E., Schirripa, M.J., 2009. A framework for modelling fish and shellfish responses to future climate change. ICES J. Mar. Sci. 66 (7), 1584-1594.
- Houde, E.D., 1987. Fish early life dynamics and recruitment variability. Am. Fish. Soc. Symp. 2, 17-29.
- Hunt Jr., G.L., Stabeno, P.J., 2002. Climate change and the control of energy flow in the southeastern Bering Sea. Prog. Oceanogr. 55, 5-22.
- Hunt Jr., G.L., Stabeno, P.J., Walters, G., Sinclair, E., Brodeur, R.D., Napp, J.M., Bond, N.A., 2002. Climate change and control of the southeastern Bering Sea pelagic ecosystem. Deep-Sea Res. II 49, 5821-5853.
- Hunt Jr., G.L., Coyle, K.O., Eisner, L., Farley, E.V., Heintz, R., Mueter, F.J., Napp, J.M., Overland, J.E., Ressler, P.H., Salo, S., Stabeno, P.J., 2011. Climate impacts on eastern Bering Sea foodwebs: A synthesis of new data and an assessment of the Oscillating Control Hypothesis. ICES J. Mar. Sci. 68(6), 1230-1243.
- Hurst, T.P., 2007. Causes and consequences of winter mortality in fishes. J. Fish Biol. 71, 315-345.
- Ianelli, J.N., Honkalehto, T., Barbeaux, S., Kotwicki, S., Aydin, K., Williamson, N., 2011. Assessment of the walleye pollock stock in the Eastern Bering Sea. In: Stock Assessment and Fishery Evaluation Report for the Groundfish Resources of the Bering Sea/Aleutian Islands Regions. North Pacific Fishery Management Council, 605 W. 4th Ave., Suite 306, Anchorage, AK 99501. 118 pp.

- Kachel, N.B., Hunt Jr., G.L., Salo, S.A., Schumacher, J.D., Stabeno, P.J., Whitley, T.E., 2002. Characteristics and variability of the inner front of the southeastern Bering Sea. *Deep-Sea Res. II* 49, 5889-5909.
- Kendall Jr., A.W., Nakatani, T., 1992. Comparisons of early-life-history characteristics of walleye pollock *Theragra chalcogramma* in Shelikof Strait, Gulf of Alaska. *Fish. Bull.* 90, 129-138.
- Kendall Jr., A.W., Incze, L.S., Ortner, P.B., Cummings, S.R., Brown, P.K., 1994. The vertical distribution of eggs and larvae of walleye pollock, *Theragra chalcogramma*, in Shelikof Strait, Gulf of Alaska. *Fish. Bull.* 92, 540-554.
- Kooka, K., Yamamura, O., Nishimura, A., Hamatsu, T., Yanagimoto, T., 2007. Optimum temperature for growth of juvenile walleye pollock *Theragra chalcogramma*. *J. Exp. Mar. Biol. Ecol.* 347, 69-76.
- Litzow, M.A., Bailey, K.M., Prahl, F.G., Heintz, R., 2006. Climate regime shifts and reorganization of fish communities: the essential fatty acid limitation hypothesis. *Mar. Ecol. Prog. Ser.* 315, 1-11.
- Matarese, A.C., Kendall Jr., A.W., Blood, D.M., Vinter, B.M., 1989. Laboratory Guide to Early Life History Stages of Northeast Pacific fishes. NOAA Tech. Rep. NMFS 80, 652 pp.
- Mazur, M.M., Wilson, M.T., Dougherty, A.B., Buchheister, A., Beauchamp, D.A., 2007. Temperature and prey quality effects on growth of juvenile walleye pollock *Theragra chalcogramma* (Pallas): a spatially explicit bioenergetics approach. *J. Fish Biol.* 70, 816-836.
- Megrey, B.A., Hollowed, A.B., Hare, S.R., Macklin, S.A., Stabeno, P.J., 1996. Contribution of FOCI research to forecast of year class strength of walleye pollock in the Shelikof Strait, Alaska. *Fish. Oceanogr.* 5 (S1), 189-203.
- Moss, J.H., Beauchamp, D.A., Cross, A.D., Myers, K.W., Farley Jr., E.V., Murphy, J.M., Helle, J.H., 2005. Evidence for size-selective mortality after the first summer of ocean growth by pink salmon. *Trans. Am. Fish. Soc.* 134, 1313-1322.
- Moss, J.H., Farley, E.V., Feldman, A.M., Ianelli, J.N., 2009. Spatial distribution, energetic status, and food habits of eastern Bering Sea age-0 walleye pollock. *Trans. Am. Fish. Soc.* 138, 497-505.
- Mueter, F.J., Ladd, C., Palmer, M.C., Norcross, B.L., 2006. Bottom-up and top-down controls of walleye pollock (*Theragra chalcogramma*) on the Eastern Bering Sea shelf. *Prog. Oceanogr.* 68, 152-183.

Norcross, B.N., Brown, E.D., Foy, R.J., Frandsen, M., Gay, S.M., Kline Jr., T.C., Mason, D.M., Patrick, E.V., Paul, A.J., and Stokesbury, K.D.E., 2001. A synthesis of the life history and ecology of juvenile Pacific herring in Prince William Sound, Alaska. *Fish. Oceanogr.* 10(S1), 42-57.

Paul, A.J., Paul, J.M., 1998. Comparisons of whole body energy content of captive fasting age zero Alaskan Pacific herring (*Clupea pallasii* Valenciennes) and cohorts overwintering in nature. *J. Exp. Mar. Biol. Ecol.* 226, 75-86.

Paul, A.J., Paul, J.M., 1999. Interannual and regional variations in body length, weight and energy content of age-0 Pacific herring from Prince William Sound, Alaska. *J. Fish Biol.* 54, 996-1001.

Post, J.R., Parkinson, E.A., 2001. Energy allocation strategy in young fish: allometry and survival. *Ecology* 82(4), 1040-1051.

Schultz, E.T., Conover, D.O., Ehtisham, A., 1998. The dead of winter: size-dependent variation and genetic differences in seasonal mortality among Atlantic silverside (*Atherinidae: Menidia menidia*) from different latitudes. *Can. J. Fish. Aquat. Sci.* 55, 1149-1157.

Schultz, E.T., Conover, D.O., 1999. The allometry of energy reserve depletion: test of a mechanism for size-dependent winter mortality. *Oecologia* 119, 474-483.

Shima, M., Bailey, K.M., 1994. Comparative analysis of ichthyoplankton sampling gear for early life stages of walleye pollock (*Theragra chalcogramma*). *Fish. Oceanogr.* 3(1), 50-59.

Smart, T.I., Siddon, E.C., Duffy-Anderson, J.T., in press. Vertical distributions of the early life stages of a common gadid in the eastern Bering Sea (*Theragra chalcogramma*, walleye pollock). *Deep-Sea Res.* II.

Sogard, S.M., Olla, B.L., 1996. Food deprivation affects vertical distribution and activity of a marine fish in a thermal gradient: potential energy-conserving mechanisms. *Mar. Ecol. Prog. Ser.* 133, 43-55.

Sogard, S.M., Olla, B.L., 2000. Endurance of simulated winter conditions by age-0 walleye pollock: effects of body size, water temperature and energy storage. *J. Fish Biol.* 56, 1-21.

Stabeno, P.J., Schumacher, J.D., Ohtani, K., 1999. Physical oceanography of the Bering Sea. In: *The Bering Sea: A Summary of Physical, Chemical and Biological Characteristics and a Synopsis of Research*. T.R. Loughlin and K. Ohtani (eds.). North Pacific Marine Science Organization, PICES, Alaska Sea Grant Press, pp. 1-28.

Stabeno, P.J., Bond, N.A., Kachel, N.B., Salo, S.A., Schumacher, J.D., 2001. On the temporal variability of the physical environment over the south-eastern Bering Sea. *Fish. Oceanogr.* 10 (1), 81-98.

Stabeno, P.J., Kachel, N.B., Moore, S.E., Napp, J.M., Sigler, M., Yamaguchi, A., Zerbini, A.N., 2012. Comparison of warm and cold years on the southeastern Bering Sea shelf and some implications for the ecosystem. *Deep-Sea Res. II* 65-70, 31-45.

Sturdevant, M.V., Brase, A.L.J., Hulbert, L.B., 2001. Feeding habits, prey fields, and potential competition of young-of-the-year walleye pollock (*Theragra chalcogramma*) and Pacific herring (*Clupea pallasii*) in Prince William Sound, Alaska, 1994-1995.

Van Handel, E., 1985. Rapid determination of total lipids in mosquitoes. *J. Am. Mosq. Control Assoc.* 1 (3), 302-304.

Vollenweider, J.J., Heintz, R., Schaufler, L., Bradshaw, R., 2011. Seasonal cycles in whole-body proximate composition and energy content of forage fish vary with water depth. *Mar. Biol.* 158, 413-27.

Walsh, J.J., McRoy, C.P., 1986. Ecosystem analysis in the southeastern Bering Sea. *Cont. Shelf Res.* 5, 259-288.

Wespestad, V.G., Quinn II, T.J., 1996. Importance of Cannibalism in the Population Dynamics of Walleye Pollock, *Theragra chalcogramma*. NOAA Tech. Rep. NMFS 126, 212-217.

Wood, S.N., 2006. *Generalized Additive Models: An introduction with R*. Chapman & Hall/CRC, Boca Raton, FL. 422 pp.

Table 2.1. Year, season, sampling dates, and gear used to collect age-0 and age-1 walleye pollock (*Theragra chalcogramma*). The mean (\pm standard error, n) energy density, % lipid, and standard length (mm) are shown for each cruise by age class.

Age-0							
Year	Season	Dates	Gear	Mesh size	Energy density (kJ/g)	% lipid	Standard Length (mm)
2008	Spring	May 12 – 21	Bongo	505 (μm)		8.51 (0.94, 13)	5.67 (0.07, 274)
2008	Mid-summer	July 3 - 17	MOCNESS	505 (μm)	17.99 (0.68, 6)	11.36 (0.45, 18)	10.61 (0.14, 168)
2008	Late-summer	September 7 - 30	Rope trawl	1.2 cm codend liner	23.35 (0.22, 37)	21.49 (0.82, 31)	62.7 (1.25, 102)
2008	Late-summer	September 9 - 20	Beam trawl	7 mm; 3 mm codend liner	22.36 (0.18, 34)		66.82 (1.34, 33)
2009	Mid-summer	June 14 - July 12	MOCNESS	505 (μm)	16.95 (0.68, 4)	8.34 (0.26, 89)	8.79 (0.14, 251)
2009	Late-summer	September 2 - 30	Rope trawl	1.2 cm codend liner	22.81 (0.14, 50)	17.98 (0.84, 46)	67.1 (1.08, 100)

Table 2.1. Continued

2010	Spring	May 6 - 18	Bongo	505 (µm)		2.15 (0.30, 22)	5.67 (0.05, 164)
2010	Mid-summer	June 16 - July 14	MOCNESS	505 (µm)	15.39 (0.88, 3)	6.0 (0.23, 66)	8.88 (0.14, 135)
2010	Late-summer	August 16 - September 26	Rope trawl	1.2 cm codend liner	22.64 (0.11, 89)		59.8 (0.76, 104)
2010	Late-summer	September 2 - 15	Beam trawl	7 mm; 3 mm codend liner	22.43 (0.25, 34)		62.38 (1.9, 34)
Age-1							
2008	Summer	June 2 - July 31	Methot Trawl	2x3 mm; 1 mm codend liner	23.13 (0.12, 49)	19.44 (0.52, 49)	132.46 (1.67, 49)
2009	Summer	June 9 - August 7	Methot Trawl	2x3 mm; 1 mm codend liner	22.99 ^a (0.18, 34)	17.97 (1.0, 34)	138.45 (3.46, 34)
2009	Late-summer	September 2 - 30	Rope trawl	1.2 cm codend liner	23.51 ^a (0.34, 18)	18.8 (1.66, 18)	155.04 (6.23, 19)
2010	Summer	June 5 - August 7	Methot trawl	2x3 mm; 1 mm codend liner	24.41 (0.17, 34)	25.58 (0.72, 34)	148.25 (2.98, 34)

^aEnergy density values were predicted from % lipid values based on the regression relationship:

$$\text{energy density} = 20.1 + 0.76 * \% \text{ lipid}$$

Table 2.2. Summary of generalized additive mixed model (GAMM) fits for energy density, % lipid, and standard length showing terms, coefficient estimates, standard error (SE) for fixed coefficients, degrees of freedom (d.f.; number of parameters for each term in the model, estimated for smooth terms), and P -values. P -values for parametric terms (intercept, year coefficients) based on t-test of the null hypothesis that the coefficient is equal to zero; for smooth terms (f_i) based on an approximate F-test (Wood, 2006); for random effects term (σ_a) based on likelihood ratio test. The intercept (α) corresponds to the 2008 means and the subsequent year effects (Y_k) correspond to the difference between that year's mean and the intercept; f_1, f_2 , and f_4 are smooth terms (SL = standard length; date = sampling date); f_3 and f_5 are smooth spatial surfaces (lat=latitude; long=longitude) by year k , and ε_{ik} is within-station residual variability.

Model (Adjusted R ²)	Term	Estimate	SE	d.f.	P-value
Energy density (0.688)	Intercept (α)	22.93	0.15	1	< 0.001
	Y_{2009}	-1.09	0.26	1	< 0.001
	Y_{2010}	-0.52	0.19	1	0.007
	f_1 (SL)			3.7	< 0.001
	f_3 (lat, long) ₂₀₀₈			2.9	< 0.001
	f_3 (lat, long) ₂₀₀₉			2	< 0.001
	f_3 (lat, long) ₂₀₁₀			2	0.16
	$\sigma(a_i)$	0.49		1	< 0.001
	$\sigma(\varepsilon_{ik})$	0.71		1	

Table 2.2 Continued

<hr/>					
% Lipid (0.847)					
Intercept (α)	13.22	0.50	1	<0.001	
Y_{2009}	-2.65	0.59	1	<0.001	
Y_{2010}	-5.50	0.69	1	<0.001	
$f_1(\text{SL})$			3.9	<0.001	
$f_2(\text{date})$			1	<0.001	
$\sigma(a_i)$	1.58		1	<0.001	
$\sigma(\varepsilon_{ik})$	2.06		1		
<hr/>					
Standard length (0.955)					
Intercept (α)	20.53	1.22	1	<0.001	
Y_{2009}	6.84	1.89	1	<0.001	
Y_{2010}	2.1	1.65	1	0.2	
$f_4(\text{date})$			6.36	<0.001	
$f_5(\text{lat, long})_{2008}$			2	<0.001	
$f_5(\text{lat, long})_{2009}$			2.89	<0.001	
$f_5(\text{lat, long})_{2010}$			2	0.46	
$\sigma(a_i)$	5.68		1	<0.001	
$\sigma(\varepsilon_{ik})$	3.79		1		

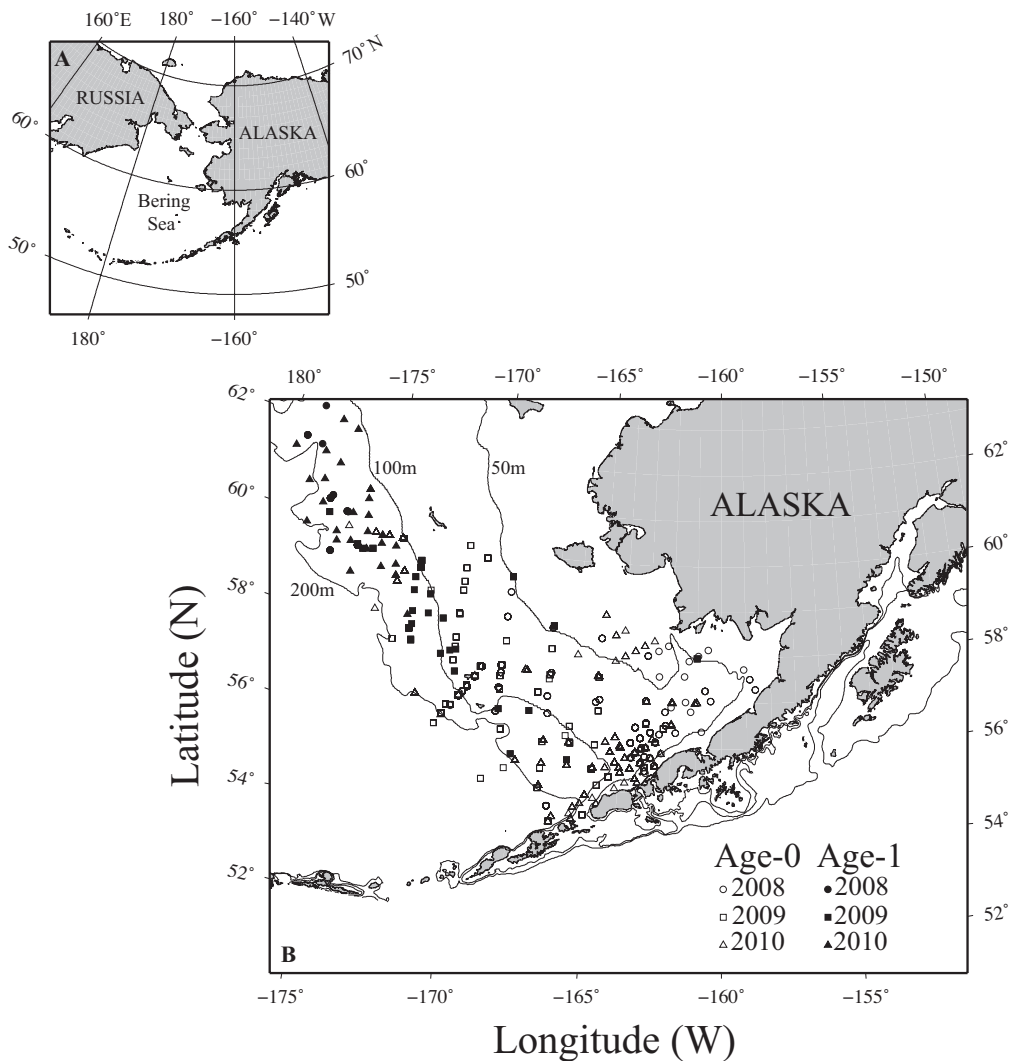


Figure 2.1. (A) Map showing the location of the Bering Sea. (B) Map of the southeastern Bering Sea showing the location of sample collections by age class and year. Sampling for age-0 fish is assumed to encompass the bulk of their distribution based on historical data, while age-1 fish were predominantly sampled from the outer shelf domain (between 100 and 200 m isobaths). Depth contours are shown for the 50 m, 100 m, and 200 m isobaths.

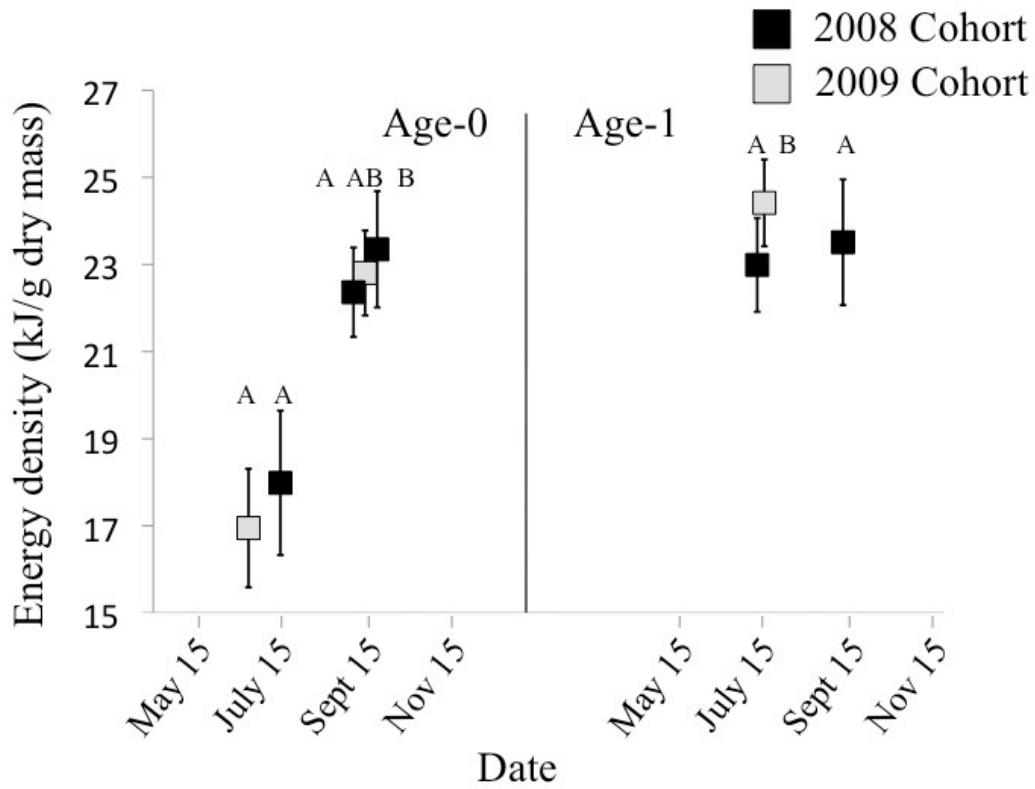


Figure 2.2. Plot of energy density (kJ/g dry mass) for the 2008 and 2009 cohorts of walleye pollock (*Theragra chalcogramma*). Errors bars are plotted as ± 1 standard deviation to show the variability in energy density estimates for each sampling interval. Different letters indicate significant differences in energy density within season. Note x-axis is mean sampling date across the age-0 and age-1 seasons.

(A)

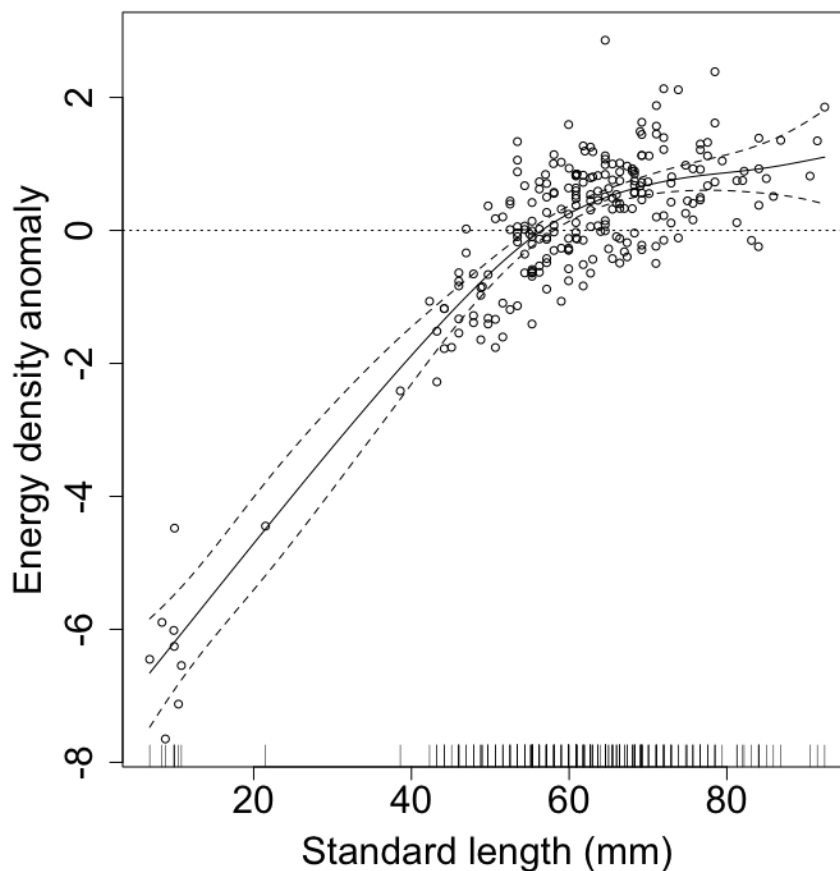


Figure 2.3. Results from generalized additive mixed model (GAMM) regression analyses showing the estimated effects on energy density (kJ/g dry mass) of (A) standard length (SL; mm), (B) spatial location (by year), and (C) year for age-0 walleye pollock (*Theragra chalcogramma*). Dashed lines denote 95% confidence intervals in (A) and (C). Energy densities in (A) are plotted as anomalies because actual values depend on location and year. Spatial contours in (B) correspond to the estimated energy density for a fish of 60 mm SL on September 1. Depth contours are shown for the 50 m, 100 m, and 200 m isobaths. The partial fits by year (C) show the average energy density by year with other covariates fixed at their mean values.

(B)

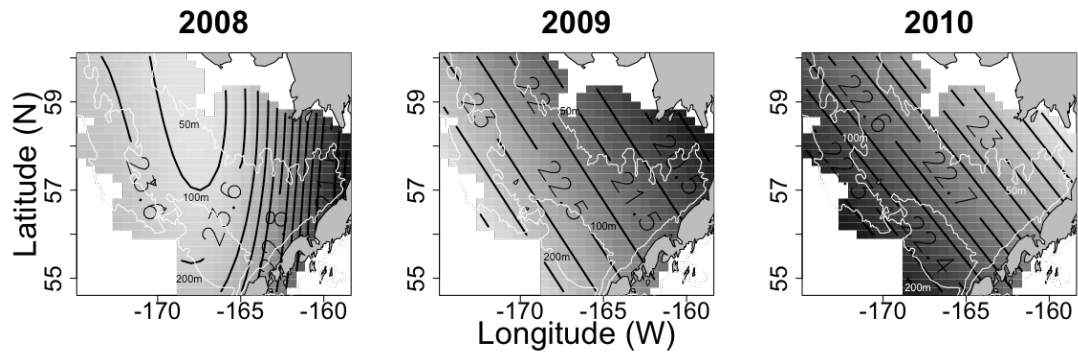


Figure 2.3. Continued

(C)

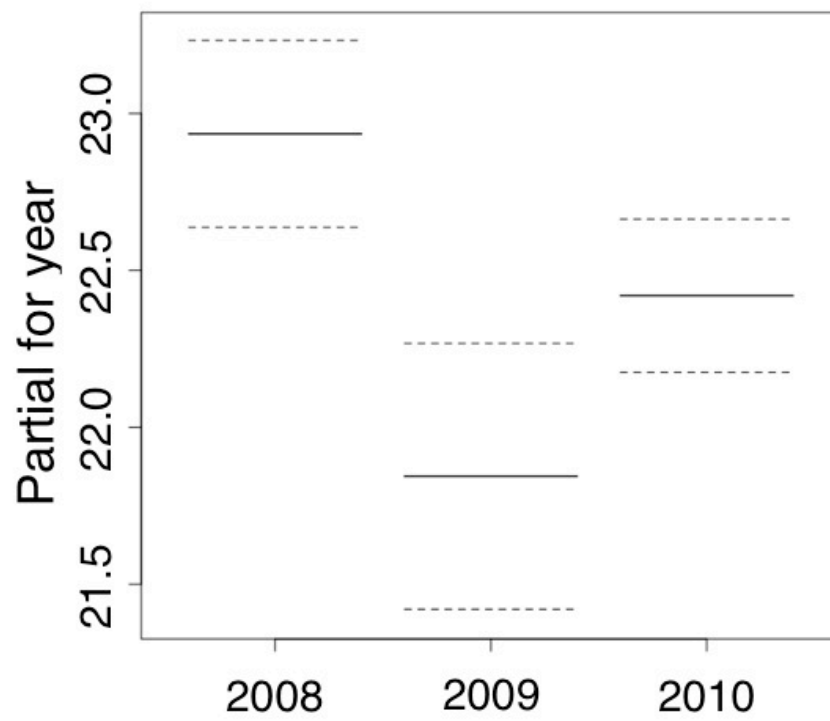


Figure 2.3. Continued

(A)

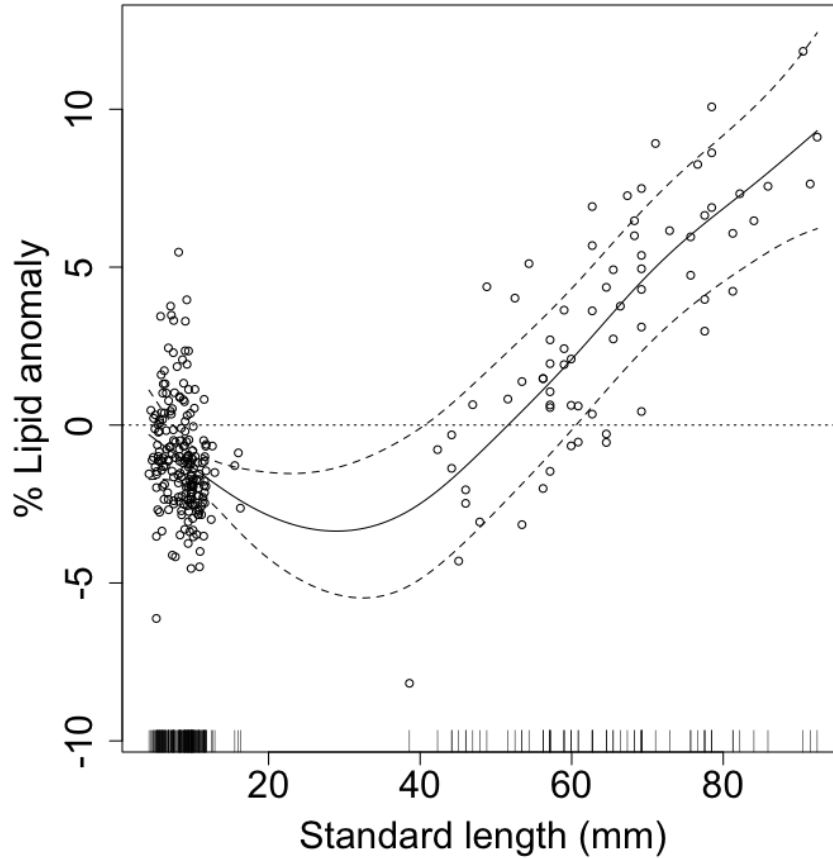


Figure 2.4. Results from generalized additive mixed model (GAMM) regression analyses showing the estimated effects on % lipid (on a dry mass basis) of (A) standard length (SL; mm), (B) sampling date, and (C) year for age-0 walleye pollock (*Theragra chalcogramma*). Dashed lines denote 95% confidence intervals. % Lipid values in (A) and (B) are plotted as anomalies because actual values depend on sampling date and year. The range of y-axis values are comparable between (A) and (B), indicating SL and sampling date are similarly important in explaining variability in % lipid. The partial fits by year (C) show the average % lipid by year with other covariates fixed at their mean values.

(B)

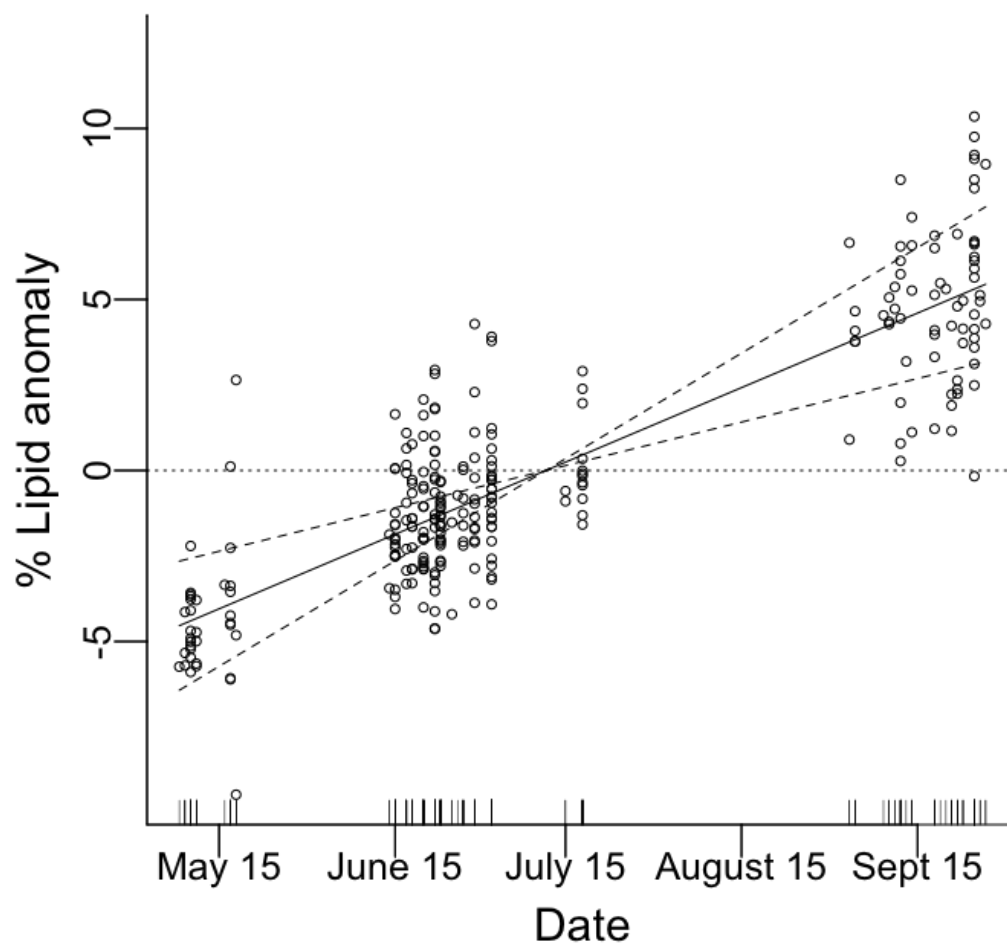


Figure 2.4. Continued

(C)

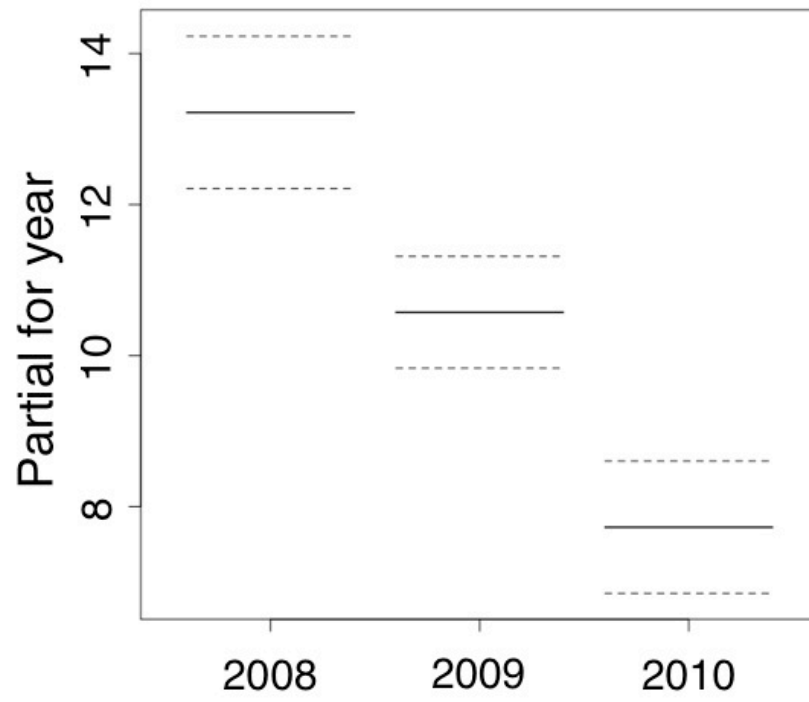


Figure 2.4. Continued

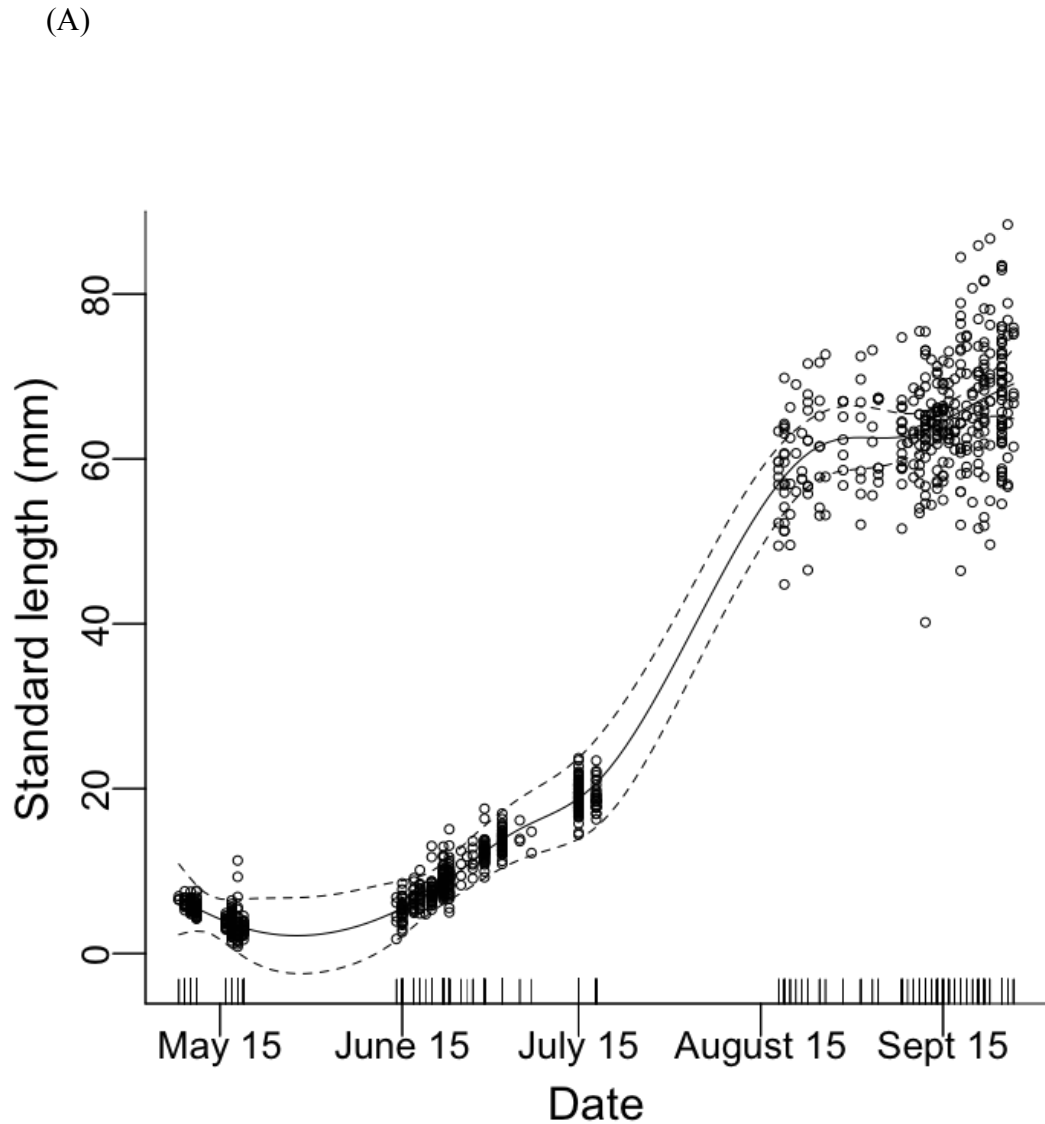


Figure 2.5. Results from generalized additive mixed model (GAMM) regression analyses showing the estimated effects on standard length (SL; mm) of (A) sampling date and (B) year for age-0 walleye pollock (*Theragra chalcogramma*). Dashed lines denote 95% confidence intervals. The partial fits by year (B) show the average SL by year with other covariates fixed at their mean values.

(B)

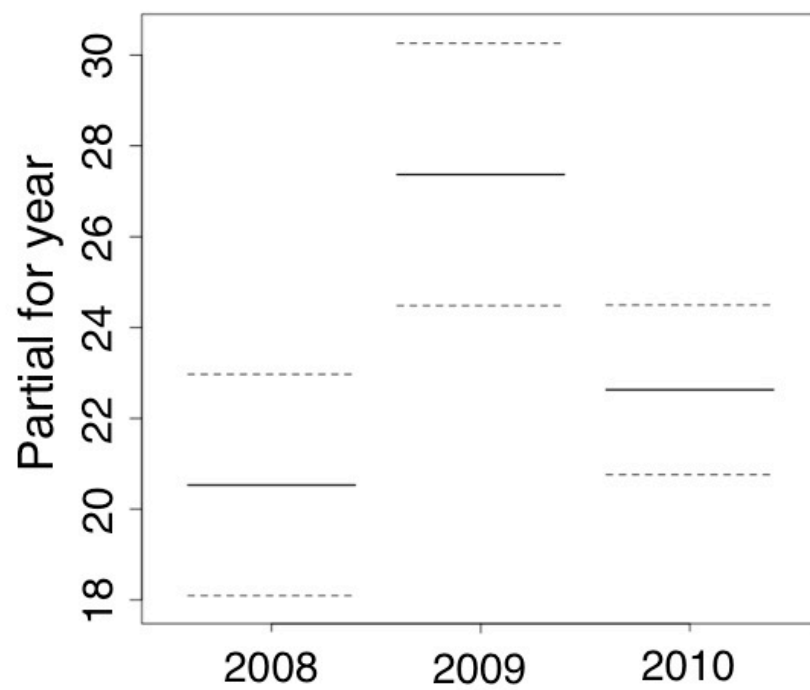


Figure 2.5. Continued

**Chapter 3: Spatial match-mismatch between juvenile fish and prey
explains recruitment variability across contrasting climate conditions
in the eastern Bering Sea⁴**

Abstract

Understanding mechanisms behind variability in early life survival of marine fishes through modeling efforts can improve predictive capabilities for recruitment success under changing climate conditions. Walleye pollock (*Theragra chalcogramma*) support the largest single-species commercial fishery in the United States and represent an ecologically important component of the Bering Sea ecosystem. Variability in walleye pollock growth and survival is structured in part by climate-driven bottom-up control of zooplankton composition. We used two modeling approaches, informed by observations, to understand the roles of prey quality, prey composition, and water temperature on juvenile walleye pollock growth: (1) a bioenergetics model that included local predator and prey energy densities, and (2) an individual-based model that included a mechanistic feeding component dependent on larval development and behavior, local prey densities and size, and physical oceanographic conditions. Prey composition in late-summer shifted from predominantly smaller copepod species in the warmer 2005 season to larger species in the cooler 2010 season, resulting in different growth conditions and year-class survival. Observed diets reflected temporal variability in zooplankton composition,

⁴ Siddon, E.C., Kristiansen, T., Mueter, F.J., Holsman, K., Heintz, R.A., and Farley, E.V. In preparation for journal submission. Spatial match-mismatch between juvenile fish and prey explains recruitment variability across contrasting climate conditions in the eastern Bering Sea. In preparation to be submitted to PLoS ONE.

corroborating hypothesized bottom-up control of survival. In 2010, the main prey of juvenile walleye pollock were more abundant (37%), had greater biomass (64%), and had higher mean energy density (12%), resulting in greater recruitment to age-1 (42%) compared to 2005. Spatial patterns in prey composition and water temperature lead to areas of enhanced growth, or growth ‘hot spots’, for juvenile walleye pollock and survival may depend on the overlap between fish and these areas. This study provides evidence that a spatial mismatch between juvenile walleye pollock and growth ‘hot spots’ in 2005 contributed to poor recruitment while a higher degree of overlap in 2010 resulted in improved recruitment. Our results indicate that climate-driven changes in prey composition and quality can impact growth of juvenile walleye pollock, severely affecting recruitment variability.

3.1 Introduction

The match-mismatch hypothesis [1] proposes that predator survival is dependent on the temporal and spatial overlap with prey resources [2]. Factors affecting temporal overlap, such as climate variability through altered phenology, can lead to changes in survival at critical life stages [3]. Temporal variation in spatial patterns of physical or biological conditions may concurrently affect survival. For example, in temperate and sub-arctic marine ecosystems, the timing of the spring bloom varies between years, driven by physical oceanographic conditions that change due to climate variability (e.g. [4]). These conditions, such as the onset of stratification, turbulence, and light availability, also affect the spatial patterns of zooplankton abundance, which further influences the feeding success of planktivorous fish species. Hence, variability in the spatial overlap of predator and prey, as well as differences in prey quality [5,6], may directly affect differences in year-class success of many marine fish species [7,8].

Variability in year-class strength of gadids is often associated with changing physical conditions [9,10]. In the North Sea, temperature increases since the mid-1980s have led to a mismatch of Atlantic cod (*Gadus morhua*) and their prey; under warmer conditions, a shift in species composition decreased the prey size and energy content, which reduced recruitment success of Atlantic cod [9]. The eastern Bering Sea (EBS) has experienced multi-year periods of both warm and cold conditions since the turn of the 21st century [11], with cold years having much higher walleye pollock (*Theragra chalcogramma*) recruitment on average [12]. In the EBS, changes in zooplankton composition between these periods have been identified as an important driver of

recruitment success for walleye pollock [8,13], but the mechanistic links remain poorly understood.

Walleye pollock is an ecologically important component of the Bering Sea ecosystem, and the focus of the largest commercial fishery in the U.S. Interannual changes in ocean temperatures [11] and shifts in the spatio-temporal distribution of prey [13] make walleye pollock an ideal case study to better understand drivers of recruitment success in sub-arctic marine fish. Larger zooplankton taxa, such as lipid-rich *Calanus* spp., were less abundant during recent warm years in the EBS, possibly causing reduced growth rates and subsequent year-class strength of juvenile walleye pollock (hereafter juvenile pollock). In contrast, higher abundances of lipid-rich prey, combined with lower metabolic demands in cold years, may have allowed pollock to acquire greater lipid reserves by late summer and experience increased overwinter survival [8]. Although the energetic condition of juvenile pollock in late summer is recognized as a predictor of age-1 abundance during the following summer in the EBS [12], the causal mechanism linking differences in prey abundance and quality to walleye pollock survival remains untested.

We utilized two modeling approaches, informed by observations of the prey field and environmental conditions, to better understand the roles of prey composition, prey quality, and temperature on juvenile pollock growth. Variability in these habitat characteristics contributes to bottom-up control of fish growth and survival. Comparing alternative model-based predictions of growth allows a better understanding of the mechanisms behind variability in growth patterns and an evaluation of the importance of different parameters in the models.

The objectives of this study were to (1) estimate spatial differences in maximum growth potential of juvenile pollock on the EBS shelf using a bioenergetics modeling approach, (2) quantify the impact of temperature and prey quality on spatial variability in growth potential, (3) compare maximum growth potential to predicted growth from an individual-based model (IBM), and (4) compare observed and predicted (from IBM) prey preferences in order to better understand mechanistic prey selection leading to differences in modeled growth. We hypothesize that differences in prey species composition and quality lead to bottom-up control of juvenile pollock growth and survival in representative warm and cold years in the EBS.

3.2 Materials and methods

3.2.1 Ethics statement

Collection of physical and biological oceanographic data and fish samples during the US Bering-Aleutian Salmon International Surveys (BASIS) conducted on the EBS shelf was approved through the National Marine Fisheries Service, Scientific Research Permit numbers 2005-9 and 2010-B1. Collection of biological data in the US Exclusive Economic Zone by federal scientists to support fishery research is granted by the Magnuson - Stevens Fishery Conservation and Management Act.

3.2.2 Modeling approaches

Two alternative modeling approaches allowed for a comparison of maximum growth potential from a Wisconsin-type bioenergetics model parameterized for juvenile pollock (modified from [14]) and predicted growth from a mechanistic individual-based model

(IBM; [15]). Growth ($\text{g} \cdot \text{g body wet weight}^{-1} \cdot \text{day}^{-1}$) was estimated for 65 mm standard length (SL; 2.5 g) juvenile pollock, corresponding to the average size of age-0 fish observed in late summer (2005: 64.1 ± 6.7 mm SL [mean \pm SD] and 1.97 ± 0.93 g; 2010: 64.3 ± 9.2 mm SL and 2.39 ± 0.94 g). The IBM also provided estimates of average predicted fish depth (m) in the water column as well as station-specific prey preferences (i.e., Chesson's index; [16]) that were compared with observed prey preferences from stomach contents of juvenile pollock in late summer.

Models were parameterized based on samples of juvenile pollock and oceanographic data collected during the US Bering-Aleutian Salmon International Surveys (BASIS) conducted on the EBS shelf from mid-August to October 2005 and 2010 ([17]; Fig. 3.1). Model inputs included water column temperature, zooplankton abundance and biomass, energy density estimates of selected zooplankton taxa and of juvenile pollock for the bioenergetics model, and vertical distribution of zooplankton taxa for the IBM.

We selected 2005 (warm) and 2010 (cold) for our analyses based on data availability and on the pronounced contrast in ocean conditions between these years (e.g., depth-averaged temperature anomalies over the middle shelf; [11]). Extensive spatial coverage of the surveys, combined with varying climate conditions between years, provided ample data with which to inform the models and compare differences in predicted growth between a representative warm year and a representative cold year in the EBS.

3.2.3 Field observations

3.2.3.1 Juvenile pollock abundance

Juvenile pollock were collected using a midwater rope trawl that was 198 m long, had hexagonal mesh in wings and body, and had a 1.2 cm mesh liner in the codend. The rope trawl was towed at 6.5 to 9.3 km•hr⁻¹, at or near the surface, and had a typical spread of 55 m horizontally and 25 m vertically. Trawl stations were generally sampled during daytime and tow duration generally lasted 30 minutes and covered 2.8 to 4.6 km.

Catch per unit effort (CPUE; #•m⁻²) of juvenile pollock was calculated as:

$$CPUE_i = \frac{n_i}{d_i \cdot h} \quad \text{Eq. 1}$$

where n_i is the number of fish collected in a given haul i , d_i is the trawl distance (m) calculated from starting and ending ship position, and h is the horizontal spread of the trawl net (m). Haul-specific average fish weights were calculated as the total weight of juvenile pollock divided by the number caught in each haul. Only surface tows at pre-defined stations were used to compute CPUE because midwater tows specifically targeted acoustic sign of walleye pollock.

3.2.3.2 Water temperature

Vertical profiles of water temperature were collected at each station sampled for oceanography using a Sea-Bird Electronics (SBE) conductivity-temperature-depth (CTD) profiler SBE-25 (2005) or SBE-911 (2010). The average temperature in the upper 30 m of the water column was used in the bioenergetics model, assuming juvenile pollock collected from surface trawls were concentrated within the upper 30 m [17]. For the IBM, the water column was divided into 1-m discrete depth bins. For all IBM simulations, the depth of the water column was set to the upper 100 m of all deeper stations ($n=9$ of 116

in 2005, $n=27$ of 160 in 2010) because MOCNESS data used to develop vertical profiles of zooplankton distribution (see '*Zooplankton vertical profiles*' below) was limited to 100 m. For stations with missing temperature data ($n=1$ for 2005), data from the nearest station with similar depth was used. For stations with incomplete temperature profiles ($n=1$ for 2005), temperatures were linearly interpolated between depths.

3.2.3.3 Zooplankton data

3.2.3.3.1 Determination of main prey taxa

Juvenile pollock (<100 mm FL) collected from both surface (2005 and 2010) and midwater (2010 only) tows were used in the analysis to characterize diets across the EBS shelf in two contrasting years ($n=26$ stations in 2005, $n=47$ stations in 2010 [$n=16$ surface tows, $n=31$ midwater tows]). Stomach content analyses followed standard methods as described in [18]. Briefly, fish stomach contents were examined onboard the ship by removing and pooling the contents of the entire food bolus from up to 20 randomly selected individuals of similar size per trawl. Stomach contents were sorted and identified to the lowest feasible taxonomic group. Individual prey taxa were allocated a proportional contribution to total stomach contents, as % volume, of each prey taxon to the diet. To compute overall average diet composition, contributions were weighted by the CPUE of juvenile pollock at each station and averaged across stations. All prey taxa of juvenile pollock that cumulatively accounted for at least 90% of the diet by volume and individually accounted for at least 2% of the diet by volume were included in the bioenergetics and IBM models (Table 3.1). Main prey taxa from either year were included in models for both years for comparing growth across years.

3.2.3.3.2 Zooplankton size

The length and width of each species/stage of zooplankton comprising the main prey taxa in each year were used in the mechanistic feeding component of the IBM. Literature values of stage-specific length and width were used when available; voucher collections from the EBS were used for length and width measurements when literature values were not available (Table 3.A.1).

3.2.3.3.3 Zooplankton abundance

Water-column estimates of abundance for small and large zooplankton taxa were collected using a Juday [19] and bongo net, respectively, in both years. Zooplankton tows were generally conducted during daylight hours. The Juday net (0.1 m² with 168- μ m mesh) was towed vertically from near-bottom (or to a maximum depth of 200 m) to the surface at approximately 1 m•s⁻¹. Double oblique tows from the surface to near-bottom (or to a maximum depth of 200 m) were made with a bongo net (60-cm with 505- μ m mesh); volume filtered was measured with General Oceanics flowmeters. Samples were quantified under a microscope and abundance (#•m⁻³) of each species/stage was determined. Catch coefficients (corrections for net avoidance) were applied to Juday data (see [19]). Zooplankton abundance was allocated into 1-m discrete depth bins according to vertical profiles of zooplankton distribution (see ‘*Zooplankton vertical profiles*’ below), scaled to station depth, and used as input to the IBM. Small zooplankton representing main prey taxa sampled using the Juday net included *Acartia clausi*, *Acartia* spp. (2010 only), *Centropages abdominalis*, and *Pseudocalanus* sp. Large zooplankton sampled using the bongo net included *Calanus marshallae*, *Eucalanus bungii*, *Limacina*

helicina, *Neocalanus cristatus*, *N. plumchrus* (2005 only), *Oikopleura* sp., *Thysanoessa inermis*, *T. inspinata*, and *T. raschii*.

3.2.3.3.4 Zooplankton biomass

Total sample wet weights (g, WW) of taxa collected from the Juday net were computed from wet weight tables [19]. Wet weights ($\text{g}\cdot\text{m}^{-3}$) of taxa collected from the bongo net were measured during sample processing at the University of Alaska Fairbanks (2005; [20]) and NOAA/NMFS/Alaska Fisheries Science Center (2010). A biomass-weighted mean prey energy density was calculated for each station based on Juday and bongo data and used as input to the bioenergetics model. At each station, the biomass of individual taxa was divided by the total prey biomass, multiplied by the taxa-specific energy density (see ‘*Zooplankton energy density*’ below) for each year, and summed across all taxa present at a given station. The year-specific average biomass of individuals of a given taxon was calculated by dividing the sum of the biomass of all specimens weighed (i.e., subsample) by the total number of specimens subsampled in a given year (Table 3.A.1).

3.2.3.3.5 Zooplankton energy density

Taxa-specific energy density (ED; $\text{kJ}\cdot\text{g}^{-1}$ WW) values obtained from available zooplankton collections from the EBS during 2004 (warm; no ED data available from 2005) and 2010 (cold) were used to estimate average ED values during warm and cold conditions for the main prey taxa as input to the bioenergetics model (Table 3.A.1). For taxa lacking sufficient information to estimate separate ED values, a single estimate was used in both years. In these cases, only differences in abundance and biomass contributed to differences in average prey energy between years in the models.

Estimates of ED and % lipid were available for several copepod species (*C. marshallae*, *N. cristatus*, and *N. plumchrus/flemingeri*) from 2010 (see [21] for details on the biochemical processing). A linear regression was developed to predict species specific ED (ω_i) from % lipid values for other copepod species and/or climate conditions (Table 3.A.1), such that:

$$\omega_i = \alpha + \beta L_i + \varepsilon_i, \text{ where } \varepsilon_i \sim N(0, \sigma^2) \quad \text{Eq. 2}$$

where α and β represent the intercept and slope of the regression, respectively, L_i is the lipid composition (%) of the individual copepod sample i and ε_i is a residual. The residuals, ε_i , are assumed to be independent and normally distributed with mean 0 and variance σ^2 ($\alpha = 19.3$, $p = 0.02$; $\beta = 0.41$, $p = 0.07$; $R^2=0.98$).

3.2.3.3.6 Zooplankton vertical profiles

To account for diel vertical migrations, taxa-specific vertical profiles for day and night were developed for all main prey taxa as input for the IBM. Vertical profiles were based on summer MOCNESS surveys that provided depth-stratified abundance estimates. MOCNESS data were available for 2004 (warm) and 2009 (cold); these vertical profiles were applied to late-summer model runs for 2005 and 2010, respectively, assuming that the vertical behavior of zooplankton taxa is conserved seasonally and across years within similar oceanographic conditions. To assess this assumption, a sensitivity analysis was conducted using constant abundances by depth (see ‘IBM sensitivity analyses’ below).

In 2004, MOCNESS data were available at 47 stations over the EBS shelf [20]; 5 stations were sampled during daytime and 42 stations were sampled during nighttime. In 2009, MOCNESS data were available at 29 stations over the EBS shelf (A. Pinchuk,

unpubl. data); 7 stations were sampled during daytime and 22 stations were sampled during nighttime. Daytime extended from approximately 07:00 (sunrise) to 23:30 (sunset) Alaska Daylight Savings Time during the sampling periods; stations sampled during crepuscular periods were excluded from the analysis. The depth increments of the MOCNESS varied depending on water depth; therefore, data were binned to the finest resolution available (i.e., 5-20 m). Zooplankton abundance was assumed to be uniform within sampling depths and averaged across all daytime and nighttime tows within a given year to obtain four vertical profiles for each taxon (day vs. night, 2004 vs. 2009).

3.2.4 Bioenergetics model

A bioenergetics model was used to estimate spatially explicit maximum growth potential of juvenile pollock by station. We used the broadly applied Wisconsin bioenergetics modeling approach [22,23] that has been adapted for walleye pollock including appropriate model validation ([14, 24]; Table 3.A.2). The model estimates temperature- and weight-specific maximum daily (d) consumption for an individual fish at station k in year t ($C \max_{d,kt}$; $g \cdot g^{-1} \cdot d^{-1}$ in terms of grams wet body weight) as:

$$C \max_{d,kt} = \alpha W^{\beta} \cdot f(T_{d,kt}) \quad \text{Eq. 3}$$

where $C \max_{d,kt}$ is parameterized from independent laboratory observations of consumption rates for the species, absent competitor or predator interference, and is assumed to scale exponentially with fish weight (W) according to α and β (the allometric intercept and slope of consumption) and thermal experience according to the temperature scaling function $f(T)$ (Table 3.A.2).

Realized individual daily consumption rates ($C_{d,kt}$; $g \cdot g^{-1} \cdot d^{-1}$) based on *in situ* fish are typically much lower than $C_{\max_{d,kt}}$ because inter- and intra-species competition, mismatched prey phenology or distributions, and predator avoidance behaviors by prey species often limit capture and consumption rates [14,25]. The ratio of realized consumption to maximum consumption (i.e., $\bar{\eta} = C_{d,kt} / C_{\max_{d,kt}}$), or the mean relative foraging rate, is a measure of *in situ* foraging efficiency. $\bar{\eta}$ can be estimated using field observations of growth or it can be set to a specific value and used to predict daily growth ($G_{d,kt}$) using the mass balance equation where growth is the difference between energy consumed ($C_{d,kt}$) and energy lost to metabolism and waste ($[\delta | C_{d,kt}, W_{d-1}, T_{d,kt}]$), such that:

$$G_{d,kt} = (C_{d,kt} - [\delta | C_{d,kt}, W_{d-1}, T_{d,kt}]) \cdot \bar{\xi}_{kt} \quad \text{Eq. 4}$$

where $G_{d,kt}$ is the estimated daily specific growth ($g \cdot g^{-1} \cdot d^{-1}$), $C_{d,kt}$ is realized consumption ($C_{d,kt} = \bar{\eta} \cdot C_{\max_{d,kt}}$), W_{d-1} is the weight of an individual fish at the start of the simulation day d , $T_{d,kt}$ is the water temperature on simulation day d , and $\bar{\xi}_{kt}$ is the ratio of annual mean predator (\bar{v}_t) energy density for year t to station (k) specific prey energy densities (\bar{w}_k) and is used to convert consumed biomass of prey into predator biomass (for more information see [25]).

Empirically derived or inferred values for the energy density of different prey species (see *Zooplankton energy density* above) were used to derive mean station-specific (k) available prey energy density for both years (\bar{w}_{kt}); diet composition was assumed to be proportional to the relative biomass of zooplankton prey at each station. Individual

fish energy density (v_i) was determined using biochemical processing (see [21]). At stations where sufficient numbers of juvenile pollock were collected ($n=91$ in 2005 and $n=12$ in 2010), 2-8 fish were selected to represent the size range of juvenile pollock at each station. Station-specific mean energy density in a given year (\bar{v}_{kt}) was weighted by CPUE and the number of fish processed at each station to calculate the average fish energy density by year (\bar{v}_t).

We ran the model for a single simulation day (i.e., $d=1$) using base scenario input parameter values (Table 3.2; see also [14] Tables I and II) that were kept constant across stations and years (i.e., $W=2.5$ and $\bar{\eta}=1$), were constant across stations but varied by year (i.e., \bar{v}_t), or varied by station and year (i.e., T_{kt} and $\bar{\omega}_{kt}$). Because the model is size-specific, running the model for a single simulation day minimized compound errors that can accumulate over multiple simulation days when predicting growth and allowed for a comparative index of growth across stations. Keeping starting weights (W) constant allowed us to evaluate spatial effects of changes in the other parameters; setting $\eta=1$ implies that growth was constrained by physiological processes, but not by prey consumption, hence we evaluated variability in maximum growth potential. Annual average fish energy density was applied across stations in each year ($\bar{v}_{2005}=3.916 \text{ kJ}\cdot\text{g}^{-1}$ WW; $\bar{v}_{2010}=5.292 \text{ kJ}\cdot\text{g}^{-1}$ WW). The average water temperature in the upper 30 m (T_{kt}) and the biomass-weighted mean prey energy density ($\bar{\omega}_{kt}$) varied by station (k) and year (t).

3.2.4.1 Bioenergetics sensitivity analyses

To test the sensitivity of the model to variability in the inputs, individual input parameters were increased and decreased by 1 standard deviation (SD) and the change in growth relative to maximum predicted growth under the base scenario was recorded. A pooled SD was calculated across stations after removing the annual means. Relative foraging rate ($\bar{\eta}$) was held at 1 for all sensitivity model runs in order to compare the relative effect of other parameters on maximum growth potential.

Station-specific parameters (i.e., T_{kt} and $\bar{\omega}_{kt}$) were increased and decreased by 1 SD at each station to evaluate the relative effect of different inputs on predicted growth and to examine resulting changes in spatially explicit growth patterns in each year. To evaluate the effect of variability in fish start weight and energy density (W_{d-1} and \bar{v}_t , respectively) on estimated growth in 2005 and 2010, we used Monte Carlo simulations at a representative station (see Fig. 3.1). A single station was used because mean fish weight and energy density did not vary across stations in the model; hence the spatial pattern in estimated growth is not affected by increasing or decreasing these values by a constant amount. The model was run 1000 times using parameter values drawn at random from a normal distribution with the observed mean and SD for each parameter. The resulting distribution of predicted maximum growth potential ($g \cdot g^{-1} \cdot d^{-1}$) was visually examined.

3.2.5 Mechanistic individual-based model

A mechanistic, depth-stratified individual-based model (IBM) was used to predict average growth ($g \cdot g^{-1} \cdot d^{-1}$) and depth (m) of 100 simulated juvenile pollock by station. The details of the IBM and model validation are described in [15,26], who modeled growth and foraging of larval Atlantic cod and compared results to observational data

from a macrocosm study in Norway and Georges Bank. For this study, the IBM was reparameterized for juvenile pollock and forced with input data for water column temperatures and prey availability in 1 m discrete depth bins.

The IBM predicted average growth and depth using a mechanistic prey selection component that simulated the feeding behavior of juvenile pollock on zooplankton. The size and species composition of zooplankton available to the fish were based on observations. The simulated feeding ecology depended on juvenile pollock development (e.g., swimming speed, gape width, eye sensitivity) and vertical migratory behavior, prey densities and size, as well as light and physical oceanographic conditions (for details see [15]). Gape width was calculated as a function of fish size; conversion between length and weight followed [27]. Juvenile feeding processes were modeled with light-dependent prey encounter rates and prey-capture success (see [28]). Optimal prey size was estimated to be 5-8% of fish length based on research on larval Atlantic cod [28,29]; juvenile pollock are predicted to have nearly 100% capture success of prey smaller than 5% of fish length, while the probability of capture success decreases with larger prey [15].

Vertical migratory behavior was modeled assuming that juvenile pollock would seek deeper depths to avoid predation risk as long as ingestion rates would sustain metabolism and growth. If not, juvenile fish would seek the euphotic zone where light enhances feeding success, but also increases predation risk. Prey distributions switched between daytime to nighttime profiles when the light level (i.e., irradiance) reached $1 \mu\text{mol}\cdot\text{m}^{-2}\cdot\text{s}^{-1}$ [26]. The cost of vertical migration was included as a maximum of 10% of standard metabolic rates if the fish swims up or down at its maximum velocity, and

scaled proportionally for shorter vertical displacements. Swimming velocity was a function of juvenile fish size [30].

Gut fullness was estimated based on the amount of prey that was ingested and digested per time step (1 hour) according to the feeding module. Prey biomass flowing through the alimentary system supplied growth up to a maximum growth potential (C_{max} ; [24]), and standard metabolic cost, egestion, excretion, and specific dynamic action [14] were subtracted. Both maximum growth and metabolic costs were functions of fish weight and water temperature.

For all base model scenarios, the initial weight of the fish was held constant across stations, while zooplankton abundance and vertical distribution varied according to observations. Initial fish weight was $2.5 \text{ g} \pm 30\%$ assuming a random uniform distribution around the mean. Year-specific vertical profiles (day and night) for the main prey taxa and station-specific temperature and prey abundance profiles were applied. The model scenarios were run for 72 hours, but only the last 24 hours of the simulations were used for the analysis to avoid the early part of the simulations that may be unduly influenced by random initial conditions.

3.2.5.1 IBM sensitivity analyses

To test the sensitivity of the model, we varied starting fish weights and the vertical prey profiles; resulting growth and average depth predictions were compared to predicted values under the base model scenario (see [26] for sensitivity of the IBM model to variability in other parameters). To evaluate the effect of fish size separately from the effects of environmental controls, estimated growth based on starting weights of $2.0 \text{ g} \pm$

30% was compared to the base scenario ($2.5 \text{ g} \pm 30\%$), encompassing the mean weight of juvenile pollock from the BASIS surveys in 2005 ($1.97 \pm 0.93 \text{ g}$, mean \pm SD) and 2010 ($2.39 \pm 0.94 \text{ g}$, mean \pm SD). To test the effect of vertical distributions and diel migrations of prey taxa, model runs assuming a uniform distribution of prey with depth were compared to the base scenario, highlighting the effects of non-uniform zooplankton distribution and diel vertical migrations on juvenile pollock prey selection.

3.2.6 Comparison of observed and predicted prey preferences

Stomach contents of juvenile pollock (<100 mm SL) were identified from selected stations across the EBS shelf to compare observed diet composition, model-predicted diets, and available prey. Chesson's prey preference index [16] was calculated for the main prey taxa in each year and compared to IBM-based estimates of prey preference at corresponding stations. Chesson's index (α_i) for a given prey taxon i is the ratio between ingested prey items (r_i) and the frequency of their occurrence in the environment (n_i), standardized by the sum of the ratios over all m prey types:

$$\alpha_i = \frac{\frac{r_i}{n_i}}{\sum_{j=1}^m \frac{r_j}{n_j}} \quad \text{Eq. 5}$$

The standardization implies that neutral selection (α_{neu}) corresponds to $1/m$ and a specific prey item or group was actively selected if the index is $> \alpha_{neu}$, as they appear more frequently in the diet than their abundance in the environment would suggest. To calculate Chesson's index for observed diets, % volume in the diet was used as a proxy for biomass consumed (r_i) relative to prey biomass in the environment (n_i).

Chesson's prey preference indices for main prey taxa in each year, based on observed and predicted diets, were compared at each station for which observed diet, predicted diet, and zooplankton composition was available and where at least 90% of the observed prey taxa (by % volume) were accounted for in the zooplankton data ($n=7$ in 2005; $n=9$ in 2010). Zooplankton samples that did not include a known prey item were not considered for this analysis because the lack of a known prey item in zooplankton samples collected at the same station suggests that the sample is not representative of prey availability due to small-scale patchiness, or indicates a spatial and/or temporal mismatch between where captured juvenile pollock were foraging and where samples were collected. To compare observed (α^{obs}) and predicted (α^{pre}) prey preferences, we computed differences between these prey preferences relative to neutral selection:

$$\alpha_i^{obs} / \alpha_{neu} - \alpha_i^{pre} / \alpha_{neu} \quad \text{Eq. 6}$$

and averaged them across all stations within each year, as well as by domain (i.e., inner: 0-50 m isobath, middle: 50-100 m isobath, and outer: 100-200 m isobath).

3.3 Results

3.3.1 Field observations

3.3.1.1 Juvenile pollock abundance

Juvenile pollock abundance and distribution had distinct spatial patterns in the surface layer between warm and cold years, with a more northerly distribution in warm years. Specifically, during warm late-summer conditions juvenile pollock were distributed over a broad extent of the middle and outer domain, while in the cooler late summer of 2010

fish were concentrated over small regions of the southern shelf and outer domain (Fig. 3.2). Abundance also varied between years with higher mean CPUE observed in 2005 as compared to 2010 (CPUE = $0.08 \text{ fish}\cdot\text{m}^{-2}$ vs. $0.001 \text{ fish}\cdot\text{m}^{-2}$, respectively) at positive catch stations.

3.3.1.2 Water temperature

The average water temperature in the upper 30 m of the water column during the BASIS survey was 8.8°C in 2005 and 7.6°C in 2010, while the average temperature between 40 m and the substratum was 4.5°C in 2005 and 2.9°C in 2010. The warmest surface temperatures occurred in nearshore waters, while 2005 had warm temperatures over much of the southern shelf (Fig. 3.3, top panel). Bottom temperatures show the extent of the cold pool (waters $<2^{\circ}\text{C}$), which was limited to the northern portion of the study area in 2005 and covered much of the shelf in 2010 (Fig. 3.3, bottom panel).

3.3.1.3 Zooplankton

3.3.1.3.1 Prey taxa

Diets of juvenile pollock shifted from smaller copepod species in the warmer 2005 summer season (e.g., *Pseudocalanus* sp., *C. abdominalis*, and *A. clausi*), to larger species in the cooler 2010 summer season (e.g., *N. cristatus*, *N. plumchrus*, and *E. bungii*).

Several zooplankton species were present in the diets across years, including *L. helicina*, which was the predominant prey item in both years, as well as *C. marshallae* and *T. raschii* (Table 3.1). In 2010, the main prey taxa of juvenile pollock collected in surface tows was similar to those from midwater tows, with the exception of *E. bungii* accounting for 0% and 3% of surface and midwater tows, respectively. *Eucalanus bungii* was

included in further analyses because it represented approximately 3% of combined diets by volume (Table 3.1).

3.3.1.3.2 Zooplankton abundance

Changes in juvenile pollock diet composition reflect spatial and temporal variability in zooplankton species composition and availability. In 2005, the abundance of available prey was highest in the inner domain and decreased towards the outer domain and northern Bering Sea. The abundance of prey in 2010 was greater in the inner domain in the southern region of the shelf, but shifted to the middle and outer domains farther north (Fig. 3.4, a and c). The lowest abundance of zooplankton in 2010 occurred in the southern region of the outer domain (Fig. 3.4c), corresponding to higher concentrations of juvenile pollock predators (Fig. 3.2). The total abundance of zooplankton within the optimal prey size range for 65 mm SL juvenile pollock (species with mean length within 5-8% of fish length) revealed that optimal prey was more abundant in the northwest region of the study area and over the southern shelf in the outer domain in 2005, with lesser overlap with juvenile pollock (Fig. 3.4e). In 2010, optimal prey was located across the middle and outer domains with highest abundances in the southern region, mirroring the distribution of juvenile pollock (Fig. 3.4g). Spatial patterns of zooplankton abundance accounting for all taxa <8% of fish length (not shown) reflected total abundance patterns in both years, indicating that areas of highest zooplankton abundance are driven by small (<5% of fish length) zooplankton taxa (comparison of total abundance plots [Fig. 3.4, a and c] and optimal prey size plots [Fig. 3.4, e and g]).

3.3.1.3.3 Zooplankton biomass

The biomass of available prey was highest in the inner domain and generally lower in the middle and outer domains in 2005, similar to the spatial patterns in abundance (Fig. 3.4b). In 2010, the highest concentrations of prey biomass were located in the southern region of the shelf (south of 60 °N) due to the high abundance of large zooplankton species in this region and overall biomass was higher (Fig. 3.4d).

3.3.1.3.4 Zooplankton energy density

In 2005, available prey energy (i.e., biomass-weighted mean $\bar{\omega}_{kt}$) was highest in the northwest region of the shelf, with low prey energy over most of the shelf south of 60 °N where juvenile pollock abundances were greater (Fig 3.4f). In 2010, concentrations of very high available prey energy were found across much of the southern shelf, particularly within the cold pool, where juvenile pollock were more abundant (Fig. 3.4h). Spatial patterns in high available prey energy were similar to spatial patterns of abundance for optimal prey size classes because highest energy prey taxa are within 5-8% of fish length.

3.3.1.3.5 Zooplankton vertical profiles

Species-specific vertical profiles of abundance suggest a non-uniform distribution with depth and strong diel vertical migrations for some species (Fig. 3.5). *Centropages abdominalis* were not collected by the MOCNESS; because the distribution of *C. abdominalis* during the 2005 and 2010 BASIS surveys was predominantly at shallow, well-mixed stations of the inner domain (inside of the 50 m isobath), a uniform distribution throughout the water column was applied for both years. *Oikopleura* sp. did not occur in daytime tows in 2004; therefore, the 2009 daytime vertical distribution was

applied for both 2005 and 2010 model runs. *Thysanoessa inspinata* were rarely collected by the MOCNESS ($n=1$ for 2005; $n=3$ for 2010), therefore an average vertical profile based on all *Thysanoessa* sp. was applied.

3.3.2 Bioenergetics model

The bioenergetics model results suggest pronounced differences in the spatial patterns of maximum growth potential ($g \cdot g^{-1} \cdot d^{-1}$) of juvenile pollock between a warm and a cold year in the EBS. In the warm year of 2005, growth potential was highest in the northwest region of the shelf (north of 60 °N) and lowest in the inner domain with one station having negative growth. Gradients in growth potential, from low to high, occurred from the inner to outer domains and from southern to northern regions of the shelf (Fig. 3.6a). In the cold year of 2010, growth was positive at all stations. Highest growth potential occurred over the southern region of the shelf with lower growth predicted in the northeast region (Fig. 3.6b).

3.3.2.1 Bioenergetics sensitivity analyses

3.3.2.1.1 Effect of water temperature and prey energy density

In the warm year of 2005, the effect of increasing temperatures by 1 SD varied across the region, with areas of decreased growth at shallow inner domain and southern shelf stations where water temperatures already approached thermal thresholds. Growth could not be estimated at one inner domain station because the increased temperature exceeded 15°C, the maximum temperature for consumption (T_{cm}) in the model (Fig. 3.6c). The effect of decreasing water temperature was also greatest at shallow inner domain and southern shelf stations (not shown), resulting in increased growth, because temperature-

dependent control of growth is magnified where temperatures are close to thermal thresholds. In 2010, the effect of increasing water temperatures was an order of magnitude less than in 2005 (Table 3.3), but the spatial patterns were similar with shallow stations in the inner domain being most sensitive, as well as a small area in the outer domain (Fig. 3.6d).

Increasing available prey energy ($\bar{\omega}_{kt}$) resulted in increases in predicted growth rates across the region in 2005 (Fig. 3.6e), with weaker effects in the inner domain and northwest region. In 2010, increasing prey energy also resulted in increased growth, but effect strengths were much lower than in 2005, and the spatial pattern differed; stronger effects occurred in the inner domain and southern region of the outer domain (Fig. 3.6f).

Predicted maximum growth potential generally increases with temperature and prey energy until temperature-dependent controls limit growth. Predicted growth is negative when available prey energy cannot meet metabolic demands under increased temperatures. Interpolating over the range of observed temperatures and prey energy across 2005 and 2010 provided a continuous scale of growth over a broad range of possible environmental and biological scenarios (Fig. 3.7). Water temperatures were warmer in 2005, therefore juvenile pollock experienced conditions at or near their metabolic threshold at some stations. Colder water temperatures and higher available prey ED in 2010 resulted in better growing conditions over the shelf.

3.3.2.1.2 Effect of fish weight and fish energy density

Increasing fish weight by 1 SD resulted in lower predicted growth rates in both years because larger fish have higher metabolic demands (Table 3.3). Increasing fish energy

density (\bar{v}_t) by 1 SD had a variable effect across stations in 2005, with some stations showing a decrease in growth and other stations showing an increase. In general, the effect of varying fish energy is dependent on initial fish energy and the relative available prey energy ($\bar{\omega}_{kt}$) at each station. In 2010, increasing fish energy density resulted in lower predicted growth rates across stations when available prey energy was held constant (Table 3.3).

Variability in fish starting weight resulted in a broader distribution of predicted growth rates than variability in fish energy for both 2005 and 2010, indicating that the model was more sensitive to inputs of fish weight. The simulated mean predicted growth rates, when varying fish starting weight or fish energy, were lower and less variable for 2005 than for 2010 (Fig. 3.8).

3.3.3 Mechanistic individual-based model

Predicted mean growth rates from the IBM were 30% (2005) and 46% (2010) lower than maximum growth potential from the bioenergetics model (Tables 3.3 and 3.4) as relative foraging rates are restricted in the IBM based on stomach fullness and the prey selection module (i.e., capture success). The reduction in growth was greater in 2010, resulting in similar predicted growth rates from the IBM in 2005 and 2010. In addition, predicted growth rates from the IBM have a narrower range than maximum growth potential from the bioenergetics model.

In 2005, growth was positive across the region with moderate growth predicted across the southern Bering Sea shelf. In the northern Bering Sea (north of 60 °N), predicted growth rates decreased from inner to outer domain (Fig. 3.9a). The average

depth (m) of juvenile pollock was 44 m (Table 3.4), with shallower distributions in the northeast region and deeper distributions in the southern region of the outer domain (Fig. 3.9b). In 2010, growth was positive across the region, with highest predicted growth in the inner domain and areas of lower growth in the middle domain (Fig. 3.9c). The spatial patterns of average depth of juvenile pollock (Fig. 3.9d) mirrored those of 2005 with a slightly deeper average depth of 47 m (Table 3.4).

3.3.3.1 IBM sensitivity analyses

The effect of smaller starting fish weights on predicted growth was positive across the region, with stronger effects in 2005 than 2010 (Table 3.4). Similarly, effect strengths varied spatially in both years with areas of higher predicted growth in the middle domain (Fig. 3.9, e and g). In 2005, smaller starting fish weights resulted in shallower depth distributions across the region (mean=-2.6 m; Table 3.4), with much shallower depths at two stations in the middle domain (Fig. 3.9f). The average change in depth distribution was similar in 2010 (mean=-2.4 m; Table 3.4), but spatially more variable than in 2005. In the outer domain south of 60 °N, changes in fish distribution ranged from 22 m deeper to 43 m shallower (Fig. 3.9h).

Applying uniform vertical distributions to prey taxa had variable effects on predicted growth rates in both years, with similarly small effect strengths (Table 3.4). In 2005, uniform distributions resulted in increased predicted growth rates at several stations in the northern-most region of the shelf (Fig. 3.9i). While the average depth of juvenile pollock was 2.1 m deeper across the region, fish at some of the northern-most stations had shallower depths (Fig. 3.9j). In 2010, strongest effects were observed in the middle

domain of the southern shelf, with high spatial variability (Fig. 3.9k). Changes in the depth of fish in response to uniform prey distributions mirrored spatial patterns in growth effects; stations showing deeper mean depths also resulted in a decrease in growth and vice versa (Fig. 3.9l).

3.3.4 Spatial comparison of bioenergetics- and IBM-predicted growth

While average predicted growth rates from the IBM were within the range of maximum growth potential from the bioenergetics model, spatial patterns varied due to differences in input parameters of each model. In both years, the bioenergetics model predicted higher growth rates than the IBM over the middle and outer domains. The greatest difference occurred in the northwest region of the shelf in 2005 (Fig. 3.10a) and over the southern region of the middle domain in 2010 (Fig. 3.10b). The IBM predicted moderately higher growth in the shallow, well-mixed inner domain in both years.

3.3.5 Comparison of observed and predicted prey preferences

Modeled diets from the IBM were comparable to observed diets from the 2005 and 2010 surveys (Figs. 3.11 and 3.12; most differences overlap zero), indicating that the model may adequately capture predator-prey dynamics. Relatively small differences between observed and predicted prey preference were consistent across domains in both years.

Limacina helicina, the predominant component of diets across years, was more prevalent in observed diets (except in the inner domain south of 60 °N in 2005), as was *T. raschii*.

Modeled diets, however, consistently overestimated consumption of *C. marshallae* and *E. bungii* (2010 only) across domains.

3.4 Discussion

This study demonstrates that warm and cold conditions in the EBS are associated with spatial differences in zooplankton species composition, energy content, and abundance, which subsequently affect the feeding ecology and growth of juvenile pollock.

Particularly, prey distribution and quality in combination with water temperatures create spatial patterns of increased growth potential ('hot spots') that vary with climate conditions. Spatial heterogeneity in growth conditions results from a combination of prey quality and quantity, water temperature, and metabolic costs, which may contribute to size-dependent fish survival and subsequent annual variability in recruitment. We provide evidence that a spatial mismatch between juvenile pollock and growth 'hot spots' in 2005 contributed to poor recruitment to age-1 while a higher degree of overlap in 2010 resulted in 42% greater [31] recruitment to age-1.

Multiple factors affect the early life survival of marine fishes and seminal hypotheses address the interplay of biological and physical controls (e.g., 'critical period hypothesis' [32]; 'stable ocean hypothesis' [33]). Results from our modeling efforts and sensitivity analyses highlight the importance of both prey dynamics and physical oceanographic conditions on juvenile pollock growth. The premise of the match-mismatch hypothesis [1], and the majority of research to date [9,34], is that temporal overlap of predator needs and resource availability regulates recruitment [35]; we expand this to demonstrate that spatial overlap can also modify survival and recruitment success. Additionally, spatial distribution and resource availability can be modified under climate variability [2,36,37,this study].

In the EBS, changes in oceanographic conditions can impact juvenile fish distributions through front formation [38] and subsequent changes in drift trajectories [39]. The resultant variability in larval and early juvenile distributions relative to their prey during late summer and fall may be particularly important because the time period after the completion of larval development and before the onset of winter has been identified as a critical period for energy storage in juvenile pollock [21]. In addition, the late-summer energetic status is considered a reliable predictor of overwinter survival [12]. Therefore, as the spatial distribution of fish, including spawning locations of adult walleye pollock, and zooplankton prey vary under alternate climate conditions, so do patterns in juvenile fish growth and subsequent recruitment success (Fig. 3.13). Here, we find support for the argument that warm years produce smaller, less energy-rich prey and that this reduced prey quality, in combination with higher metabolic demands, results in lower growth of juvenile pollock. Conversely, cold years produce larger, more energy-rich prey which, when combined with lower metabolic demands, are favorable for juvenile pollock growth and survival. Thus, mechanisms responsible for controlling growing conditions during the critical pre-winter period can be linked to variability in recruitment.

Varying model parameters in the sensitivity analyses helped to identify when and where favorable growth conditions may occur across the EBS shelf under alternate climate conditions. Projected declines in walleye pollock recruitment [10] do not account for adaptive behaviors or changes to phenology that could enable fish to maintain higher growth rates under changing climate conditions. In the bioenergetics model, varying fish

size had a stronger effect on growth potential than changes in initial fish energy density. Larger fish have greater capacity for growth due to increased gape size, which allows them to take advantage of larger, more energy rich prey resources (e.g., euphausiids) prior to winter. Increasing water temperatures in the bioenergetics sensitivity runs had a weaker effect in the cold year of 2010 because fish under those conditions had a broader range of temperatures over which growth potential was relatively high (Fig. 3.7), including warmer surface waters and a colder refuge in deeper waters that allows fish to conserve energy and avoid predation. Increasing available prey energy also had a stronger effect in the warm year of 2005 because metabolic demands were greater and mean prey energy density was lower than in 2010.

The relative foraging rate was held constant at $\eta=1$ across all bioenergetics model scenarios to estimate maximum growth potential, but lower values would better reflect realistic foraging rates and could exacerbate thermal constraints on growth. To maintain positive growth rates at half of all the stations required relative foraging rates of $\eta=0.71$ in 2005 and $\eta=0.57$ in 2010. These values correspond to a 29% and 43% reduction in achieved growth relative to maximum growth potential (i.e., $\eta=1$) and are similar to the mean differences between growth rates in the bioenergetics and IBM models (i.e., 30% in 2005 and 46% in 2010), providing support of model agreement. A higher relative foraging rate was required in 2005 in order to achieve positive growth at half of all stations, similar to results based on larger juvenile and adult walleye pollock [24], indicating that juvenile pollock growth was more prey limited and constrained by temperature in 2005 than in 2010. Thus, a greater reduction in both achieved growth from

the IBM relative to maximum growth potential and relative foraging rates was observed in 2010 compared to 2005.

While the horizontal distribution of larval and early juvenile pollock is largely determined by oceanographic conditions, changes in vertical behavior could lead to increased growth potential. The IBM allows for complex larval and juvenile behavioral responses to changes in the environment. Vertical behavior in the model aims to maximize prey ingestion while minimizing predation risk. Predation risk was based on the visibility of juvenile pollock to predators at the given light conditions. Smaller (i.e., younger) fish were predicted to move shallower in the water column to improve prey detection, which is dependent on eye development and light availability. Moving into the surface layer also exposed juvenile pollock to higher predation risk because of the stronger light intensity and thereby visibility to predators. Applying uniform vertical prey distributions instead of observed distributions in the IBM had very weak effects across the EBS shelf in both years. Under uniform prey distributions, modeled fish may move vertically in response to other cues (i.e., predation risk, thermal boundaries) regardless of diel patterns.

A comparison of observed and IBM predicted diets provided a better understanding of prey preferences and the importance of individual prey taxa under varying climate conditions. For example, shifts in *C. marshallae* abundance between warm and cold years in the EBS have been proposed as a major contributor to differences in juvenile pollock condition and survival [13]. However, observed diets of juvenile pollock (<100 mm SL) in 2005 and 2010 do not reflect its relative importance to growth

because *C. marshallae* was less prevalent than expected. Greater prevalence of specific prey items in observed diets (e.g., *Centropages abdominalis* in 2005) indicates that the IBM model underestimates the ability of juvenile pollock to detect, capture, and ingest that prey item. Alternatively, the prey could have been more abundant in the areas where juvenile pollock were feeding than in the area sampled by the bongo and/or Juday net due to patchiness. Differences between observed and predicted diets may also be explained by prey escape behaviors or size-selectivity by juvenile pollock that is more complex than the prey selection component of the IBM [40]. Juvenile pollock collected in late-summer (~65 mm SL) likely feed more heavily in surface waters during crepuscular or nighttime periods [41], moving deeper during the daytime, while observed diets for this study were sampled from daytime surface hauls. However, the spatial and temporal disconnect between where juvenile pollock feed and were collected for diet analyses likely did not affect our results as previous work has shown that proportional diet compositions do not vary between day and night [41,42] and the IBM integrates predicted diets over 24 hours, encompassing diel vertical patterns.

Our comparative model approach allowed us to evaluate the relative role of prey availability and water temperature on juvenile pollock growth. Spatial patterns in growth differed between the models; these differences elucidate underlying mechanisms in the feeding potential and ultimately possible causes for growth 'hot spots' and variability in recruitment success between warm and cold climate conditions. The bioenergetics model incorporates a biomass-weighted mean energy density of available prey, assuming fish feed proportional to what is available in the environment. The IBM is length-based and

growth is dependent on prey size selection, gut fullness, and vertical movements to minimize predation risk. By comparing spatial patterns in growth between the models, similar trends emerged that indicate mechanisms leading to areas of increased growth. In the middle and outer domains where the water column is stratified, the bioenergetics model predicted higher growth than the IBM; the bioenergetics model allowed fish to feed at maximum consumption ($\eta=1$) while the IBM indicates fish move deeper in the water column to conserve energy or avoid predation. In the inner domain, the IBM predicted higher growth; here juvenile pollock may opt to take advantage of available prey and warmer water temperatures to maximize growth because predator avoidance in deeper waters is not an option.

Behavioral responses of modeled juvenile pollock in the IBM moderate predicted growth rates leading to differences across domains in the EBS based on stratification. In the middle and outer domains, once sufficient growth is attained fish will move deeper to seek refuge from predation. While the bioenergetics and IBM models were run at all stations in both years, observed juvenile pollock abundances were concentrated over the middle and outer domains in 2005 and over small regions of the southern shelf and outer domain in 2010. Few fish were observed in the well-mixed inner domain, possibly due to reduced growth potential based on available prey energy or lack of stratification and predation refuge in deeper waters. Additionally, the inner front, which delineates the stratified middle domain from the well-mixed inner domain [38], may act as a barrier to juvenile pollock distribution [43].

The importance of prey quality, temperature-dependent relationships, and size selective predation differ between warm and cold years for the EBS. In 2005 (a warm year), predicted growth was more sensitive to increases in temperature than changes in prey energy, resulting in greater reductions in growth. Further, both models predicted similar spatial patterns in 2005 indicating that prey energy (input to bioenergetics model) and size selection (IBM input) have less influence than temperature on estimates of growth in that year. The relative effect of increasing temperatures was greater in 2005 than in 2010 because fish in 2005 were near thermal limits based on temperature-dependent functions in the bioenergetics model over much of the EBS shelf; hence further increases in temperature are predicted to result in negative growth. In addition to warmer water temperatures in 2005, the spatial overlap of juvenile pollock and growth ‘hot spots’ was lower than in 2010, further limiting fish growth. In 2010, the effect of increased temperatures was an order of magnitude less than in 2005; therefore, prey quality appears more indicative of growth in cold years under maximum consumption scenarios.

Warm temperature conditions are predicted to result in reduced prey quality and low energy density of juvenile pollock in late summer [8,12]. Warmer water temperatures are associated with decreased growth [this study], resulting in lower overwinter survival and recruitment to age-1 [31]. The warm years of 2002-2005 had 67% lower average recruitment to age-1 relative to the cold years of 2008-2010 [31]. These findings agree with projected declines in recruitment of age-1 walleye pollock [10] under increased summer sea surface temperatures of 2°C predicted by 2050 [44]. Our results corroborate

these previous studies and suggest that climate-driven increases in water temperature will have the largest effect on recruitment during anomalously warm years.

3.5 Conclusions

This study provides evidence that climate-driven changes in prey dynamics may have ecosystem-level consequences via bottom-up control of fish populations in sub-arctic marine ecosystems (Fig. 3.13). This work has improved our understanding of the mechanisms behind recruitment variability, in particular the underlying spatial patterns that drive relationships between prey availability, water temperature, growth, and survival. Our findings inform ongoing discussions of climate effects on predator-prey interactions and recruitment success of marine fishes.

3.6 Acknowledgements

We thank NOAA's Bering Aleutian Salmon International Survey (BASIS) program for data collection and database management as well as the officers and crew of the R/V *Oscan Dyson* and F/V *Sea Storm*. The BASIS program is funded in part by the North Pacific Anadromous Fish Commission. MOCNESS data were provided from the PROBES (2004) and BEST-BSIERP (2009) surveys. The North Pacific Research Board provided funding for this project.

3.7 References

1. Cushing DH (1990) Plankton production and year-class strength in fish populations – an update of the match mismatch hypothesis. *Advances in Marine Biology* 26: 249-293.
2. Durant JM, Hjermann DO, Ottersen G, Stenseth NC (2007) Climate and the match or mismatch between predator requirements and resource availability. *Climate Research* 33: 271-283.
3. Edwards M, Richardson AJ (2004) Impact of climate change on marine pelagic phenology and trophic mismatch. *Nature* 430: 881-884.
4. Hunt GL Jr, Stabeno PJ, Walters G, Sinclair E, Brodeur RD, Napp JM, Bond NA (2002) Climate change and control of the southeastern Bering Sea pelagic ecosystem. *Deep-Sea Research II* 49: 5821-5853.
5. Sogard SM, Olla BL (2000) Endurance of simulated winter conditions by age-0 walleye pollock: effects of body size, water temperature and energy storage. *Journal of Fish Biology* 56: 1-21.
6. Litzow MA, Bailey KM, Prahlg FG, Heintz R (2006) Climate regime shifts and reorganization of fish communities: the essential fatty acid limitation hypothesis. *Marine Ecology Progress Series* 315: 1–11.
7. Paul AJ, Paul JM (1998) Comparisons of whole body energy content of captive fasting age zero Alaskan Pacific herring (*Clupea pallasii* Valenciennes) and cohorts over-wintering in nature. *Journal of Experimental Marine Biology and Ecology*. 226: 75–86.
8. Hunt GL Jr, Coyle KO, Eisner L, Farley EV, Heintz R, Mueter FJ, Napp JM, Overland JE, Ressler PH, Salo S, Stabeno PJ (2011) Climate impacts on eastern Bering Sea foodwebs: A synthesis of new data and an assessment of the Oscillating Control Hypothesis. *ICES Journal of Marine Sciences* 68(6): 1230-1243.
9. Beaugrand G, Brander KM, Lindley JA, Souissi S, Reid PC (2003) Plankton effect on cod recruitment in the North Sea. *Nature* 426: 661-664.
10. Mueter FJ, Bond NA, Ianelli JN, Hollowed AB (2011) Expected declines in recruitment of walleye pollock (*Theragra chalcogramma*) in the eastern Bering Sea under future climate change. *ICES Journal of Marine Science* 68: 1284–1296.

11. Stabeno PJ, Kachel NB, Moore SE, Napp JM, Sigler M, Yamaguchi A, Zerbini AN (2012) Comparison of warm and cold years on the southeastern Bering Sea shelf and some implications for the ecosystem. *Deep-Sea Research II* 65-70: 31-45.
12. Heintz RA, Siddon EC, Farley EV Jr, Napp JM (In press) Correlation between recruitment and fall condition of age-0 walleye pollock (*Theragra chalcogramma*) from the eastern Bering Sea under varying climate conditions. *Deep-Sea Research II*.
13. Coyle KO, Eisner LB, Mueter FJ, Pinchuk AI, Janout MA, Ciciel KD, Farley EV, Andrews AG (2011) Climate change in the southeastern Bering Sea: impacts on pollock stocks and implications for the Oscillating Control Hypothesis. *Fisheries Oceanography* 20(2): 139-156.
14. Ciannelli L, Brodeur RD, Buckley TW (1998) Development and application of a bioenergetics model for juvenile walleye pollock. *Journal of Fish Biology* 52: 879-898.
15. Kristiansen T, Lough RG, Werner FE, Broughton EA, Buckley LJ (2009) Individual-based modeling of feeding ecology and prey selection of larval cod on Georges Bank. *Marine Ecology Progress Series* 376: 227-243.
16. Chesson J (1978) Measuring preference in selective predation. *Ecology* 59: 211-215.
17. Farley EV, Murphy JM, Wing BW, Moss JH, Middleton A (2005) Distribution, migration pathways, and size of western Alaska juvenile salmon along the eastern Bering Sea shelf. *Alaska Fishery Research Bulletin* 11: 15-26.
18. Moss JH, Farley EV Jr, Feldmann AM, Ianelli JN (2009) Spatial distribution, energetic status, and food habits of eastern Bering Sea age-0 walleye pollock. *Transactions of the American Fisheries Society* 138: 497-505.
19. Volkov AF, Efimkin AY, Kuznetsova NA (2007) Characteristics of the plankton community of the Bering Sea and several regions of the North Pacific in 2002 – 2006. *Izvestiya Tikhookeanskiy Nauchno-Issledovatel'skiy Institut Rybnogo Khozyaystva I Okeanografii* 151: 338–364 (in Russian).
20. Coyle KO, Pinchuk AI, Eisner LB, Napp JM (2008) Zooplankton species composition, abundance and biomass on the eastern Bering Sea shelf during summer: the potential role of water column stability and nutrients in structuring the zooplankton community. *Deep Sea Research II* 55: 1755–1791.

21. Siddon EC, Heintz RA, Mueter FJ (2013) Conceptual model of energy allocation in walleye pollock (*Theragra chalcogramma*) from age-0 to age-1 in the southeastern Bering Sea. Deep-Sea Research II. <http://dx.doi.org/10.1016/j.dsr2.2012.12.007>.
22. Kitchell JF, Stewart DJ, Weininger D (1977) Applications of a bioenergetics model to perch (*Perca flavescens*) and walleye (*Stizostedion vitreum*). Journal of the Fisheries Research Board of Canada 34: 1922–1935.
23. Ney JJ (1990) Trophic economics in fisheries: assessment of demand–supply relationships between predators and prey. Reviews in Aquatic Sciences 2:55–81.
24. Holsman KK, Aydin K (In prep) Comparative field and bioenergetics-based methods for evaluating climate change impacts on the foraging ecology of Alaskan walleye pollock (*Theragra chalcogramma*), Pacific cod (*Gadus macrocephalus*), and arrowtooth flounder (*Atheresthes stomias*).
25. Hanson P, Johnson T, Schindler D, Kitchell J (1997) Fish Bioenergetics 3.0. Madison, WI: University of Wisconsin Sea Grant Institute.
26. Kristiansen T, Fiksen Ø, Folkvord A (2007) Modelling feeding, growth, and habitat selection in larval Atlantic cod (*Gadus morhua*): observations and model predictions in a macrocosm environment. Canadian Journal of Fisheries and Aquatic Sciences 64: 136-151.
27. Buchheister A, Wilson MT, Foy RJ, Beauchamp DA (2006) Seasonal and geographic variation in condition of juvenile walleye pollock in the western Gulf of Alaska. Transactions of the American Fisheries Society 135: 897-907.
28. Fiksen O, MacKenzie BR (2002) Process-based models of feeding and prey selection in larval fish. Marine Ecology Progress Series 243: 151–164.
29. Munk P (1997) Prey size spectra and prey availability of larval and small juvenile cod. Journal of Fish Biology 51(Suppl A): 340–351.
30. Peck MA, Buckley LJ, Bengtson DA (2006) Effects of temperature and body size on the swimming speed of larval and juvenile Atlantic cod (*Gadus morhua*): implications for individual-based modelling. Environmental Biology of Fishes 75: 419–429.
31. Ianelli JN, Honkalehto T, Barbeaux S, Kotwicki S, Aydin K, Williamson N (2012) Assessment of the walleye pollock stock in the Eastern Bering Sea. In: Stock assessment and fishery evaluation report for the groundfish resources of the

- Bering Sea/Aleutian Islands regions. North Pacific Fishery Management Council, 605 W. 4th Ave., Suite 306, Anchorage, AK 99501. 106 pp.
32. Hjort J (1914) Fluctuations in the great fisheries of Northern Europe viewed in the light of biological research. *Rapports et Procès-Verbaux des Réunions du Conseil International pour l'Exploration de la Mer* 20: 1–228.
 33. Lasker R (1975) Field criteria for the survival of anchovy larvae: the relation between inshore chlorophyll maximum layers and successful first feeding. *Fishery Bulletin* 73: 847–855.
 34. Brander KM, Dickson RR, Shepherd JG (2001) Modelling the timing of plankton production and its effect on recruitment of cod (*Gadus morhua*). *ICES Journal of Marine Science* 58: 962–966.
 35. Leggett WC, Deblois E (1994) Recruitment in marine fishes: is it regulated by starvation and predation in the egg and larval stages? *Netherlands Journal of Sea Research* 32(2): 119-134.
 36. Chick JH, Van Den Avyle MJ (1999) Zooplankton variability and larval striped bass foraging: evaluating potential match/mismatch regulation. *Ecological Applications* 9(19): 320–334.
 37. Kristiansen T, Drinkwater KF, Lough RG, Sundby S (2011) Recruitment variability in North Atlantic cod and match-mismatch dynamics. *PLoS ONE* 6(3): e17456. doi:10.1371/journal.pone.0017456.
 38. Kachel NB, Hunt GL Jr, Salo SA, Schumacher JD, Stabeno PJ, Whitley TE (2002) Characteristics and variability of the inner front of the southeastern Bering Sea. *Deep-Sea Research II* 49: 5889–5909.
 39. Duffy-Anderson JT, Busby MS, Mier KL, Deliyaniades CM, Stabeno PJ (2006) Spatial and temporal patterns in summer ichthyoplankton assemblages on the eastern Bering Sea shelf 1996–2000. *Fisheries Oceanography* 15: 80–94.
 40. Petrik CM, Kristiansen T, Lough RG, Davis CS (2009) Prey selection of larval haddock and cod on copepods with species-specific behavior: a model-based analysis. *Marine Ecology Progress Series* 396: 123-143.
 41. Brodeur RD, Wilson MT, Ciannelli L (2000) Spatial and temporal variability in feeding and condition of age-0 walleye pollock (*Theragra chalcogramma*) in frontal regions of the Bering Sea. *ICES Journal of Marine Science* 57: 256–264.
 42. Schabetsberger R, Brodeur RD, Ciannelli L, Napp JM, Swartzman GL (2000)

- Diel vertical migration and interaction of zooplankton and juvenile walleye pollock (*Theragra chalcogramma*) at a frontal region near the Pribilof Islands, Bering Sea. *ICES Journal of Marine Science* 57: 1283–1295.
43. Logerwell EA, Duffy-Anderson JT, Wilson M, McKelvey D (2010) The influence of pelagic habitat selection and interspecific competition on productivity of juvenile walleye pollock (*Theragra chalcogramma*) and capelin (*Mallotus villosus*) in the Gulf of Alaska. *Fisheries Oceanography* 19: 262-278.
 44. Hollowed AB, Bond NA, Wilderbuer TK, Stockhausen WT, A'mar ZT, Beamish RJ, Overland JE, Schirripa MJ (2009) A framework for modelling fish and shellfish responses to future climate change. *ICES Journal of Marine Science* 66: 1584–1594.
 45. Gardner GA, Szabo I (1982) British Columbia pelagic marine copepoda: an identification manual and annotated bibliography. Canadian Special Publication of Fisheries and Aquatic Sciences 62. 536 p.
 46. Yamamoto T, Teruya K, Hara T, Hokazono H, Hashimoto H, Suzuki N, Iwashita Y, Matsunari H, Furuita H, Mushiake K (2008) Nutritional evaluation of live food organisms and commercial dry feeds used for seed production of amberjack *Seriola dumerili*. *Fisheries Science* 74: 1096-1108.
 47. Lough RG, Buckley LJ, Werner FE, Quinlan JA, Edwards KP (2005) A general biophysical model of larval cod (*Gadus morhua*) growth applied to populations on Georges Bank. *Fisheries Oceanography* 14: 241-262.
 48. Lee RF, Hagen W, Kattner G (2006) Lipid storage in marine zooplankton. *Marine Ecology Progress Series* 307: 273-306.
 49. Tomita M, Ikeda T, Shiga N (1999) Production of *Oikopleura longicauda* (Tunicata: Appendicularia) in Toyama Bay, southern Japan Sea. *Journal of Plankton Research* 21(12): 2421-2430.
 50. Frost BW (1989) A taxonomy of the marine calanoid copepod genus *Pseudocalanus*. *Canadian Journal of Zoology* 67: 525-551.
 51. Peters J (2006) Lipids in key copepod species of the Baltic Sea and North Sea – implications for life cycles, trophodynamics and food quality. PhD Dissertation. University of Bremen. 177 p.
 52. Pinchuk AI, Coyle KO (2008) Distribution, egg production and growth of euphausiids in the vicinity of the Pribilof Islands, southeastern Bering Sea, August 2004. *Deep-Sea Research II* 55: 1792-1800.

53. Pinchuk AI, Hopcroft RR (2007) Seasonal variations in the growth rates of euphausiids (*Thysanoessa inermis*, *T. spinifera*, and *Euphausia pacifica*) from the northern Gulf of Alaska. *Marine Biology* 151: 257-269.
54. Kathman RD, Austin WC, Saltman JC, Fulton JD (1986) Identification manual to the Mysidacea and Euphausiacea of the northeast Pacific. Canadian Special Publications of Fisheries and Aquatic Sciences 93. 411 p.
55. Falk-Petersen S (1985) Growth of the euphausiids *Thysanoessa inermis*, *Thysanoessa raschii*, and *Meganyctiphanes norvegica* in a subarctic fjord, North Conway. *Canadian Journal of Fisheries and Aquatic Sciences* 42: 14-22.

Table 3.1. Dominant prey taxa included in the models for 2005 and 2010. Prey items cumulatively accounting for at least 90% of the diet by % volume and individually accounting for at least 2% of the diet by % volume were included.

Prey taxa common to both years are shown in **bold**.

2005			2010		
Taxa	Individ % Vol	Cum % Vol	Taxa	Individ % Vol	Cum % Vol
<i>Limacina helicina</i>	26.33		<i>Limacina helicina</i>	35.45	
<i>Pseudocalanus</i> sp.	26.04	52.4	<i>Thysanoessa inermis</i>	27.08	62.5
<i>Oikopleura</i> sp.	11.86	64.2	<i>Calanus marshallae</i>	13.87	76.4
<i>Centropages abdominalis</i>	8.98	73.2	<i>Neocalanus cristatus</i>	4.84	81.2
<i>Thysanoessa raschii</i>	8.48	81.7	<i>Thysanoessa inspinata</i>	3.16	84.4
<i>Thysanoessa</i> sp.	4.63	86.3	<i>Thysanoessa raschii</i>	3.09	87.5
<i>Acartia clausi</i>	3.40	89.7	<i>Neocalanus plumchrus</i> *	2.98	90.5
<i>Calanus marshallae</i>	1.71	91.4	<i>Eucalanus bungii</i>	2.95	93.4

**Neocalanus plumchrus* was not identified in the 2010 bongo data, but did occur in the Juday data (small-mesh; not quantitative for large zooplankton taxa). Due to the absence in the bongo data, *N. plumchrus* was excluded from further analyses.

Table 3.2. Parameter definitions and values used in the bioenergetics model to estimate maximum growth potential ($g \cdot g^{-1} \cdot d^{-1}$) of juvenile walleye pollock. Parameters were used as inputs to the bioenergetics model described in [14].

Parameter	Definition (units)	Value	Reference
C	Consumption ($g \cdot g^{-1} \cdot d^{-1}$)		
η	Relative foraging rate	0-1	<i>a</i>
O_2 cal	Activity multiplier; convert g $O_2 \rightarrow$ g prey	13560	<i>a</i>
α	Intercept of the allometric function for C	0.119	<i>a</i>
β	Slope of the allometric function for C	-0.46	<i>a</i>
Q_c	Temperature dependent coefficient	2.6	<i>b</i>
T_{co}	Optimum temperature for consumption	10	<i>b</i>
T_{cm}	Maximum temperature for consumption	15	<i>b</i>
R	Respiration ($g O_2 \cdot g^{-1} \cdot day^{-1}$)		
A_r	Intercept of the allometric function for R	0.0075	<i>b</i>
B_r	Slope of the allometric function for R	-0.251	<i>b</i>
Q_r	Temperature dependent coefficient	2.6	<i>b</i>
T_{ro}	Optimum temperature for respiration	13	<i>b</i>
T_{rm}	Maximum temperature for respiration	18	<i>b</i>
D_s	Proportion of assimilated energy lost to Specific Dynamic Action	0.125	<i>b</i>
A_m	Multiplier for active metabolism	2	<i>b</i>
F	Egestion		
F_a	Proportion of consumed energy	0.15	<i>b</i>
U	Excretion		
U_a	Proportion of assimilated energy	0.11	<i>b</i>

^a [24]; ^b [14]

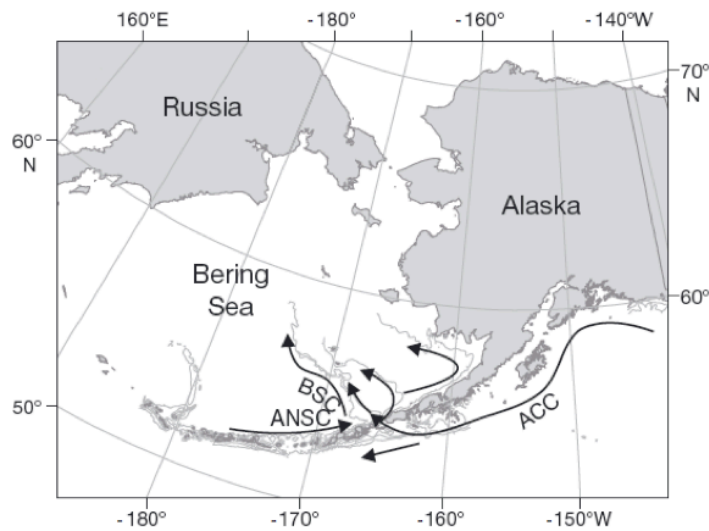
Table 3.3. Summary of sensitivity analyses for the bioenergetics model in 2005 and 2010 showing the minimum, mean, and maximum growth potential over all stations. Base values are predicted maximum growth potential ($g \cdot g^{-1} \cdot d^{-1}$) from the base model scenarios ($W=2.5$ g, Temp=average temperature in upper 30 m, $P=1.0$, ω_k =prey energy density, $\bar{v}_{2005}=3.916$ $\text{kJ} \cdot \text{g}^{-1}$ WW; $\bar{v}_{2010}=5.292$ $\text{kJ} \cdot \text{g}^{-1}$ WW). All other values denote the change in growth rate resulting from indicated changes in inputs; therefore (-) effects indicate that varied conditions resulted in lower predicted growth and vice versa. Pooled standard deviations (SDs) for each parameter were calculated across stations after removing the annual means. W and v_t are constant values applied across all station, so changes (± 1 SD) act as a scalar and results in similar spatial patterns across the area. Temperature and ω_k vary across stations.

		2005			2010		
Parameter	SD	min	mean	max	min	mean	max
Base		-0.00557	0.01458	0.02913	0.00687	0.01716	0.0272
$W + 1$ SD	0.935	-0.00562	-0.00407	-0.00169	-0.00516	-0.0037	-0.00225
$W - 1$ SD	0.935	0.00343	0.00758	0.01025	0.00414	0.0068	0.00939
Temp + 1 SD	1.75	-0.02269	-0.00527	0.00172	-0.00708	-0.00074	0.00178
Temp - 1 SD	1.75	-0.00276	0.00178	0.01293	-0.00257	0.00075	0.00301
$\omega_k + 1$ SD	497.5	0.00457	0.0061	0.00645	0.00321	0.00436	0.00477
$\omega_k - 1$ SD	497.5	-0.00645	-0.0061	-0.00457	-0.00477	-0.00436	-0.00321
$v_t + 1$ SD	395.93	-0.00267	-0.00134	0.00051	-0.00189	-0.00119	-0.00048
$v_t - 1$ SD	395.93	-0.00062	0.00164	0.00328	0.00056	0.00139	0.0022

Table 3.4. Summary of sensitivity analyses for the IBM model in 2005 and 2010 showing the minimum, mean, and maximum growth potential and depth over all stations. Base values are predicted growth ($g \cdot g^{-1} \cdot d^{-1}$) and depth of juvenile walleye pollock over 24 hours from the base model scenarios ($W=2.5$ g, zooplankton prey distributed according to vertical profiles). All other values are predicted changes in growth and depth. Negative changes in depth indicate a shallower distribution; positive values indicate a deeper distribution. Weight is a constant value applied across all station, so varying the parameter acts as a scalar and results in similar spatial patterns across the area. The effect of applying a uniform distribution of zooplankton prey with depth varies across stations.

		2005			2010		
Parameter		min	mean	max	min	mean	max
Base	Growth	0.0062	0.0102	0.01213	0.00554	0.00922	0.01227
	Depth	10	44.2	80.9	15	47.4	93
W (2.0 g)	Growth	0.00401	0.01843	0.05115	0.00196	0.00681	0.02539
	Depth	-0.14	2.6	30.5	-21.7	2.4	43.3
Prey distribution (Uniform)	Growth	-0.00094	0.005	0.00583	-0.00342	0.00095	0.00635
	Depth	-15.8	-2.1	21.4	-35.2	1.8	42.9

a)



b)

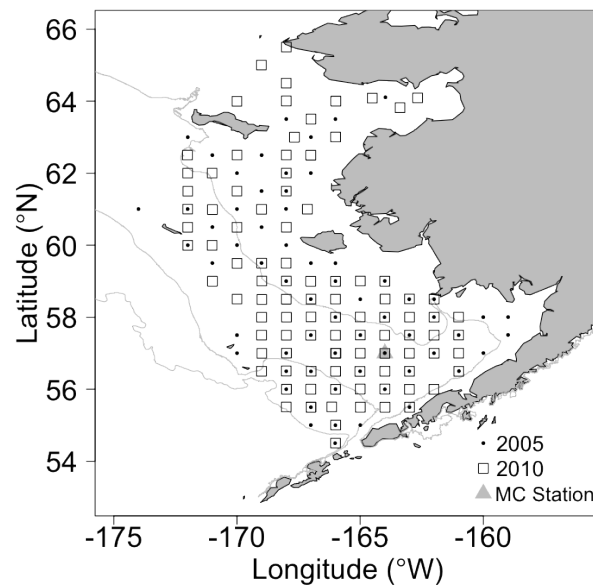


Figure 3.1. (a) Bering Sea with predominant currents in the study region, including the Aleutian North Slope Current (ANSC), the Bering Slope Current (BSC), and the Alaska Coastal Current (ACC). (b) Eastern Bering Sea with locations of sampling stations at which the bioenergetics model and IBM models were run in 2005 (•) and 2010 (□). MC Station (▲) is the representative station used for Monte Carlo simulations. Depth contours are shown for the 50 m, 100 m, and 200 m isobaths.

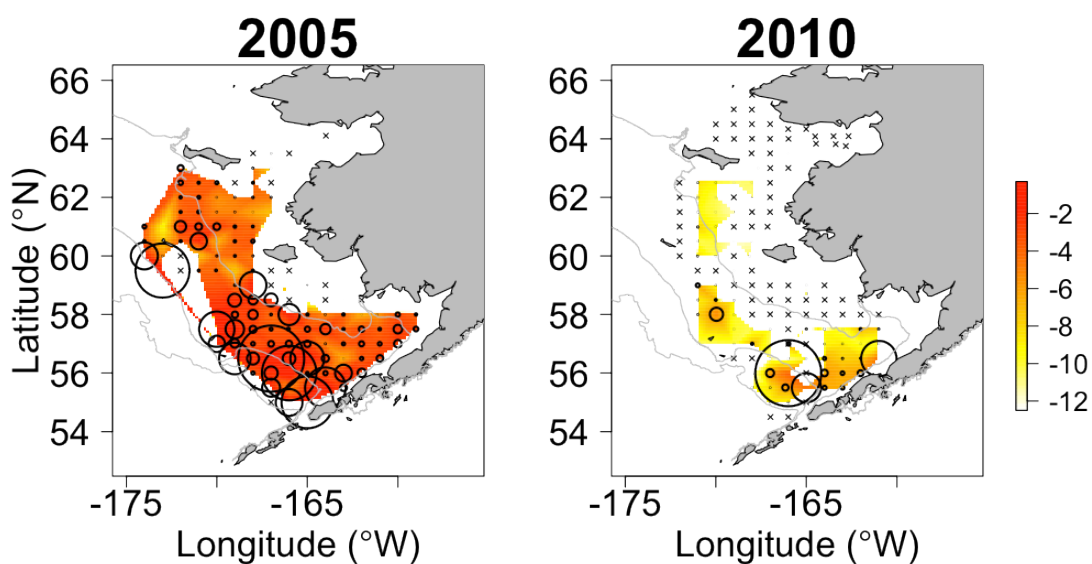


Figure 3.2. Log(CPUE) of juvenile walleye pollock collected in surface trawls in 2005 (a) and 2010 (b). Circle size is proportional to catch at each station; stations with zero catch (x) are on white background.

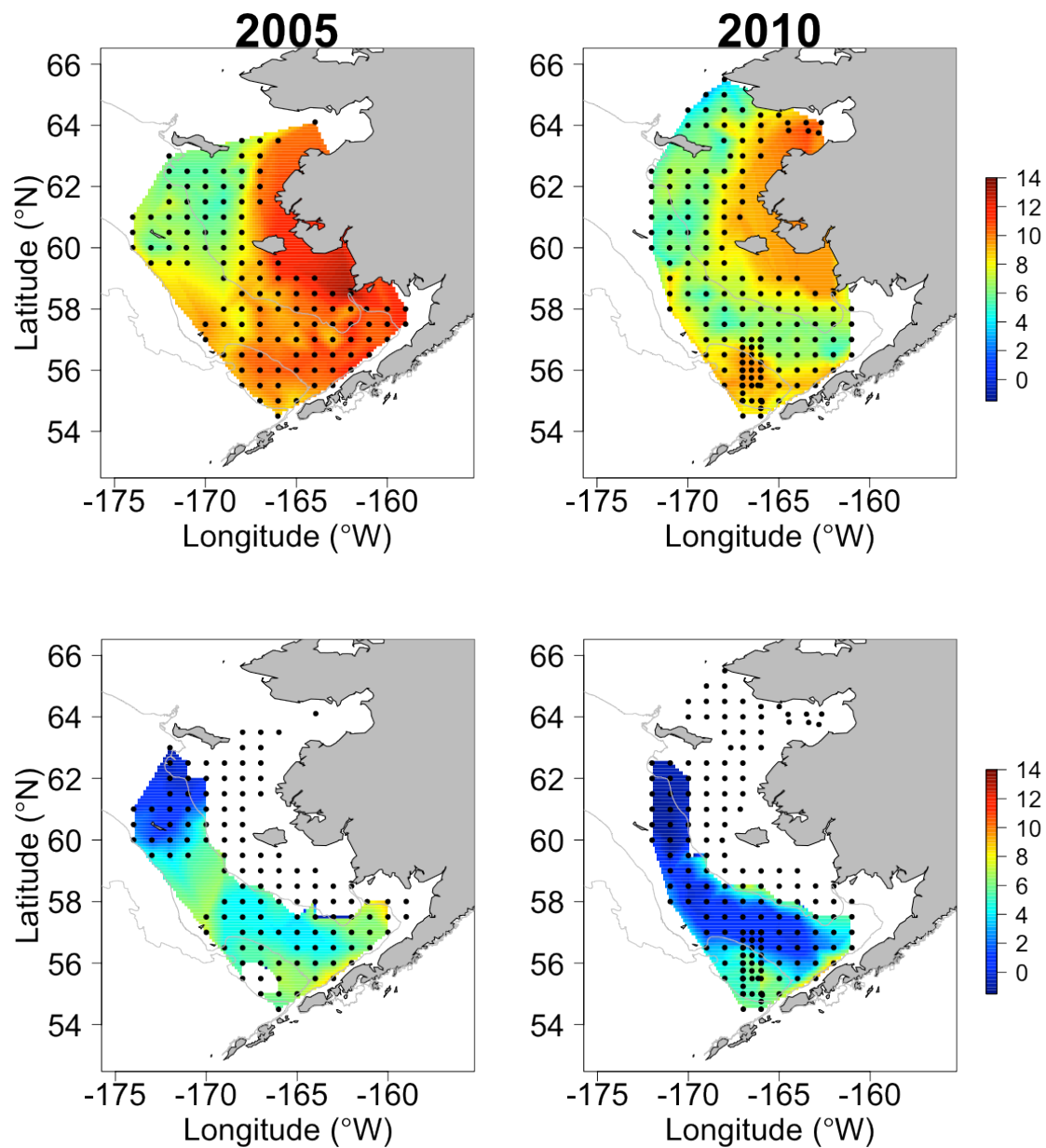


Figure 3.3. Water temperatures in 2005 and 2010 interpolated across all stations (•) sampled by the CTD. Upper row shows the mean temperature in the upper 30 m of the water column. Lower row shows the mean temperature below 40 m.

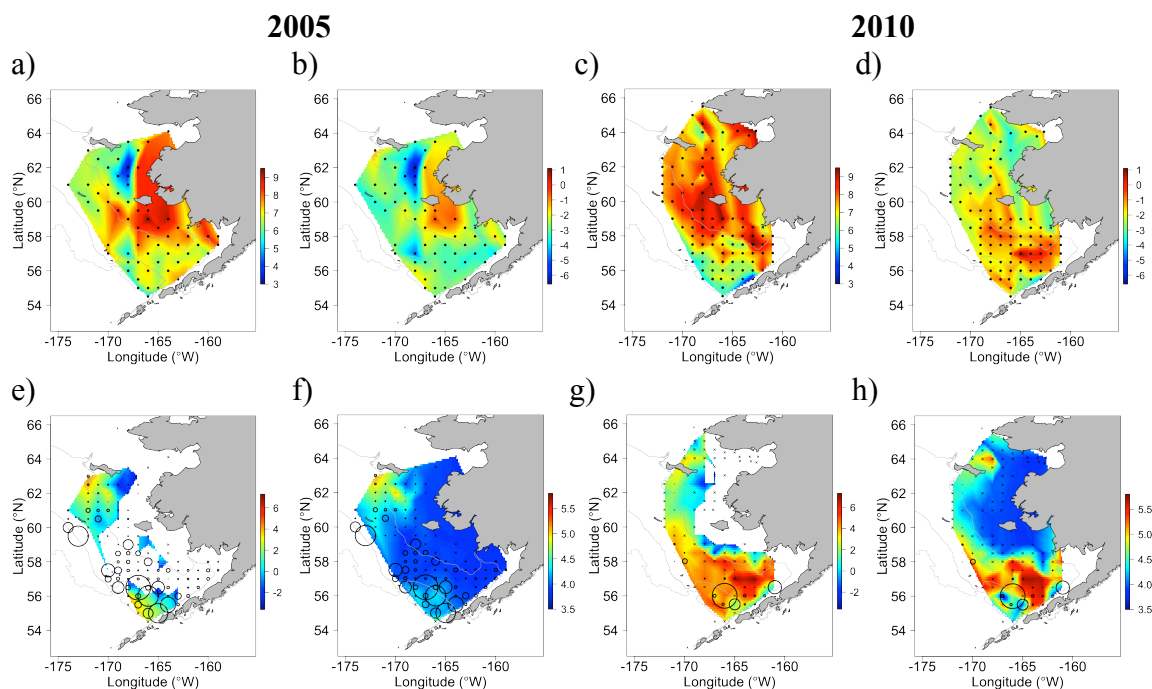


Figure 3.4. Zooplankton prey availability in the eastern Bering Sea in 2005 and 2010.

Upper row shows the log of total abundance (a and c) and log of total biomass (g WW; b and d) in each year. Lower row shows the log of total abundance for zooplankton within the optimal size range for 65 mm SL juvenile walleye pollock (5-8% of fish length; e and g) and the biomass-weighted mean energy density (f and h) of available zooplankton prey in each year. The CPUE of juvenile walleye pollock collected in surface trawls is overlaid in e-h. Circle size is proportional to catch at each station (\times =zero catch).

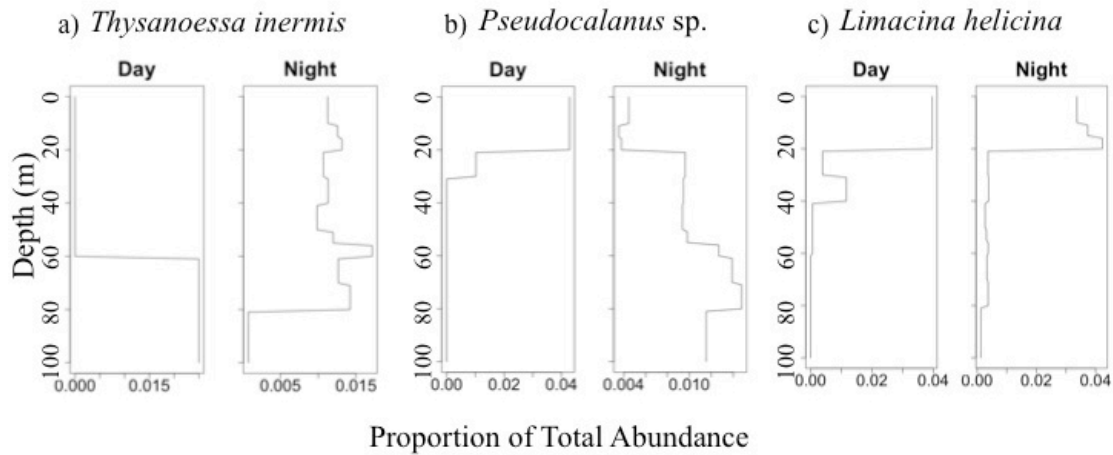


Figure 3.5. Vertical profiles of abundance for representative main prey taxa from a cold year. (a) *Thysanoessa inermis* has a strong diel migration with distribution shifting from deeper during day to more shallow at night. (b) *Pseudocalanus* sp. displays an opposite behavior, shallow distribution during the day and deeper at night. (c) *Limacina helicina*, the dominant prey item in 2005 and 2010, does not display strong diel migration, with a shallow distribution during day and night.

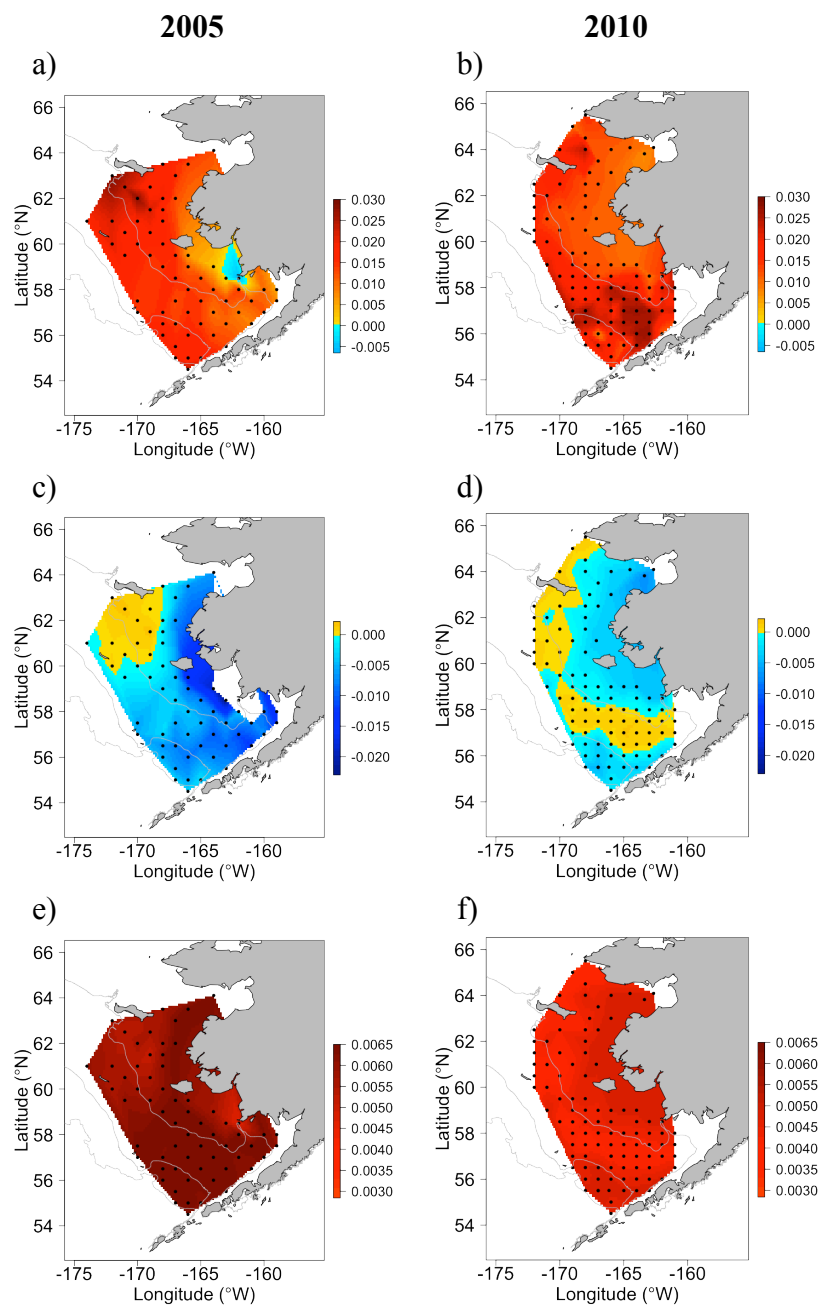


Figure 3.6. Maximum predicted growth of juvenile walleye pollock ($g \cdot g^{-1} \cdot d^{-1}$) from the bioenergetics model. Top row shows growth under the base scenarios for 2005 and 2010 (a and b, respectively). Middle row (c-d) shows changes in predicted growth when

Figure 3.6. Continued

temperature is increased by 1 standard deviation (SD). Predicted growth could not be estimated at one station (panel c) in the inner domain under increased temperatures because the water temperature in the upper 30 m was greater than 15 °C ($T_{cm} = 15$ °C in the model). Lower row shows changes in predicted growth when prey energy density is increased by 1 SD in 2005 and 2010 (e and f, respectively). Spatial plots of predicted growth when parameters are lowered by 1 SD are not shown, but can be visualized by subtracting the anomalies (lower two rows) from the base scenario plots (top row).

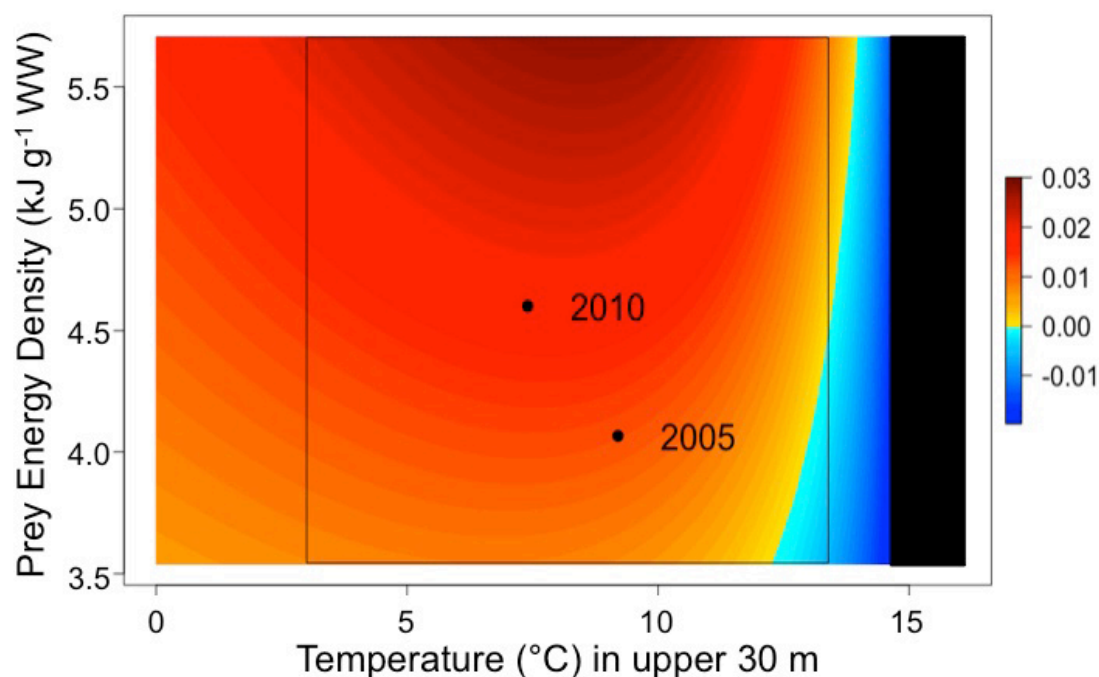


Figure 3.7. Predicted growth ($g \cdot g^{-1} \cdot d^{-1}$) of juvenile walleye pollock over the range of observed temperatures and prey energy density (ω_k) across both 2005 and 2010. The observed fish energy density (v_k) was higher in 2010 ($v_{2010} = 5.292 \text{ kJ} \cdot g^{-1} \text{ WW}$; used in plot shown), thus higher metabolic demands, therefore this interpolation demonstrates the range of predicted growth for fish with high energy density. Temperatures included 0-16 °C to show possible range under variable climate conditions; observed range of ω_k across warm and cold years. Black rectangle encompasses the range of temperatures and ω_k observed across 2005 and 2010. Points are shown for average temperature and ω_k conditions in 2005 and 2010. Predicted growth above 15 °C was not possible (black) because the bioenergetics model has a temperature threshold of 15 °C.

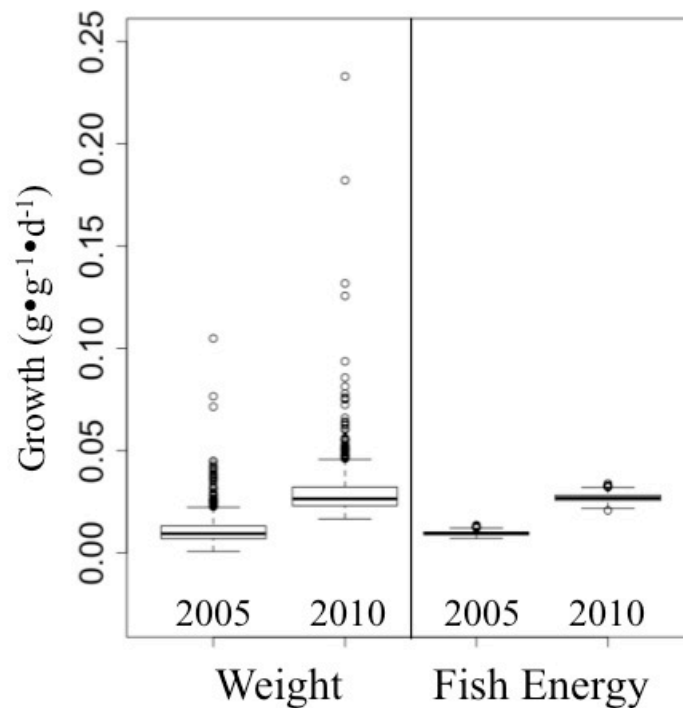


Figure 3.8. Simulated distribution of growth rates ($g \cdot g^{-1} \cdot d^{-1}$) when fish weight (W) and fish energy (v_t) at a single representative station (see Fig. 3.1) in 2005 and 2010 is varied over the range of observed values (random draws from a normal distribution with observed mean and SD). Using the base scenario ($W=2.5$ g; $v_{2005} = 3.916$ kJ \cdot g $^{-1}$ WW; $v_{2010} = 5.292$ kJ \cdot g $^{-1}$ WW) ± 1 standard deviation (SD), the model was run 1000 times to estimate the distribution around mean predicted growth. Parameter SDs were calculated across stations after removing the annual means.

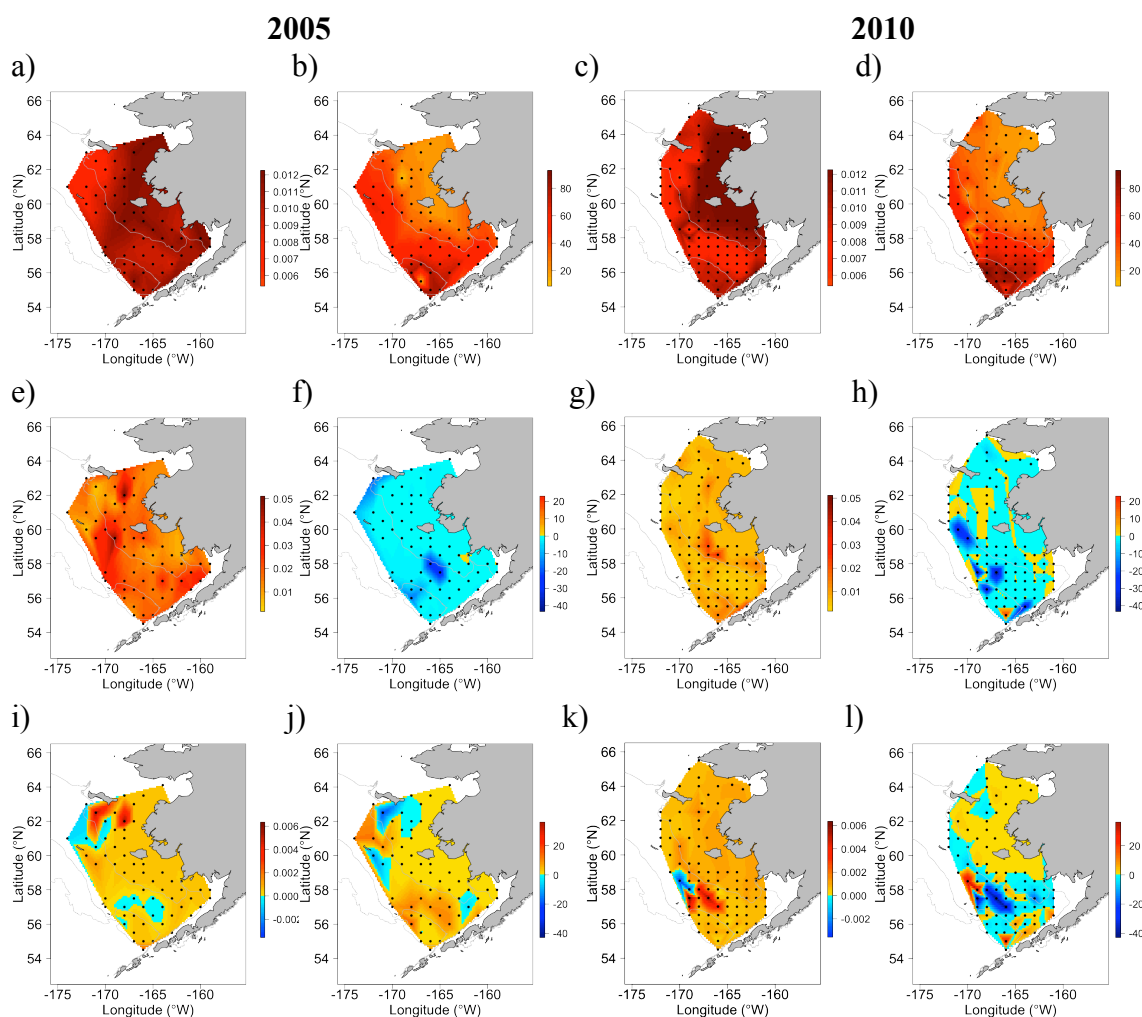


Figure 3.9. Maximum predicted growth ($g \cdot g^{-1} \cdot d^{-1}$) and average depth of juvenile walleye pollock over 24 hours from the IBM. Top row shows growth (a and c) and average depth (b and d) under the base scenario for a 2.5 g fish in 2005 and 2010. Middle row shows changes in predicted growth (e and g) and average depth (f and h) for 2.0 g fish, highlighting the relative importance of fish size and water temperature (between years). Lower row shows changes in predicted growth (i and k) and average depth (j and l) when uniform vertical distributions of prey are implemented, highlighting the effect of

Figure 3.9. Continued

zooplankton diel vertical distribution and migrations on juvenile walleye pollock prey selection. Negative changes in depth indicate a shallower distribution; positive values indicate a deeper distribution.

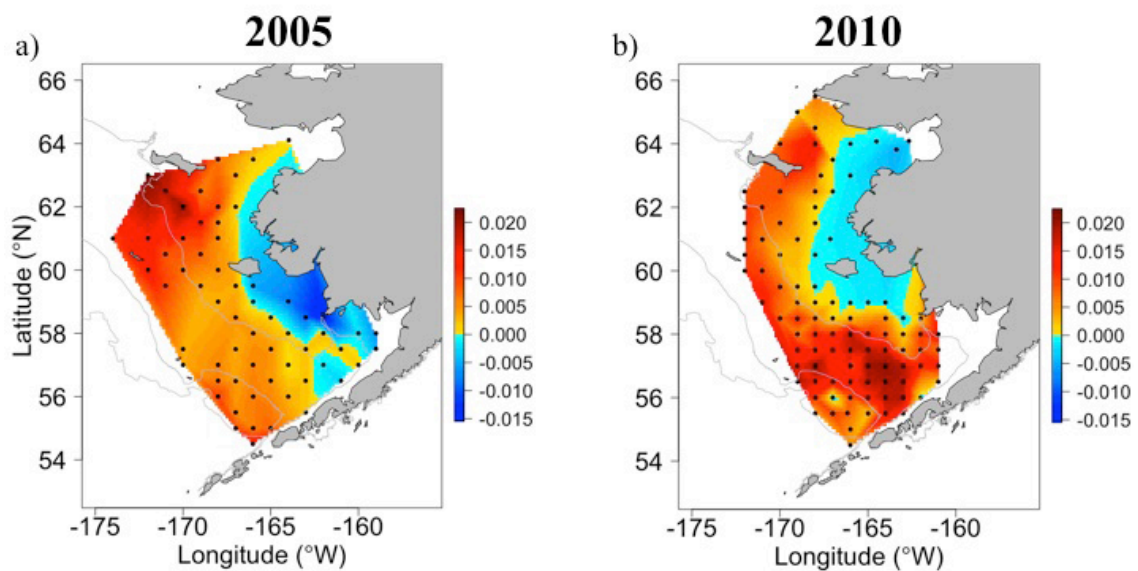


Figure 3.10. Difference in predicted growth of juvenile walleye pollock ($g \cdot g^{-1} \cdot d^{-1}$) between the bioenergetics model and the IBM for 2005 (a) and 2010 (b). Areas of positive differences indicate where maximum growth potential from the bioenergetics model was higher than predicted growth from the IBM.

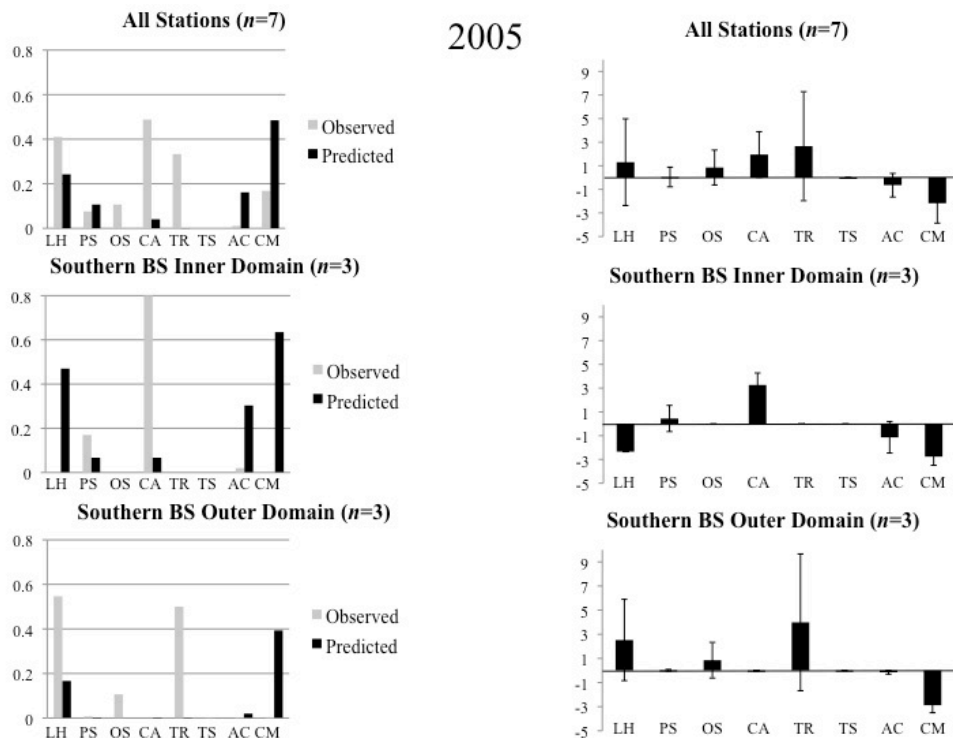


Figure 3.11. Diet comparisons between observed and predicted (IBM) diets of juvenile walleye pollock for main prey taxa (see Table 3.1) in 2005. The left-hand panel shows the mean Chesson indices (unitless) for each prey taxon for observed and predicted diets. Neutral selection varied across stations depending on the number of taxa present. The right-hand panel shows the difference (± 1 standard deviation) in the relative preference of each prey taxa; Chesson values were divided by neutral selection for each station and then predicted values subtracted from observed. Positive values indicate the prey is more prevalent in observed diets (e.g., a value of 2 indicate the taxa is twice as prevalent in observed diets as predicted). Prey taxa abbreviations are as follows: LH = *Limacina helicina*; PS = *Pseudocalanus* sp.; OS = *Oikopleua* sp.; CA = *Centropages abdominalis*; TR = *Thysanoessa raschii*; TS = *Thysanoessa* sp.; AC = *Acartia clausi*; CM = *Calanus marshallae*.

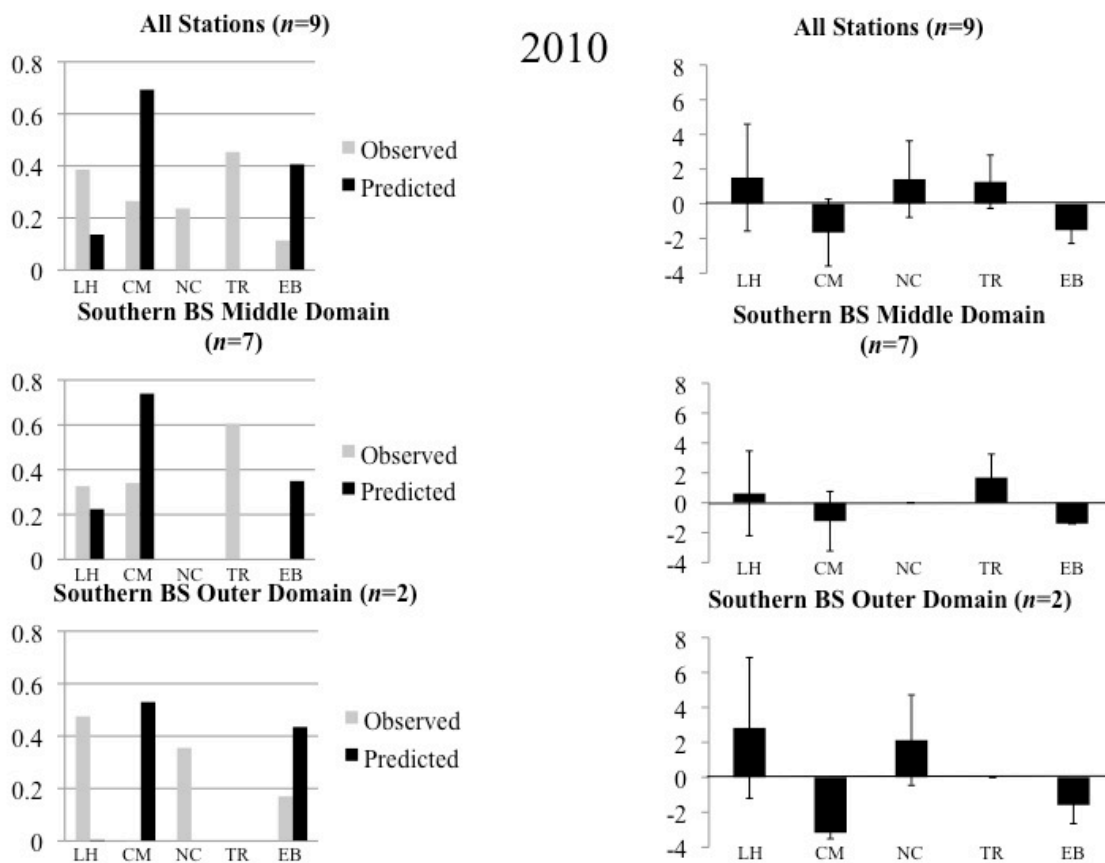


Figure 3.12. Diet comparisons between observed and predicted (IBM) diets of juvenile walleye pollock for main prey taxa (see Table 3.1) in 2010. See Figure 3.11 legend for explanation. Prey taxa abbreviations are as follows: LH = *Limacina helicina*; CM = *Calanus marshallae*; NC = *Neocalanus cristatus*; TR = *Thysanoessa raschii*; EB = *Eucalanus bungii*.

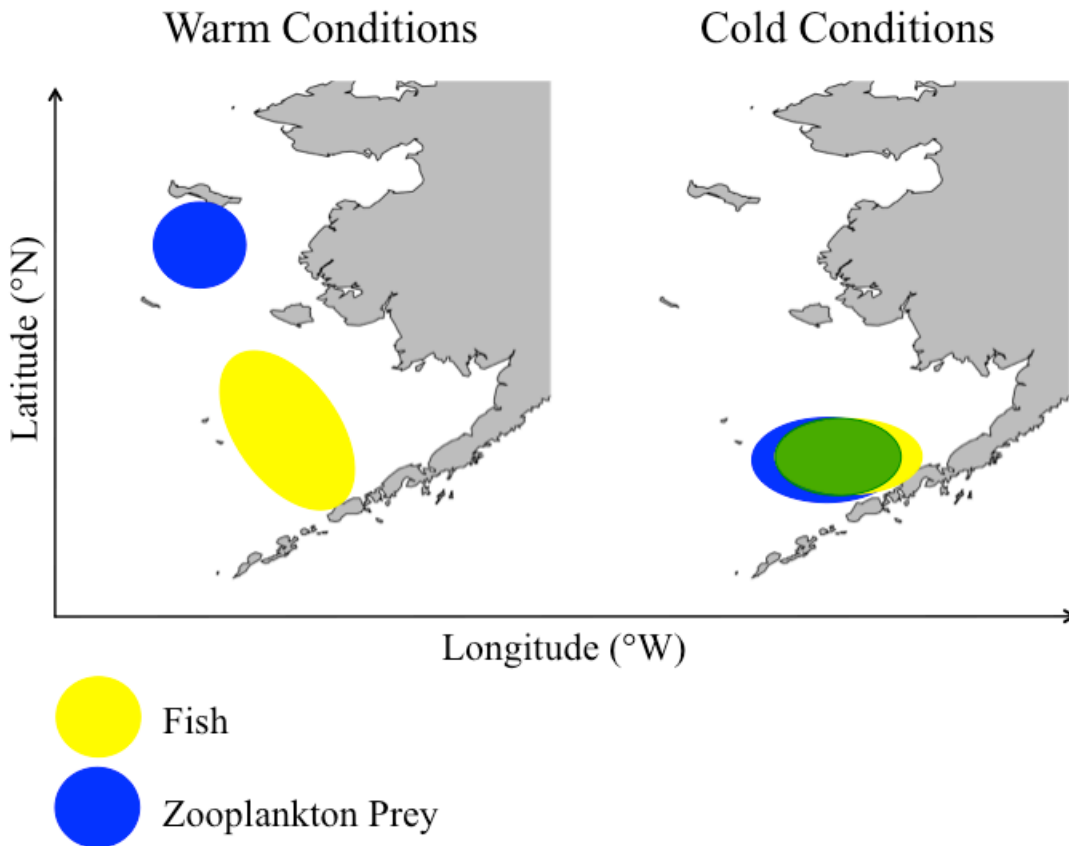


Figure 3.13. Conceptual figure of the spatial relationship between juvenile fish abundance (yellow) and zooplankton prey availability (blue). Where these areas overlap (green), juvenile fish are predicted to have higher growth rates and increased survival. Under warm climate conditions, there is reduced spatial overlap between juvenile fish and prey availability, resulting in lower overwinter survival and recruitment success to age-1. In colder conditions, increased spatial overlap between juvenile fish and prey availability results in increased overwinter survival and recruitment to age-1.

Table 3.A.1. Stage, sampling gear, length range, width, biomass (g wet weight), and energy density ($\text{kJ}\cdot\text{g}^{-1}$ wet weight) values for the main prey items of juvenile walleye pollock in late summer 2005 and 2010. Biomass estimates were obtained during processing of the zooplankton samples from 2005 (warm) and 2010 (cold) (NA=stage was not collected); energy density values were obtained from zooplankton collected in the EBS during 2004 (warm) and 2010 (cold). Single estimates of energy density (shown in bold) were used when year-specific information was not available for individual taxa.

Species	Stage	Gear	Length range (mm TL)	Width (mm)	Warm Biomass (g WW)	Cold Biomass (g WW)	Warm Energy Density ($\text{kJ}\cdot\text{g}^{-1}$ WW)	Cold Energy Density ($\text{kJ}\cdot\text{g}^{-1}$ WW)	Comments
<i>Acartia clausi</i>	A	Juday	0.25 – 1.4 ^a	0.22 ^b	3.5 E-05	3.5 E-05	3.816^c	3.816^c	
	AF	Juday	0.8 – 1.4 ^a	0.29 ^b	NA	4.5 E-05			
	AM	Juday	0.8 – 1.2 ^a	0.27 ^b	NA	2.5 E-05			
<i>Acartia</i> sp.	A	Juday	0.25 – 0.93 ^a	0.16 ^b	1.85 E-05	1.9 E-05			
	I	Juday	0.25 – 0.42 ^a	0.09 ^b	NA	4.1 E-06			Length range for <i>A. clausi</i>

Table 3.A.1. Continued

	II	Juday	0.42 – 0.51 ^a	0.12 ^b	NA				Length range for <i>A. clausi</i>
						9.4 E-06			
	III	Juday	0.51 – 0.65 ^a	0.16 ^b	NA				Length range for <i>A. clausi</i>
						1.7 E-05			
	IV	Juday	0.65 – 0.76 ^a	0.19 ^b	1.0 E-05				Length range for <i>A. clausi</i>
						2.5 E-05			
	V	Juday	0.76 – 0.93 ^a	0.23 ^b	2.7 E-05				Length range for <i>A. clausi</i>
						4.0E-05			
<i>Calanus marshallae</i>	AF	Bongo	3.2 – 4.2 ^a	0.78 ^d	0.003	0.002	5.325 ^f	5.732 ^g	
	AM	Bongo	3.5 – 4 ^a	1.0 ^e	0.0026	0.0017			
	I	Bongo	0.5 – 0.7 ^a	0.16 ^e	5.25 E-05	5.25 E-05			
	II	Bongo	1.2 – 1.5 ^a	0.36 ^e	9.19 E-05	1.33 E-04			
	III	Bongo	1.6 – 2.3 ^a	0.68 ^d	1.9 E-04	2.7 E-04			
	I-III	Bongo	0.5 – 2.3 ^a	0.37 ^e	1.13 E-04	2.2 E-04			
	IV	Bongo	2.3 – 2.6 ^a	0.69 ^d	5.82 E-04	5.24 E-04			

Table 3.A.1. Continued

	V	Bongo	2.8 – 3.8 ^a	0.73 ^d	0.002	0.0016			
<i>Centropages abdominalis</i>	A	Juday	0.3 – 2.1 ^a	0.36 ^h	7.49 E-05	5.73 E-05	3.843ⁱ	3.843ⁱ	
	AF	Juday	1.6 – 2.1 ^a	0.53 ^h	1.61 E-4	1.36 E-4			
	AM	Juday	1.5 ^a	0.5 ^h	9.14 E-05	1.16 E-4			
	C	Juday	1.13 ^a	0.5 ^h	2.33 E-05	2.33 E-05			
	I	Juday	0.3 ^a	0.16 ^h	NA	2.92 E-05			
	II	Juday	0.38 ^a	0.22 ^h	NA	1.5 E-05			
	III	Juday	0.5 ^a	0.29 ^h	1.32 E-05	2.82 E-05			
	I-III	Juday	0.33 ^a	0.17 ^h	NA	9.1 E-06			
	IV	Juday	0.65 ^a	0.39 ^h	NA	4.25 E-05			
	V	Juday	0.85 ^a	0.5 ^h	8.55 E-05	6.89 E-05			
<i>Eucalanus bungii</i>	A	Bongo	4.8 – 8 ^a	1.7 ^e	0.0023	8.67 E-05	3.916 ^j	4.194 ^k	
	AF	Bongo	6 – 8 ^a	1.86 ^e	0.0086	0.0086			
	AM	Bongo	4.8 – 5.5 ^a	1.37 ^e	0.0031	0.0041			

Table 3.A.1. Continued

	I	Bongo	1.3 – 1.6 ^a	0.39 ^e	4.5 E-05	5.3 E-05			
	II	Bongo	2 – 2.2 ^a	0.56 ^e	1.96 E-4	1.56 E-4			
	III	Bongo	2.9 – 3 ^a	0.79 ^e	4.92 E-4	2.66 E-4			
	I-III	Bongo	1.3 – 3 ^a	0.57 ^e	2.44 E-04	8.41 E-4			
	IV	Bongo	3.36 – 3.8 ^a	0.95 ^e	0.0011	0.0009			
	V	Bongo	4.5 – 5.2 ^a	1.29 ^e	0.0027	0.0034			
<i>Limacina helicina</i>	XS	Bongo	0.1 – 0.5 ^l	0.3 ^l	NA	6.93 E-05	2.51 ^m	2.766 ^g	
	S	Bongo	0.5 – 2 ^l	1.25 ^l	9.40 E-05	1.58 E-4			
	M	Bongo	2 – 4 ^l	3 ^l	3.71 E-4	8.29 E-4			
	L	Bongo	4 - 10 ^l	7 ^l	0.0026	0.0045			
<i>Neocalanus cristatus</i>	AF	Bongo	8.5 – 10.4 ^a	2.5 ^e	NA	0.0137	3.253 ⁿ	3.39 ^g	
	III	Bongo	3.2 ^a	0.85 ^e	8.83 E-4	0.0013			
	IV	Bongo	4.9 – 5.3 ^a	1.36 ^e	0.0059	0.0025			
	V	Bongo	7.1 – 8.9 ^a	2.13 ^e	0.019	0.015			

Table 3.A.1. Continued

<i>N. plumchrus</i>	V	Bongo	4.1 – 5.2 ^a	1.24 ^e	0.00395	0.0041	4.207 ^o	4.676 ^g	
<i>Oikopleura</i> sp.	A	Bongo	0.1 – 0.6 ^p	0.35 ^p	1.73 E-4	1.7 E-4	4.076 ^q	4.025 ^r	
<i>Pseudocalanus</i> spp.	A	Juday	0.65 – 1.2 ^s	0.29 ^d	4.44 E-05	3.6 E-05	3.951^t	3.951^t	Length range for <i>P. moultoni</i>
	AF	Juday	1.05 – 2.27 ^s	0.42 ^d	8.27 E-05	8.01 E-05			
	AM	Juday	0.91 – 1.74 ^s	0.35 ^b	4.13 E-05	5.42 E-05			
	I	Juday	0.5 – 0.7 ^s	0.16 ^b	NA	5.98 E-06			
	II	Juday	0.65 – 0.8 ^s	0.19 ^b	1.01 E-05	1.08 E-05			
	III	Juday	0.8 – 1 ^s	0.24 ^b	1.26 E-05	2.0 E-05			
	I-III	Juday	0.5 – 1 ^s	0.2 ^b	NA	1.01 E-05			
	IV	Juday	1 – 1.2 ^s	0.3 ^d	3.06 E-05	3.19 E-05			
	V	Juday	1.2 – 1.5 ^s	0.37 ^d	8.89 E-05	4.93 E-05			
	II-V	Juday	0.65 – 1.5 ^s	0.29 ^d	3.55 E-05	2.8 E-05			

Table 3.A.1. Continued

<i>Thysanoessa inermis</i>	A	Bongo	10.1 – 29.2 ^u	2.4 ^d	NA	0.083	4.99^m	4.99^m	
	AF	Bongo	10.1 – 29.2 ^u	2.4 ^d		0.10			
	AM	Bongo	10.1 – 29.2 ^u	2.4 ^d	0.069	NA			
	J	Bongo	8.5 – 13.8 ^u	1.4 ^d	NA	0.011			
	J (L)	Bongo	11.1 – 13.8 ^u	1.5 ^d	0.061	0.11			
	J (S)	Bongo	8.5 – 11.1 ^u	1.2 ^d	0.011	0.024			
<i>T. inspinata</i>	J	Bongo	12 – 17 ^v	2.2 ^w	0.0012	0.0128	4.99^x	4.99^x	
<i>T. raschii</i>	A	Bongo	7 – 29.1 ^y	3.3 ^d	0.006	NA	4.308 ^{aa}	5.231 ^g	
	AF	Bongo	7 – 29.1 ^y	3.3 ^d	0.077	0.0903			
	AM	Bongo	15.3 – 20.2 ^z	2.7 ^d	0.046	0.088			
	J	Bongo	7.4 – 8.4 ^z	1.45 ^d	0.005	0.0117			
	J (L)	Bongo	7.9 – 8.4 ^z	1.5 ^d	0.0476	0.0936			
	J (S)	Bongo	7.4 – 7.9 ^z	1.4 ^d	0.0089	0.0059			

Table 3.A.1. Continued

^a [45]; ^b Estimated width = 26.7% of length (based on *Pseudocalanus* sp. relationship); ^c Energy density estimated from % lipid (2.25% wet weight assuming 80% moisture [46]) using the regression relationship: $ED = (0.4098 \cdot \% \text{ lipid}) + 19.287$; ^d E. Fergusson, NOAA/AFSC, unpublished data; ^e Estimated width = 26.6% of length (based on *C. marshallae* relationship); ^f Energy density estimated from % lipid (10.5%; R. Heintz, NOAA/AFSC, unpublished data); ^g R. Heintz, NOAA/AFSC, unpublished data; ^h [47]; ⁱ Energy density estimated from % lipid (2.6% wet weight [48]); ^j Energy density estimated from % lipid (3.55%; R. Heintz, NOAA/AFSC, unpublished data); ^k Energy density estimated as 7.1% higher in cold years (based on copepod data; [this study]); ^l C. Stark, UAF, unpublished data; ^m 2006 collection (R. Heintz, NOAA/AFSC, unpublished data); ⁿ Energy density estimated from % lipid (5.85%; R. Heintz, NOAA/AFSC, unpublished data); ^o Energy density estimated from % lipid (6.83%; R. Heintz, NOAA/AFSC, unpublished data); ^p Trunk length/width [49]; ^q Energy density estimated from % lipid of Chaetognatha (2.67%; R. Heintz, NOAA/AFSC, unpublished data); ^r Energy density estimated from % lipid of Chaetognatha (2.04%; R. Heintz, NOAA/AFSC, unpublished data); ^s [50]; ^t Energy density estimated from % lipid (4% wet weight [51]); ^u Carapace width from [52]; converted to TL using equations from [53]; ^v Length range of 'spineless' *T. longipes* [54]; ^w Estimated

Table 3.A.1. Continued

width as 15% of length; ^x Used energy density of *T. inermis*; ^y Minimum size for *T. inermis* and maximum size for *T. spinifera* [52]; converted to TL using equations from [53]; ^z Minimum size for *T. inermis* and maximum size for *T. spinifera* [55]; converted to TL using equations from [53]; ^{aa} Energy density estimated as 17.65% higher in cold years (R. Heintz, NOAA/AFSC, unpublished data).

Table 3.A.2. Component equations of the bioenergetics model used to estimate maximum growth potential ($g \cdot g^{-1} \cdot d^{-1}$) of juvenile walleye pollock.

Consumption	$C = \alpha \cdot W^\beta \cdot f(T) \cdot \eta$
	$f(T) = V^X \cdot e^{(X(1-V))}$
	$V = (T_{cm} - T) / (T_{cm} - T_{co})$
	$X = (Z^2 \cdot (1 + (1 + 40/Y)^{0.5})^2) / 400$
	$Z = \ln(Q_c) \cdot (T_{cm} - T_{co})$
	$Y = \ln(Q_c) \cdot (T_{cm} - T_{co} + 2)$
Respiration	$R = (A_r \cdot W^{Br} \cdot f(T) \cdot A_m \cdot 13560) + (D_s \cdot (C - F))$
	$f(T) = V^X \cdot e^{(X(1-V))}$
	$V = (T_{rm} - T) / (T_{rm} - T_{ro})$
	$X = (Z^2 \cdot (1 + (1 + 40/Y)^{0.5})^2) / 400$
	$Z = \ln(Q_r) \cdot (T_{rm} - T_{ro})$
	$Y = \ln(Q_r) \cdot (T_{rm} - T_{ro} + 2)$
Egestion	$F = F_a \cdot C$
Excretion	$U = U_a \cdot (C - F)$

General Conclusions

While most previous studies have focused on climate effects on adult demersal fish and shellfish communities (Brander et al. 2003, Perry et al. 2005, Mueter et al. 2007, Mueter & Litzow 2008, Spencer 2008), less work has been done to investigate changes in the pelagic community structure and ecology of early life stages of fishes (Duffy-Anderson et al. 2006, Brodeur et al. 2008, Doyle et al. 2009). The pelagic distribution of ichthyoplankton is related to the spawning locations of adult fish (Doyle et al. 2002). Therefore as the spatial distribution of spawning populations as well as zooplankton prey vary under changing climate conditions, so do patterns in larval and juvenile fish condition, growth, and subsequent recruitment success. After spawning, larval drift is subject to advection of water masses (Lanksbury et al. 2005), which is strongly influenced by wind stress and varies interannually as a result of basin-scale climate variability. Transport pathways can lead to differential survival of larvae based on life history characteristics (Doyle et al. 2009), predator abundances (Hunt et al. 2002), or availability of suitable juvenile habitat (Wilderbuer et al. 2002). Understanding variability in larval fish assemblage structure, as well as spatial and temporal patterns in fish condition and growth, may indicate ecosystem-level and/or species-specific responses to climate change.

Using a multivariate approach, shifts in larval fish community composition in response to environmental variability and delineations based on hydrographic conditions were identified in the eastern Bering Sea (EBS). This study was the first to look at such transitions over a relatively short time period that included both pronounced warm and

cold conditions. Significant differences in assemblage structure were detected, supporting the hypothesis that early life stages may be primary indicators of environmental change. Larval abundances were generally higher at the time of sampling in warm years with high abundances of walleye pollock contributing most to differences between warm and cold periods in Unimak Pass, the outer domain, and shelf areas. Assemblages over the slope were less variable between years and may be somewhat insulated from interannual variability. The slope assemblage was consistently dominated by *Sebastes* spp. with increased abundances in cold years.

Cross-shelf assemblage structure was primarily associated with a geographic and/or salinity gradient that distinguished slope and shelf communities. Salinities are higher over the slope due to the oceanic influence of the Aleutian North Slope Current and lower on the shelf due to increased freshwater from the mainland and from the Alaska Coastal Current (ACC) flowing through Unimak Pass. The cross-shelf gradient, largely driven by differences in spawning habitat for slope and shelf species, appears resilient to environmental variability between warm and cold years.

The advection of ACC waters through Unimak Pass (Ladd et al. 2005) may affect the distribution of larval fish on the EBS shelf. Species entrained in, or advected by, ACC waters within Unimak Pass and the Bering Sea shelf included Pacific cod (*Gadus macrocephalus*) and northern rock sole (*Lepidopsetta polyxystra*), with higher overall abundances of these species in warm years. Unfortunately, our sampling design could not resolve whether these larvae originated in the Gulf of Alaska or were entrained in ACC waters within Unimak Pass and nearby spawning grounds. The impact of Gulf of Alaska

larvae on Bering Sea populations, and the degree to which the populations are connected, are important ecological (i.e., competition, predation) and fisheries management (number of sub-populations) questions. However, while some studies have demonstrated larval drift from the Gulf of Alaska to the Bering Sea (e.g., Lanksbury et al. 2007), for most species the role of advection through Unimak Pass and the resulting connectivity between Gulf of Alaska and Bering Sea populations is still largely unknown.

Multiple factors during the early life stages of fishes result in variable recruitment success, including environmental conditions (Cushing 1982) and prey availability. Variability in the spatial and temporal overlap of predator and prey (match/mismatch hypothesis; Cushing 1969, 1990), as well as differences in prey quality (Sogard & Olla 2000, Litzow et al. 2006), affect fish growth and energy storage, which may directly affect differences in year-class success of many marine fish species, such as walleye pollock (Hunt et al. 2011). In addition, cold water temperatures generally delay ontogenetic development of walleye pollock (Blood 2002, Smart et al. in press) while also lowering routine metabolic demands (Ciannelli et al. 1998). Such constraints affect larval fishes' ability to achieve sufficient size and energy reserves prior to their first winter (Sogard & Olla 2000, Heintz & Vollenweider 2010).

Differences in energy storage result from differences in the quantity and quality of prey during the age-0 period (Heintz et al. in press). Higher abundances of larger, lipid-rich zooplankton taxa during cold years, combined with lower metabolic demands, allow age-0 walleye pollock to acquire greater lipid reserves by late summer, resulting in increased overwinter survival (Hunt et al. 2011). In the cold years of 2006-2010, the

zooplankton community over the Bering Sea shelf was dominated by large copepods (e.g., *Calanus marshallae*) and euphausiids (e.g., *Thysanoessa raschii*). Under warmer conditions (2002-2005), smaller zooplankton taxa were dominant (e.g., *Pseudocalanus* spp., *Acartia* spp., Coyle et al. 2011, Stabeno et al. 2012) and the lack of larger prey appeared to have had a limiting effect on growth and energy storage of walleye pollock, leading to poor energy levels and reduced year-class recruitment. The limited availability of large zooplankton coincided with increased rates of cannibalism by older age-classes of walleye pollock, as well as high predation rates by juvenile salmon, further reducing age-0 survival in warm years (Coyle et al. 2011). Hence, prey quality may be as important as the thermal regime for determining overwinter survival (Hurst 2007), although prey availability and prey quality were closely linked to temperature conditions in recent years (Coyle et al. 2011).

I quantified the seasonal progression in energy content of age-0 walleye pollock during three cold years in the EBS (Stabeno et al. 2012), therefore delayed development times likely resulted in smaller fish sizes relative to warmer years (Smart et al. in press). Age-0 juvenile walleye pollock reached an asymptotic length at approximately 60 mm SL in late summer, which may correspond to a shift in prey preferences with increasing gape size (i.e., switch to euphausiids; Brodeur 1998) and associated foraging capability (e.g., Ciannelli et al. 2002). An asymptotic energy density occurred when fish reached approximately 75 mm SL, similar to that observed for walleye pollock near the Pribilof Islands (asymptotic energy density at 80 mm SL) during 1994-1996 and 1999, with 1995 and 1999 also being cold years (Ciannelli et al. 2002).

Larval and juvenile walleye pollock face competing physiological demands of somatic growth versus lipid storage (Post & Parkinson 2001) for available energy resources. I identified differing energy allocation strategies indicating that distinct ontogenetic stages face different survival constraints. Larval fish favored allocation to somatic growth, presumably in order to escape size-dependent predation, while juvenile fish allocated energy to lipid storage in late summer. My results support the idea that late summer (July-September) represents a critical period for energy storage in age-0 walleye pollock, and that overwinter survival is dependent on sufficient storage in the previous growing season and may be an important determinant of recruitment success.

Although the energetic condition of juvenile walleye pollock in late summer is recognized as a predictor of age-1 abundance during the following summer in the EBS (Heintz et al. in press), the causal mechanism linking differences in prey abundance and quality to walleye pollock survival remains untested. Comparing alternative model-based predictions of growth allows a better understanding of the mechanisms behind variability in growth patterns and an evaluation of the importance of different parameters in the models. I found that differences in prey species composition and quality lead to bottom-up control of juvenile walleye pollock growth and survival in representative warm and cold years in the EBS.

Prey distribution and quality in combination with water temperatures create spatial patterns of increased growth potential ('hot spots') that vary with climate conditions. Spatial heterogeneity in growing conditions results from combined prey quality and quantity and metabolic costs, which may contribute to size-dependent

survival and subsequent annual variability in recruitment success. The premise of the match-mismatch hypothesis (Cushing 1990) is that temporal overlap of predator needs and resource availability regulates recruitment (Leggett & DeBlois 1994). Additionally, spatial distribution and resource availability can be modified under climate variability (Chick & Van Den Avyle 1999, Durant et al. 2007, Kristiansen et al. 2011).

The comparative model approach allowed me to evaluate the relative role of prey and temperature on juvenile walleye pollock growth. Spatial patterns in growth differed between two alternative models; these differences elucidate underlying mechanisms in the feeding potential and ultimately possible causes for growth ‘hot spots’ and variability in recruitment success between warm and cold climate conditions. The relative effect of increasing temperatures was greater in 2005 than in 2010. In 2005, fish were near thermal limits based on temperature-dependent functions in the bioenergetics model over much of the EBS shelf; further increases in temperature are predicted to result in negative growth. In addition to warmer water temperatures in 2005, the spatial overlap of juvenile walleye pollock and growth ‘hot spots’ was lower than in 2010, further limiting fish growth.

This study provided evidence that climate-driven changes in prey dynamics may have ecosystem-level consequences via bottom-up control of fish populations in sub-arctic marine ecosystems. While temporal match-mismatch and the study of changes in phenology remain paramount in advancing the discussion of climate effects, I highlight the importance of simultaneous spatial match-mismatch affecting the overlap of marine fish and prey resources. This work has resulted in an improved understanding of the mechanisms behind recruitment variability, in particular the underlying spatial patterns

that drive relationships between temperature, prey availability, growth and survival. My findings thereby inform ongoing discussions of climate effects on predator-prey interactions and recruitment success of marine fishes.

References

- Bacheler NM, Ciannelli L, Bailey KM, Duffy-Anderson JT (2010) Spatial and temporal patterns of walleye pollock (*Theragra chalcogramma*) spawning in the eastern Bering Sea inferred from egg and larval distributions. *Fish Oceanogr* 19(2): 107-120
- Beamish RJ, Mahnken C (2001) A critical size and period hypothesis to explain natural regulation of salmon abundance and the linkage to climate and climate change. *Prog Oceanogr* 49: 423-437
- Blood DM (2002) Low-temperature incubation of walleye pollock (*Theragra chalcogramma*) eggs from the southeast Bering Sea shelf and Shelikof Strait, Gulf of Alaska. *Deep-Sea Res II* 49: 6095–6108
- Brander KM, Blom G, Borges MF, Erzini K, Henderson G, MacKenzie BR, Mendes H, Santos AMP, Toresen P (2003) Changes in fish distribution in the eastern North Atlantic: are we seeing a coherent response to changing temperature? *ICES Mar Sci Symp* 219: 260-273
- Brodeur RD (1998) Prey selection by age-0 walleye pollock, *Theragra chalcogramma*, in nearshore waters of the Gulf of Alaska. *Environ Biol Fish* 51: 175-186
- Brodeur RD, Peterson WT, Auth TD, Soulen HL, Parnel MM, Emerson AA (2008) Abundance and diversity of coastal fish larvae as indicators of recent changes in ocean and climate conditions in the Oregon upwelling zone. *Mar Ecol Prog Ser* 366: 187-202
- Chick JH, Van Den Avyle MJ (1999) Zooplankton variability and larval striped bass foraging: evaluating potential match/mismatch regulation. *Ecol Appl* 9:320–334
- Ciannelli L, Brodeur RD, Buckley TW (1998) Development and application of a bioenergetics model for juvenile walleye pollock. *J Fish Biol* 52: 879-898
- Ciannelli L, Paul AJ, Brodeur RD (2002) Regional, interannual and size-related variation of age 0 year walleye pollock whole body energy content around the Pribilof Islands, Bering Sea. *J Fish Biol* 60: 1267-1279
- Ciannelli L, Bailey KM, Chan KS, Stenseth NC (2007) Phenological and geographical patterns of walleye pollock (*Theragra chalcogramma*) spawning in the western Gulf of Alaska. *Can J Fish Aquat. Sci* 64: 713-722
- Coachman LK (1986) Circulation, water masses, and fluxes on the southeastern Bering Sea shelf. *Cont Shelf Res* 5(1-2): 23-108

Coyle KO, Eisner LB, Mueter FJ, Pinchuk AI, Janout MA, Cieciel KD, Farley EV, Andrews AG (2011) Climate change in the southeastern Bering Sea: impacts on pollock stocks and implications for the Oscillating Control Hypothesis. *Fish Oceanogr* 20 (2): 139-156

Cushing DH (1969) The regularity of the spawning season of some fishes. *J Cons Int Explor Mer* 33: 81-97

Cushing DH (1982) *Climate and fisheries*. Academic Press: London. ISBN 0-12-199720-0. 373 pp

Cushing DH (1990) Plankton production and year-class strength in fish populations: an update of the match/mismatch hypothesis. *Adv Mar Biol* 26: 250-293

Doyle MJ, Mier KL, Busby MS, Brodeur RD (2002) Regional variation in springtime ichthyoplankton assemblages in the northeast Pacific Ocean. *Prog Oceanogr* 53: 247-281

Doyle MJ, Picquelle SJ, Mier KL, Spillane MC, Bond NA (2009) Larval fish abundance and physical forcing in the Gulf of Alaska, 1981-2003. *Prog Oceanogr* 80: 163-187

Duffy-Anderson JT, Busby MS, Mier KL, Deliyanides CM, Stabeno PJ (2006) Spatial and temporal patterns in summer ichthyoplankton assemblages on the eastern Bering Sea shelf 1996-2000. *Fish Oceanogr* 15: 80-94

Durant JM, Hjermann DO, Ottersen G, Stenseth NC (2007) Climate and the match or mismatch between predator requirements and resource availability. *Climate Res* 33: 271-283

Hare SR, Mantua NJ (2000) Empirical evidence for North Pacific regime shifts in 1977 and 1989. *Prog Oceanogr* 47: 103-145

Heintz RA, Vollenweider JJ (2010) Influence of size on the sources of energy consumed by overwintering walleye pollock (*Theragra chalcogramma*). *J Exp Mar Biol Ecol* 393 (1-2): 43-50

Heintz RA, Siddon EC, Farley EV (In press) Climate-related changes in the nutritional condition of young-of-year (YOY) walleye pollock (*Theragra chalcogramma*) from the southeastern Bering Sea. *Deep-Sea Res II*

Hillgruber N, Haldorson, LJ, Paul AJ (1995) Feeding selectivity of larval walleye pollock *Theragra chalcogramma* in the oceanic domain of the Bering Sea. *Mar Ecol Prog Ser* 120: 1-10

Hollowed AB, Bond NA, Wilderbuer TK, Stockhausen WT, A'mar ZT, Beamish RJ,

- Overland JE, Schirripa MJ (2009) A framework for modelling fish and shellfish responses to future climate change. *ICES J Mar Sci* 66: 1584–1594
- Hunt GL Jr, Stabeno PJ (2002) Climate change and the control of energy flow in the southeastern Bering Sea. *Prog Oceanogr* 55: 5-22
- Hunt GL Jr, Stabeno PJ, Walters G, Sinclair E, Brodeur RD, Napp JM, Bond NA (2002) Climate change and control of the southeastern Bering Sea pelagic ecosystem. *Deep-Sea Res II* 49: 5821-5853
- Hunt GL Jr, Coyle KO, Eisner L, Farley EV, Heintz R, Mueter FJ, Napp JM, Overland JE, Ressler PH, Salo S, Stabeno PJ (2011) Climate impacts on eastern Bering Sea foodwebs: A synthesis of new data and an assessment of the Oscillating Control Hypothesis. *ICES J Mar Sci* 68(6): 1230-1243
- Hurst TP (2007) Causes and consequences of winter mortality in fishes. *J Fish Biol* 71: 315-345
- Ianelli JN, Barbeaux S, Honkalehto T, Kotwicki S, Aydin K, Williamson N (2009) Assessment of the Walleye Pollock stock in the Eastern Bering Sea. In: Stock assessment and fishery evaluation report for the groundfish resources of the Bering Sea/Aleutian Islands regions. North Pacific Fishery Management Council, 605 W. 4th Ave., Suite 306, Anchorage, AK 99501
- Iverson RL, Coachman LK, Cooney RT, English TS, Goering JJ, Hunt GL Jr, Macauley MC, McRoy CP, Reeburgh WS, Whitledge TE (1979) Ecological significance of fronts in the southeastern Bering Sea. In RJ Livingston (ed.) *Ecological Processes in Coastal and Marine Systems*. Plenum Press, New York, NY. p. 437-466
- Kooka K, Yamamura O, Nishimura A, Hamatsu T, Yanagimoto T (2007) Optimum temperature for growth of juvenile walleye pollock *Theragra chalcogramma*. *J Exp Mar Biol Ecol* 347: 69-76
- Kristiansen T, Drinkwater KF, Lough RG, Sundby S (2011) Recruitment variability in North Atlantic cod and match-mismatch dynamics. *PLOS ONE* 6: e17456
- Ladd C, Hunt GL Jr, Mordy CW, Salo SA, Stabeno PJ (2005) Marine environment of the eastern and central Aleutian Islands. *Fish Oceanogr* 14(Suppl. 1): 22-38
- Lanksbury JA, Duffy-Anderson JT, Mier KL, Wilson MT (2005) Ichthyoplankton abundance, distribution, and assemblage structure in the Gulf of Alaska during September 2000 and 2001. *Est Coast Shelf Sci* 64: 775-785

- Lanksbury JA, Duffy-Anderson JT, Mier KL, Busby MS, Stabeno PJ (2007) Distribution and transport patterns of northern rock sole, *Lepidopsetta polyxystra*, larvae in the southeastern Bering Sea. *Prog Oceanogr* 72: 39-62
- Leggett WC, Deblois E (1994) Recruitment in marine fishes: is it regulated by starvation and predation in the egg and larval stages? *Neth J Sea Res* 32(2): 119-134
- Litzow MA, Bailey KM, Prahlg FG, Heintz R (2006). Climate regime shifts and reorganization of fish communities: the essential fatty acid limitation hypothesis. *Mar Ecol Prog Ser* 315: 1–11
- Moss JH, Farley EV, Feldman AM, Ianelli JN (2009) Spatial distribution, energetic status, and food habits of eastern Bering Sea age-0 walleye pollock. *Trans Am Fish Soc* 138: 497-505
- Mueter FJ, Litzow MA (2008) Sea ice retreat alters the biogeography of the Bering Sea continental shelf. *Ecol Appl* 18(2): 309-320
- Mueter FJ, Ladd C, Palmer MC, Norcross BL (2006) Bottom-up and top-down controls of walleye pollock (*Theragra chalcogramma*) on the Eastern Bering Sea shelf. *Prog Oceanogr* 68: 152–183
- Mueter FJ, Hunt GL Jr, Litzow MA (2007) The Eastern Bering Sea shelf: a highly productive seasonally ice-covered sea. *ICES CM2007/D:04*: 1-10
- Mueter FJ, Bond NA, Ianelli JN, Hollowed AB (2011) Expected declines in recruitment of walleye pollock (*Theragra chalcogramma*) in the eastern Bering Sea under future climate change. *ICES J Mar Sci* 68: 1284–1296
- Perry AL, Low PJ, Ellis JR, Reynolds JD (2005) Climate change and distribution shifts in marine fishes. *Science* 308: 1912-1915
- Post JR, Parkinson EA (2001) Energy allocation strategy in young fish: allometry and survival. *Ecology* 82(4): 1040-1051
- Schumacher JD, Stabeno PJ (1998) The continental shelf of the Bering Sea. In AR Robinson and KH Brink (eds.) *The Sea: The global coastal ocean: regional studies and synthesis*. John Wiley and Sons, New York, NY. p. 789-822
- Smart TI, Siddon EC, Duffy-Anderson JT (In press) Vertical distributions of the early life stages of a common gadid in the eastern Bering Sea (*Theragra chalcogramma*, walleye pollock). *Deep-Sea Res II*

Sogard SM, Olla BL (2000) Endurance of simulated winter conditions by age-0 walleye pollock: effects of body size, water temperature and energy storage. *J Fish Biol* 56: 1-21

Spencer PD (2008) Density-independent and density-dependent factors affecting temporal changes in spatial distributions of eastern Bering Sea flatfish. *Fish Oceanogr* 17: 396-410

Stabeno PJ, Bond NA, Kachel NB, Salo SA, Schumacher JD (2001) On the temporal variability of the physical environment over the south-eastern Bering Sea. *Fish Oceanogr* 10(1): 81-98

Stabeno PJ, Hunt GL Jr, Napp JM, Schumacher JD (2006) Physical forcing of ecosystem dynamics on the Bering Sea shelf. In AR Robinson and KH Brink (eds.) *The Sea: The global coastal ocean: Interdisciplinary regional studies and syntheses, Part B*. Harvard University Press, Cambridge, MA. p. 1177–1212

Stabeno PJ, Kachel NB, Moore SE, Napp JM, Sigler M, Yamaguchi A, Zerbini AN (2012) Comparison of warm and cold years on the southeastern Bering Sea shelf and some implications for the ecosystem. *Deep-Sea Res II* 65-70: 31-45

Strasburger WW, Hillgruber N, Pinchuk AI, Mueter FJ (In press) Feeding ecology of age-0 walleye pollock (*Theragra chalcogramma*) and Pacific cod (*Gadus macrocephalus*) in the southeastern Bering Sea. *Deep-Sea Res II*

Walsh JJ, McRoy CP (1986) Ecosystem analysis in the southeastern Bering Sea. *Cont Shelf Res* 5: 259–288

Wilderbuer TK, Hollowed AB, Ingraham WJ Jr, Spencer PD, Conners ME, Bond NA, Walters GE (2002) Flatfish recruitment response to decadal climatic variability and ocean conditions in the eastern Bering Sea. *Prog Oceanogr* 55: 235-247

Wolotira RJ Jr, Sample TM, Morin M Jr (1977) Demersal fish and shellfish resources of Norton Sound, the southeastern Chukchi Sea, and adjacent waters in the baseline year 1976. NAFC Processed Report, U.S. Department of Commerce, NOAA-NMFS, Seattle, WA. 292 p

Wyllie Echeverria T, McRoy CP (1992) Larval fish distribution, p. 195-197. In P.S. Nagel (ed.) *Results of the joint U.S.-U.S.S.R. Bering and Chukchi Seas expedition (BEWRPAC), summer 1998*. U.S. Fish and Wildlife Service, Washington, DC

Wyllie-Echeverria T, Wooster WS (1998) Year-to-year variations in Bering Sea ice cover and some consequences for fish distributions. *Fish Oceanogr* 7(2): 159-170

